

地理科学学院博士研究生温都日娜2024年博士学位论文答辩及科研成果公示

2024年5月地理科学学院理学专业博士研究生温都日娜完成博士学位论文答辩，答辩委员会一致同意该研究生通过博士学位论文答辩，建议授予理学博士学位。该生在读期间发表论文及佐证材料公示如下：

学号	姓名	专业	论文名称	刊物名称	发表情况	期刊类别	发表时间	是否达到学术论发表要求
20196019006	温都日娜	地理学	Multi-Climate Factors and the Preceding Growth Stage of Vegetation Co-Regulated the Variation of the End of Growing Season in Northeast Inner Mongolia, China	IEEE Access	见刊	SCI	2020	是
			Lagged feedback of peak season photosynthetic activities on local surface temperature in Inner Mongolia, China	Environmental Research	见刊	SCI	2023	是
			Parallel acceleration of vegetation growth rate and senescence rate across the Northern Hemisphere from 1982 to 2015	Global Ecology and Conservation	见刊	SCI	2023	是
			主持项目名称	项目类型	主要参与人	是否主持	项目起止期限	项目简介
			内蒙古东北部植被枯黄期对气候变暖的不对称响应 (CXJJB20012)	2020年教育厅研究生科研创新资助项目	美丽、海慧敏、赵丽蓉、吕达	是	2020.10.23-2021.10.31	本项目将基于遥感数据、气象数据，识别内蒙古东北部2001-2017年枯黄期时空动态及其对气象因子的响应，揭示在干旱半干旱地区影响植被枯黄期变化的关键气候因子及其驱动机制。研究结果将为植被物候模拟研究及全球变化的区域响应方面具有重要的研究和实际应用价值。



薛建拉

Received November 18, 2020, accepted December 3, 2020, date of publication December 10, 2020,
date of current version December 21, 2020.

Digital Object Identifier 10.1109/ACCESS.2020.3043788

Multi-Climate Factors and the Preceding Growth Stage of Vegetation Co-Regulated the Variation of the End of Growing Season in Northeast Inner Mongolia, China

WENDU RINA^{1,2}, GANG BAO^{1,2}, SIQIN TONG^{1,3}, YUHAI BAO^{1,2}, YIN SHAN^{1,2},
XIAOJUN HUANG^{1,2}, HONG YING⁴, AND LINGTONG DU^{5,6}

¹College of Geographical Science, Inner Mongolia Normal University, Hohhot 010022, China

²Inner Mongolia Key Laboratory of Remote Sensing and Geographic Information Systems, Inner Mongolia Normal University, Hohhot 010022, China

³Inner Mongolia Key Laboratory of Disaster and Ecological Security on the Mongolian Plateau, Inner Mongolia Normal University, Hohhot 010022, China

⁴Key Laboratory of Geographical Processes and Ecological Security in Changbai Mountains, Ministry of Education, School of Geographical Sciences, Northeast Normal University, Changchun 130024, China

⁵Breeding Base for State Key Laboratory of Land Degradation and Ecological Restoration in Northwest China, Ningxia University, Yinchuan 750021, China

⁶Key Laboratory for Restoration and Reconstruction of Degraded Ecosystem in Northwest China, Ministry of Education, Ningxia University, Yinchuan 750021, China

Corresponding authors: Gang Bao (baogang@imnu.edu.cn) and Siqin Tong (tongsq223@imnu.edu.cn)

This work was supported in part by the National Natural Science Foundation of China under Grant 61631011, Grant 41961144019, Grant 41861021, and Grant 42061070; in part by the Graduate Research and Innovation Foundation of Inner Mongolia Autonomous Region under Grant CXJB20012; and in part by the Opening Foundation of Key Laboratory for Restoration and Reconstruction of Degraded Ecosystem in Northwest China of Ministry of Education, Ningxia University, under Grant 2018KF03.

ABSTRACT The end of growing season (EOS) is an effective indicator of annual vegetation growth. Previous studies have revealed the dynamics of the EOS with climate change, while the influence of vegetation growth in preceding stage and peak of growing season (POS) on the EOS has not been thoroughly documented. In this study, we used four smoothing methods to obtain EOS dates from the Normalized Difference Vegetation Index (NDVI) in northeast Inner Mongolia (NIM) between 2001–2017, assessed the differences in the spatiotemporal variations of the EOS obtained by the four smoothing methods, and then investigated the impacts of climate factors, summer/ autumn vegetation growth and POS on the EOS. The results showed that the EOS dates obtained with different smoothing methods were broadly consistent in terms of their spatial patterns and temporal trends. In terms of climate factors, the EOS was driven mainly by preseason precipitation for the majority of vegetation types and advanced with increasing precipitation. For the steppe, both minimum temperature (T_{\min}) and relative humidity (RHU) played the most important roles in regulating the variation of EOS which was delayed with an increase in T_{\min} and reduction in RHU. Furthermore, our study found an earlier POS and vigorous vegetation growth in summer would jointly advance the steppe EOS, but these relationships were the opposite of each other in meadow and forest regions. Interestingly, the EOS of NIM was more related with vegetation growth in the most recent period before the EOS. This study highlights the importance of ecological processes in the preceding growth stage for understanding the dynamics of EOS.

INDEX TERMS End of growing season, northeast Inner Mongolia, climate change, peak of growing season, preceding growth stage of vegetation.

I. INTRODUCTION

Global warming continuously affects the structure and function of terrestrial ecosystems [1], [2]. As a fundamental

The associate editor coordinating the review of this manuscript and approving it for publication was Geng-Ming Jiang¹.

indicator of ecological processes, land surface vegetation exerts a feedback on the climate system by regulating hydrothermal circulation [3] and carbon exchange at the Earth's surface [4], [5]. Phenology, i.e., the events that occur during plant growth and their development rhythm [6], [7], has become the focus of global change studies due it being

an essential element of ecosystem models [8]–[10]. Numerous studies have reported that a delayed end of growing season (EOS) is one of the major determinants of a prolonged growing season in the middle and high latitudes of the Northern Hemisphere [11], [12], which will result in an increase in the carbon storage of terrestrial ecosystems [13]. However, some researchers have reported that a later EOS would also lead to the loss of carbon by ecosystem respiration during autumn warming [14]. This suggests that a thorough monitoring of the EOS could expand our understanding of the terrestrial ecosystem carbon cycle.

The Normalized Difference Vegetation Index (NDVI), which is derived from satellite remote sensing, has been widely applied in the estimation of land surface phenology in recent years [15]–[17]. Various methods have been developed to extract the EOS from the NDVI [18], which generally involve two main steps: elimination of the noise in NDVI data and identification of the EOS [19], [20]. In the first step, several methods, such as the Savitzky–Golay filter [21], Fourier decomposition [22], and logistic function [23], have been adopted to eliminate the noise in NDVI data, which is due to contamination by cloud cover, seasonal snow, and atmospheric variability. In the next step, the predetermined thresholds and the inflection point methods are frequently used to identify the EOS on the NDVI curve [6], [24]. Previous studies have concluded that the EOS identification method has a substantial impact on the spatiotemporal pattern of the EOS [19], [25]. However, the impact of noise smoothing methods on the magnitude and trend of the EOS remain uncertain. Although some studies have revealed distinctions among the available smoothing methods [26], [27], they were mainly based on the use of one-year data to assess the performance of smoothing methods at test points. Only a few of them have quantitatively characterized the influence of various filters on the interannual changes of the EOS [27].

Most studies have attempted to explain the changes in EOS through daily mean temperature and precipitation [20], [28]. However, the temperature has experienced faster warming during the nighttime than daytime over the past five decades [29], which has an asymmetric effect on phenological parameters [30]. In addition, some studies have found that an increase in T_{\max} has a greater impact on the start of growing season (SOS) than T_{\min} in the Northern Hemisphere, which is mainly caused by the combined effects of sunshine duration and daytime temperature [2]. However, Chew *et al.* [31] proposed that the temperature effects on the flowering time were mediated mainly by sunshine duration during spring and summer days, but the nighttime temperature was found to play a pivotal role in temperature effects as days shorten in autumn in the phenology model. Yang *et al.* [32] revealed the asymmetric responses of the EOS to T_{\min} and T_{\max} in the Tibetan Plateau. However, the contribution of T_{\min} versus T_{\max} on the EOS in temperate ecosystems is not well known and how the temperature and sunshine duration co-determine the EOS also remains

uncertain. Moreover, relative humidity could trigger rainfall regardless of dry or wet soil conditions [33], which will induce the stomatal opening of plants and improve photosynthetic efficiency [34]. Therefore, it should be included in assessments to determine if humidity triggers the EOS. As the main part of the growing season, the variation of the summer vegetation growth has a residual effect on the EOS [35], [36]. Previous studies have quantified the summer vegetation growth as the average NDVI of summer and found that the summer vegetation growth increases the cost of soil water overconsumption which then advances the EOS in the Tibetan Plateau [35]. In contrast, the summer vegetation growth could delay the EOS in the Yellow River Basin, because the increasing precipitation induced by vegetation activity is sufficient to offset enhanced evapotranspiration [36]. These conflicting results imply the complex responses of biomes under different climate conditions, and none of these studies quantified the relative importance of the vegetation growth in each preceding month in determining the EOS. Furthermore, the peak of growing season (POS) of plant activity, referring to the timing of the highest degree of photosynthetic capacity, directly affects carbon uptake and water consumption [37]. Evidence from several studies has noted that the POS has shifted towards spring throughout the majority of the Northern Hemisphere mid-latitudes [12] and the earlier occurrence of POS results in vigorous vegetation activity through enhanced carbon assimilation early in the growing season [38], [39]. Yet, little is known about the impact of change in the POS on the EOS of different biome types.

Northeast Inner Mongolia (NIM) is located in a climate transitional zone, including a range of terrestrial ecosystems along the moisture gradient from semi-arid steppe and semi-humid forest, and contains a cropland region. This region contains one of the world's four largest natural pastures and the important forest area of the Mongolian Plateau, which extends over the Greater Khingan Mountains, with a low intensity of human disturbance [40]. The extensive diversity of vegetation and highly vulnerable ecosystems in the region, especially their phenological shifts, are very sensitive to global warming [41]. Consequently, it is an ideal region for investigating the response of EOS variations to climate and the preceding growth stage of vegetation. The main objectives of our study were to: (i) assess the influence of different NDVI smoothing methods on interannual changes in the EOS; (ii) investigate how the EOS changed over the NIM from 2001 to 2017; (iii) systematically analyze the effects of multiple pre-season climate factors on the EOS variation; and (iv) explore the impact of the preceding growth stage of vegetation before the EOS on the interannual variation of the EOS, especially for different plant functional types. The results of this study improve our understanding of how the multiple climate factors and the preceding growth stage of vegetation jointly affect the EOS in temperate ecosystems. It would be useful to consider these mechanisms in future carbon cycle models.

II. MATERIALS AND METHODS

A. STUDY AREA

The NIM region extends from approximately $47^{\circ}05' - 53^{\circ}20' \text{ N}$ and $115^{\circ}31' - 126^{\circ}04' \text{ E}$, covering a total area of about $2.53 \times 10^5 \text{ km}^2$. The elevation of NIM ranges from 167 m in the east to 1,675 m in the central mountains. The annual total precipitation varies widely from 195 mm in the west to 510 mm in the east, with most rainfall received in June to August. The vegetation across the NIM exhibits an extensive natural diversity along with precipitation and topography gradients, and can be divided into four major types: steppe, meadow, forest, and cropland (Fig. 1). The steppe mainly occurs in western parts of NIM, with an annual mean temperature range of -3.0° C . Forest is widely distributed in the Greater Khingan Mountains across the central part of the study area, with an annual mean temperature range of -5 to -2° C . The transition zone between steppe and forest mainly contains meadows. Cropland areas are spread across the eastern part of NIM and are scattered among mountains toward the west, with an annual mean temperature range of 0 - 2° C .

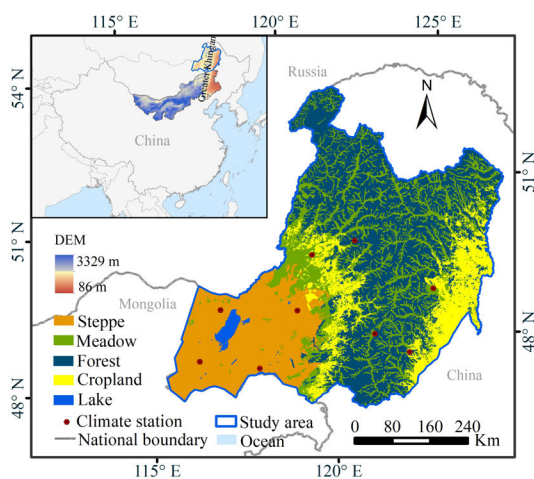


FIGURE 1. Geographic location, distribution of elevation, vegetation types, and meteorological stations of northeast Inner Mongolia (NIM).

B. DATASETS

Moderate-resolution Imaging Spectro-radiometer (MODIS) NDVI datasets spanning the period from 2001–2017 were used to retrieve the land surface phenology metrics across the study area. The 16-day maximum-value composite NDVI data (MOD13Q1) at a spatial resolution of 250 km were pre-processed and released by the Level-1 and Atmosphere Archive and Distribution System (LAADS) of the National Aeronautics and Space Administration (NASA) (<http://ladsweb.nascom.nasa.gov/>). We further processed the NDVI data, i.e., mosaicking image scenes, converting the geographic coordinate system, and clipping by boundaries. Climate records for the period of 2001–2017 were obtained from the China Meteorological Data Service Center of the China Meteorological

Administration (<http://cdc.cma.gov.cn>). The climatic datasets were collected from nine meteorological stations (Fig. 1) and then spatial interpolation data was obtained using the Kriging method [42], including the daily minimum temperature (T_{\min}), daily maximum temperature (T_{\max}), sunshine duration (SSD), relative humidity (RHU), and precipitation. The vegetation types were obtained from a vegetation map of Inner Mongolia, with a scale of 1:1000000. The data was collected in 2000 and was further grouped into steppe, meadow, forest, and cropland. Previous studies have shown that the cropland area has increased substantially in Northeast Inner Mongolia since 2000 [43]. Hence, the range of cropland in this study was updated based on the 2010 MODIS Land Cover Type Product (MCD12C1), and the remaining regions retained their original properties.

C. DETERMINATION OF THE PHENOLOGY PARAMETERS FROM THE NDVI

Original NDVI data is usually affected by residual noise despite being processed by the standard maximum value compositing (MVC) technique [44]. Therefore, we adopted the harmonic analysis of time series (HANTS), asymmetrical Gaussian function (AG), double logistic function model (DL), and Savitzky Golay (SG) filtering methods to smooth the NDVI time-series data before identifying the EOS dates (Table S1). Furthermore, we applied the cumulative NDVI based logistic regression curve method to determine the EOS from smoothed NDVI data (Table S2). This method was developed by Hou *et al.* [45] and is widely used for retrieving phenological phases. First, we calculated the cumulative NDVI based on the smoothed NDVI data and then fitted the cumulative NDVI to interpolate daily NDVI values using the logistic model. Second, we obtained the change rate of fitted logistic NDVI curves. Finally, we specified the EOS as the time when the change in the curvature rate reached its minimum value (Fig. S1b). The summer average NDVI (June, July, and August) and September NDVI represented the preceding growth stage of vegetation and was used to identify the impact on the EOS. In addition, we used the sixth-degree polynomial function [46] to interpolate daily NDVI from the 16-day NDVI, and then the timing of the occurrence of maximum NDVI in summer was defined as the POS date (Fig. S1a).

D. ANALYSES

The Theil-Sen median trend analysis and Mann-Kendall test method [47] were used to assess the spatial characteristics of EOS trends in each pixel. To further investigate the differences in EOS trends among different vegetation types, we calculated the spatial average EOS of each vegetation type to examine the overall trends. In addition, to understand the effects of the potential driving factors on the EOS, Pearson correlation coefficients [55] were calculated and a t-test was performed to assess the relationships between the EOS and both pre-season climate factors and the preceding growth stages of vegetation (June, July, August, and

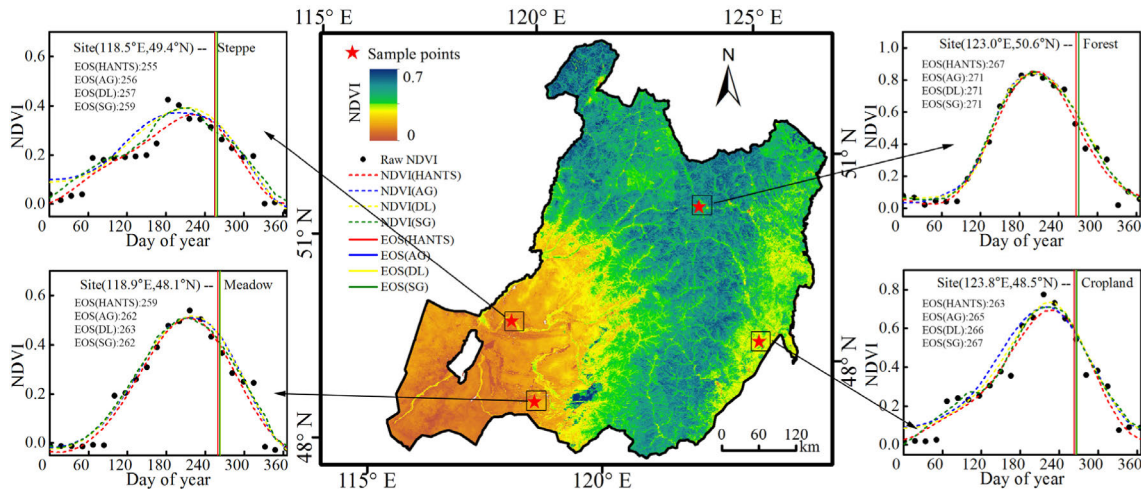


FIGURE 2. The spatial distribution of the multiyear averaged Normalized Difference Vegetation Index (NDVI). The four enlarged panels show the curves smoothed by four different methods (harmonic analysis of time series (HANTS), asymmetric Gaussian (AG) function, double logistic (DL) function, Savitzky-Golay (SG) filter) and the corresponding end of growing season (EOS). The sample pixels are in steppe (top left), meadow (bottom left), forest (top right), and cropland (bottom right).

September NDVI, summer average NDVI and POS). Here, based on the multiyear (2001–2017) spatial average EOS for each vegetation type, we determined that the last day of September could be regarded as the start of the pre-season in the steppe, meadow, and cropland regions, while the last day in mid-October was considered to be the start of the pre-season in the forest area. Furthermore, we used stepped intervals of 10 days to calculate the mean T_{min} for each of 15 periods, with durations ranging from 10–150 days (i.e., 10, 20, 30, . . . , 150) for each pixel. The same procedure was executed for the other climate factors. Hence, the pre-season length of each climate factor was defined as the period which had the largest correlation coefficient for the relationship with the EOS.

III. RESULTS

A. ANALYSIS OF THE DIFFERENT SMOOTHING METHODS TO EXTRACT THE EOS

The performance of four smoothing methods and the corresponding EOS at four sample sites selected from 2006 are displayed in Fig 2, in which each inset represents a vegetation type. It was observed that all denoising methods were effective for smoothing the time series of NDVI data. Comparing four EOS dates obtained using the different smoothing methods, we found that the dates obtained with AG, DL, and SG were extremely similar (within 3 days) for most biomes, and were even in the same day in the forest region. Moreover, the EOS date obtained with HANTS was usually earlier than the date obtained with the other three methods, which was four days earlier in most of the forest area. The spatial distribution of the multiyear average EOS, which was derived from the four filtered NDVI values during the period of 2001–2017 is shown in Fig. 3. The spatial patterns of the four EOS dates were extremely consistent with each other. The earliest EOS dates were located in the southwest and east of the study area, whereas the later EOS dates were mainly

identified in the central mountain region. We calculated the standard deviation (SD) of the EOS obtained with the four smoothing methods (Fig. 3f). Nearly 90% of the total pixels had SDs of less than 4 days, while only 10% of all pixels had SDs of more than 4 days, of which 2% of pixels had SDs of more than 6 days. In contrast, the SDs were smaller in the steppe area than in the other biomes (Fig. S2).

A comparison of the multiyear average EOS for each biome at regional scales (Fig. 4a) revealed a good resemblance among AG, DL and SG method. However, the EOS obtained from the NDVI smoothed by HANTS was approximately 5 days earlier than the value obtained using the other methods for the entire study area and the different vegetation types (Fig. 4a). Fig 4b-f shows the interannual variations of the EOS estimated from the different smoothed NDVI data and their mean values during 2001–2017 for different plant functional types. The curves of interannual changes of the EOS based on the different methods were in good agreement with each other (Fig. 4b) and the slope values were almost the same across the whole study area (Table S3). Consistent results were obtained for all vegetation types (Fig. 4c-f). Overall, the EOS results obtained using the different methods displayed similar characteristics, and therefore, we used the average value of the four EOS dates in the following analysis.

B. SPATIAL DIFFERENCES AND TEMPORAL TRENDS

The spatial distribution of multiyear average EOS is shown in Fig. 3e. The EOS was in the range of days 240–300 (late August to late October). The earlier EOS dates, ranging from days 240 to 270, were mainly located in the southwestern and eastern parts of NIM. The central and northern regions had EOS dates ranging from days 270–300. In addition, we found that the spatial average EOS date in NIM was around day 271 ± 7 (late September) (Fig. 4a). In terms of plant functional types, the earliest EOS dates were observed in steppe

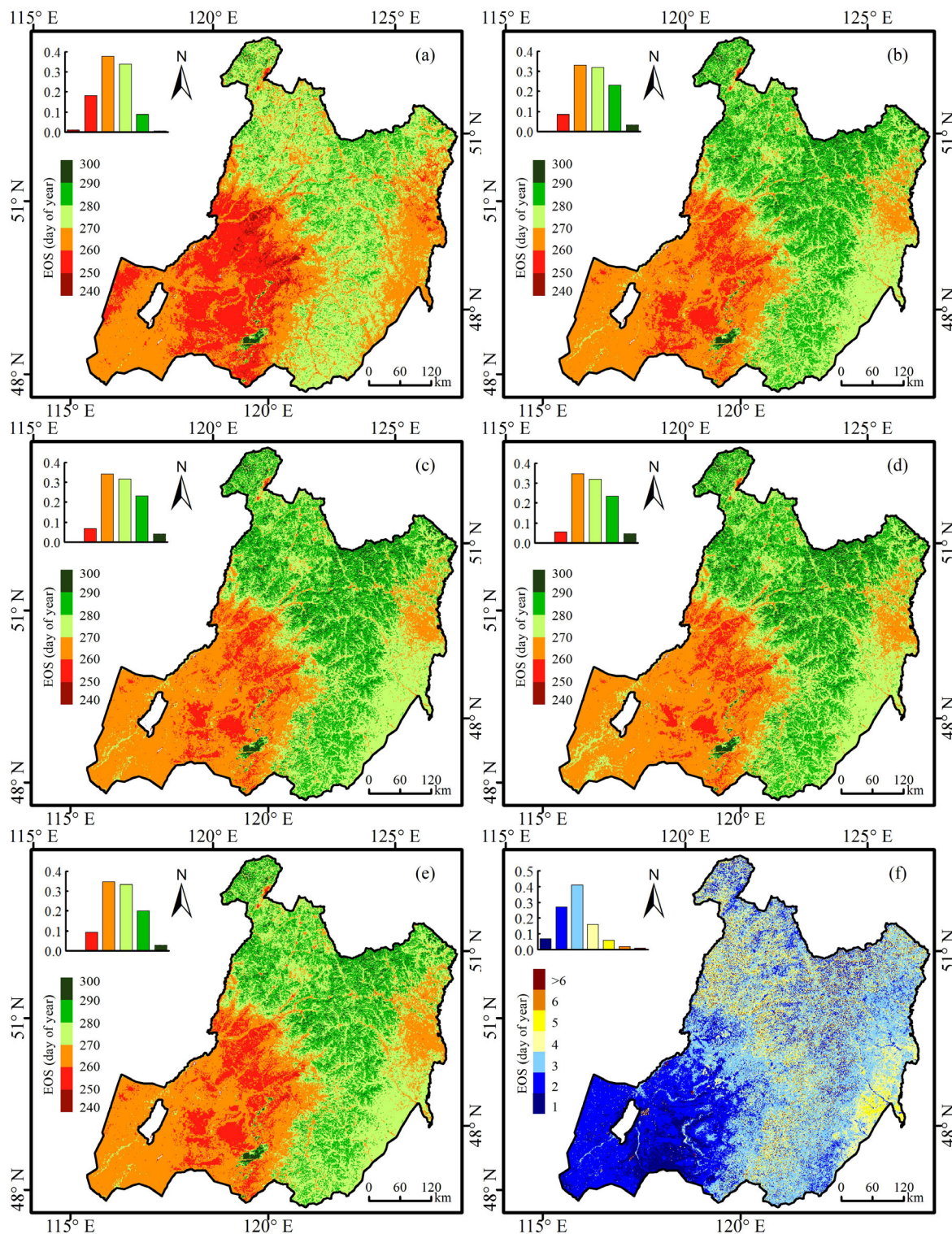


FIGURE 3. The spatial pattern of EOS in the study area obtained with the four smoothing methods and their average EOS: HANTS (a), AG function (b), DL (c), SG filter (d), mean (e), and its standard deviation (f) for the four EOS dates. The top left inset shows the percentage of each interval in which the value was indicated by the map legend.

(day 262 ± 14) and cropland (day 266 ± 10), while later EOS dates were found in meadows (day 273 ± 9) and forest (day 278 ± 6). Fig 4b-f shows the interannual changes of EOS

during the period of 2001–2017, and clearly shows discrepancies in the EOS trends for different biomes. At the regional level, the EOS across the NIM displayed no significant

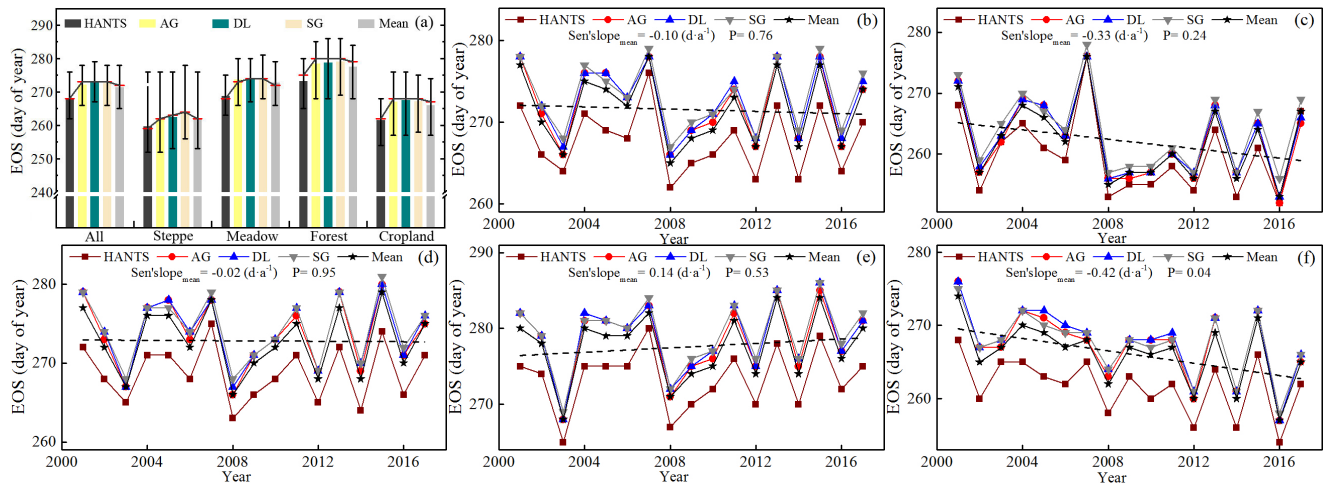


FIGURE 4. Average dates and standard deviation of EOS for the four smoothing methods and their mean (a). The interannual variations of EOS using the four smoothing methods (HANTS, AG, DL and SG) and mean EOS from 2001–2017 for entire study area (b), steppe (c), meadow (d), forest (e), and cropland (f).

advancing trend, with a rate of $0.1 \text{ d}\cdot\text{a}^{-1}$ ($P = 0.76$) (Fig. 4b). The EOS of steppe and cropland experienced advancing trends at rates of $0.33 \text{ d}\cdot\text{a}^{-1}$ ($P = 0.24$) and $0.42 \text{ d}\cdot\text{a}^{-1}$ ($P = 0.04$), respectively (Fig. 4c and f). The EOS of forest biome was delayed by $0.14 \text{ d}\cdot\text{a}^{-1}$ (Fig. 4e), but the delaying trend was not significant ($P = 0.53$). For the meadow ecosystem, there was no obvious trend (Sen's slope = -0.02 $P = 0.95$) in the EOS (Fig. 4d). We mapped the spatial distributions of EOS trends for the study period (Fig. 5). Over the study area, an advance of the EOS was observed across more than 63.7% of the total pixels, although it was significant in only 5.42% of the pixels, and the advance was more pronounced in the east of the Greater Khingan Mountains and western steppe area of NIM. In contrast, a delay in the EOS was observed in 36.3% of all pixels (significant in 3.86% of pixels), which were generally concentrated in the northern Greater Khingan Mountains.

C. RESPONSES OF THE EOS TO POTENTIAL DRIVING FACTORS

1) RESPONSES OF THE EOS TO MULTIPLE CLIMATE FACTORS

At the regional scale, both T_{\min} ($R = 0.27$, $p > 0.05$) and T_{\max} ($R = 0.41$, $P > 0.05$) exhibited a positive influence on the EOS of the NIM, which occurred approximately at pre-season day 80 (Fig. S3). In addition, the correlation between SSD and EOS was in general similar to the corresponding correlations found for T_{\min} and T_{\max} (Fig. S3), implying that a longer SSD was conducive to vegetation growth in autumn. However, the pre-season length of SSD which had the strongest effect on the EOS was generally longer than the pre-season length of T_{\min} and T_{\max} . In contrast, negative relationships between the EOS and both RHU ($R = -0.46$) and precipitation ($R = -0.62$) were observed (Fig. S3). These results implied that the EOS of NIM advanced under increased

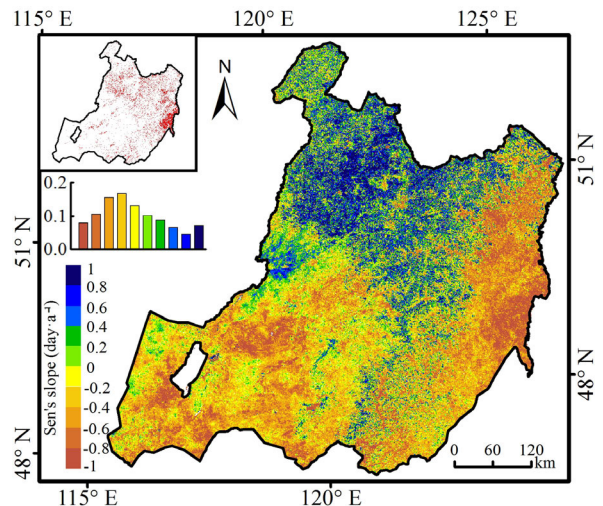


FIGURE 5. The trend of multimethod averaged EOS in NIM during 2001–2017 (the top left (upper) inset shows the pixels significant at $p < 0.05$, the top left (lower) inset shows the percentage of each interval that is indicated on the map).

RHU and precipitation. The strongest impacts of RHU and precipitation on the EOS mainly occurred in the short-term, within 10 days of the pre-season. Biome-specific correlations between the EOS and pre-season climate factors are presented in Fig. 6. It can be clearly seen that the relationship between the EOS and T_{\min} varied substantially among the plant functional types. The EOS of steppe ($R = 0.46$, $P > 0.05$) and meadow ($R = 0.26$, $P > 0.05$) were positively correlated with T_{\min} . In contrast, a negative correlation was found in forest ($R = -0.38$, $P > 0.05$) and cropland ($R = -0.44$, $P > 0.05$) regions. In general, the EOS for steppe and meadow would be delayed with a T_{\min} increase, but it would advance with a T_{\min} increase in the forest and cropland biomes. It was apparent that T_{\max} had a positive impact in most subregions,

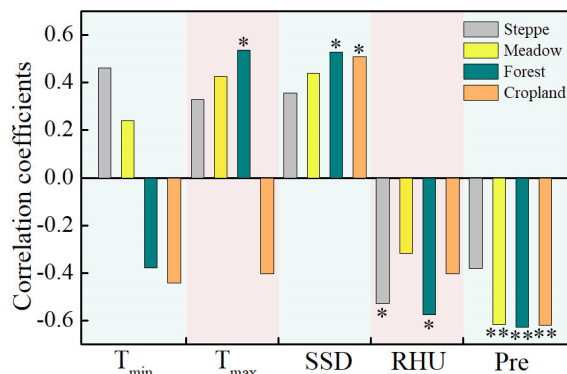


FIGURE 6. Correlation coefficients between the annual changes of the EOS with minimum temperature (T_{min}), maximum temperature (T_{max}), sunshine duration (SSD), relative humidity (RHU), and precipitation in NIM from 2001 to 2017. * and ** indicate significance at $p < 0.05$ and $p < 0.01$, respectively.

except for the cropland ($R = -0.41, P > 0.05$) area. The forest EOS was significantly related to T_{max} ($R = 0.54, P < 0.05$). This indicates that a rising T_{max} was beneficial to vegetation growth for most vegetation types, especially in the forest region, but it restricted the growth of cropland in autumn. Furthermore, the EOS of all biomes were positively correlated with SSD, particularly for the forest ($R = 0.53, P < 0.05$) and cropland ($R = 0.51, P < 0.05$) areas. However, the EOS dates in all subregions were negatively correlated with RHU and precipitation.

To determine the effects of climate factors on the EOS at the pixel scale, the correlation coefficients between the EOS and pre-season climate factors were calculated (Fig. 7a-f). Across the study area, the EOS was positively correlated with T_{min} in 48.59% of the pixels in the total area (significant in 11.96% of pixels), and there was a negative correlation in 51.41% of pixels (significant in 12.91% of pixels). The EOS was positively correlated with T_{max} in most pixels (74.17%), with the correlation being significant for 21.66% of total pixels (Fig. 7f). In most pixels (74.08%) there was a positive correlation between SSD and the EOS throughout the NIM, with 24.78% being significant. In the remaining pixels, which represented 25.92% of the total areas, there was a negative correlation (Fig. 7f). Compared with the SSD, the opposite pattern was observed in the relationship between the EOS and both RHU and precipitation. Specifically, the EOS across NIM was negatively correlated with RHU and precipitation in 82.77% and 84.03% of all pixels, of which 31.52% and 40.21% were significant at the 0.05 level, respectively (Fig. 7f). Additionally, the EOS of NIM was most closely associated with T_{min} and T_{max} during the period of days 10–110, and the mid-value occurred at days 60 and 80, respectively (Fig. S4). In contrast, the pre-season durations of SSD, RHU, and precipitation were concentrated over shorter time scales, with the mid-values mostly occurring at about day 30 (Fig. S4). In line with the across-biome results reported above, more than 70% of pixels had a positive correlation between the EOS and T_{max} for each biome, except cropland (Fig. 7b-f). The relationship between the EOS of

cropland and T_{max} was ambiguous, with positive and negative correlations in 44.96% and 55.04% of all pixels, respectively. There was a positive correlation between SSD and the EOS in more than 63% of each biome, and around 30% of these positive correlations were significant at the 0.05 level, except for the steppe (significant in 7.35%) and meadow (significant in 16.25%) regions (Fig. 7f). Consistent results were also found for RHU and precipitation, with a negative correlation between the EOS with RHU and precipitation observed at more than 68% of pixels for each vegetation type, and most were significant in more than 20% of pixels (Fig. 7f). Compared with the factors mentioned above, there were large differences in the effects of T_{min} on the EOS among the different vegetation types. For steppe, more than 86% of the pixels had a positive correlation, and about 30% of the pixels were significant at the 0.05 level (Fig. 7f). With regard to forest and cropland areas, negative correlations between the EOS and T_{min} were observed in 63.81% (forest) and 75.31% (cropland) of pixels (Fig. 7f). The meadow EOS was positively correlated with T_{min} in 48.97% of pixels and negatively correlated with T_{min} in 51.03% of pixels, although the correlation was not significant in most pixels (Fig. 7f). Overall, the EOS of NIM was most strongly related to precipitation (Fig. 7a, Fig. S5), with an average correlation coefficient of -0.33 , suggesting that the precipitation was the dominant climate factor controlling the variation of EOS. Consistent results were also found for meadow, forest, and cropland, with average correlation coefficients of $-0.36, -0.44$ and -0.33 , respectively (Fig. 7c-e, Fig. S5). For steppe, both T_{min} and RHU were the driving climate factors that best explained the trend of EOS, with average correlation coefficients of 0.33 and -0.33 , respectively (Fig. 7b, Fig. S5). Although the other climatic variables were selected in relatively few pixels, their influences on the EOS could not be ignored.

2) RESPONSES OF THE EOS TO VEGETATION GROWTH AND THE POS

The spatial patterns of correlation between the EOS and both summer average NDVI and POS are shown in Fig. 8. We found that a positive correlation between the EOS and summer average NDVI was distributed in the northern and northeastern parts of NIM (52.17% of total pixels), while a negative correlation was identified in 47.83% of pixels (Fig. 8a). The spatial distribution of the relationship between the EOS and POS had the opposite sign to the relationship between summer average NDVI and EOS in most pixels (Fig. 8b). The EOS was negatively correlated with the POS in 51.53% of pixels and positively correlated with the POS in 48.47% of pixels in the NIM.

For steppe and cropland regions, the EOS was mainly negatively correlated with summer average NDVI in 77.03% and 63.47% of their total areas, with average correlation coefficients of -0.15 and -0.11 , respectively (Fig. 8c, d). In contrast, the EOS was positively correlated with the POS in 78.39% and 65.46% of pixels, with average correlation

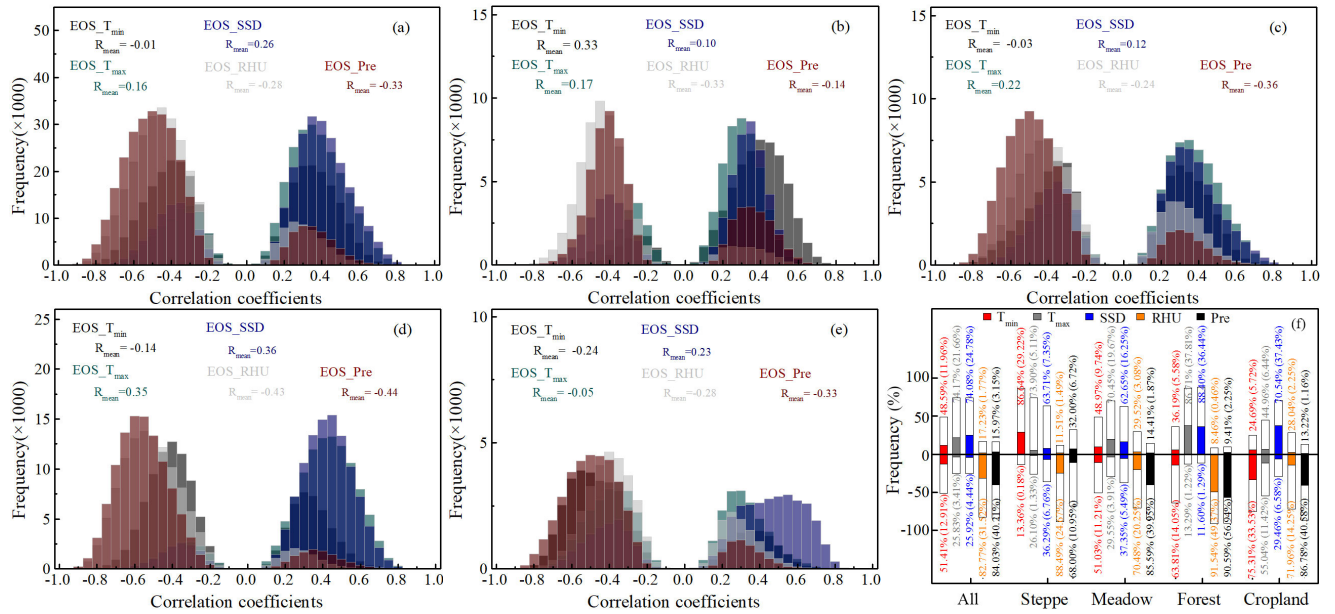


FIGURE 7. The frequency distribution of correlation coefficients between the EOS and climate factors: entire study area (a), steppe (b), meadow (c), forest (d), and cropland (e), and the percentages of correlation coefficients (f: bars above zero line represent percentage of positive correlations, and the underneath show negative percentages, colored sections show the percentage of significant correlations at $p < 0.05$).

coefficients of 0.18 and 0.13, respectively. This suggests that the EOS of steppe and cropland would advance with an increase in the summer average NDVI and an advance in the POS in most pixels. However, the summer average NDVI had a positive (67.00% of pixels) impact on the forest EOS, with an average correlation coefficient of 0.13, and the POS had a negative (64.75% of pixels) impact on the forest EOS, with an average correlation coefficient of -0.12 (Fig. 8c, d). This indicated that the forest EOS would be delayed with the growth of vegetation in summer and an advanced POS. In addition, the response of meadow EOS on the summer average NDVI and POS were ambiguous (Fig. 8c, d), with a positive/negative correlation of the EOS with summer average NDVI of 58.39% / 41.61%, respectively. The meadow EOS was positively correlated with the POS in 40.58% of pixels and negatively correlated in 59.42% of pixels. Furthermore, we obtained the relationship between the EOS and NDVI for each summer month and September. For the entire study area, we found that the EOS was negatively correlated with the NDVI in June and July, while it was positively correlated with the NDVI in August and September (Fig. S6a). A similar pattern was observed in steppe and cropland regions (Fig. S6b, e). This implied that the vegetation activity in early summer would restrict the growth of autumn vegetation, while vegetation activity in late summer and early autumn would delay the vegetation degradation. For the meadow and forest areas, the NDVI had a positive effect on the EOS in all months, especially in August and September (Fig. S6c, d), indicating that the NDVI in all periods prior to leaf senescence was sufficient to promote vegetation growth in autumn and delay the EOS.

IV. DISCUSSION

A. RESPONSES OF DIFFERENT SMOOTHING METHODS ON THE EXTRACTION OF THE EOS

Numerous studies have concluded that all smoothing methods can effectively remove the residual noise in the NDVI [18], but the different methods produce differences in the description of overall trend of vegetation dynamics [48] and in the retention of details of seasonality signals [49]. In this study, we adopted the four frequently-used methods (HANTS, AG, DL, and SG) to smooth the time series of NDVI data and then extracted the EOS in NIM during the period of 2001–2017. The results of the comparison showed that the spatial distributions of the EOS retrieved from the different smoothing methods displayed similar patterns and the SDs were mainly within 6 days (Fig. 3f). This was inconsistent with previous studies in which large disparities (range of days 20–50) were reported in the SOS and length of growing season (LOS) and that the SG filter was more reliable than the AG and DL for temperate grassland [27]. Several researchers have reported that the effects of smoothing methods on the estimation of land surface phenology vary greatly for different levels of vegetation coverage [24], [26]. In contrast, our study found that the EOS dates using different smoothing methods were similar at sample sites with different vegetation types (Fig. 2). The average SDs were relatively smaller in steppe (2 days) than the other biomes (4 days) at the pixel scale (Fig. S2). The differences in errors among the vegetation types may be caused by the signal to noise ratio of the NDVI time series, which is proportional to the confidence level for clear sky labeling [50]. Furthermore, Cong *et al.* [28] considered that the interannual changes of the EOS were mainly

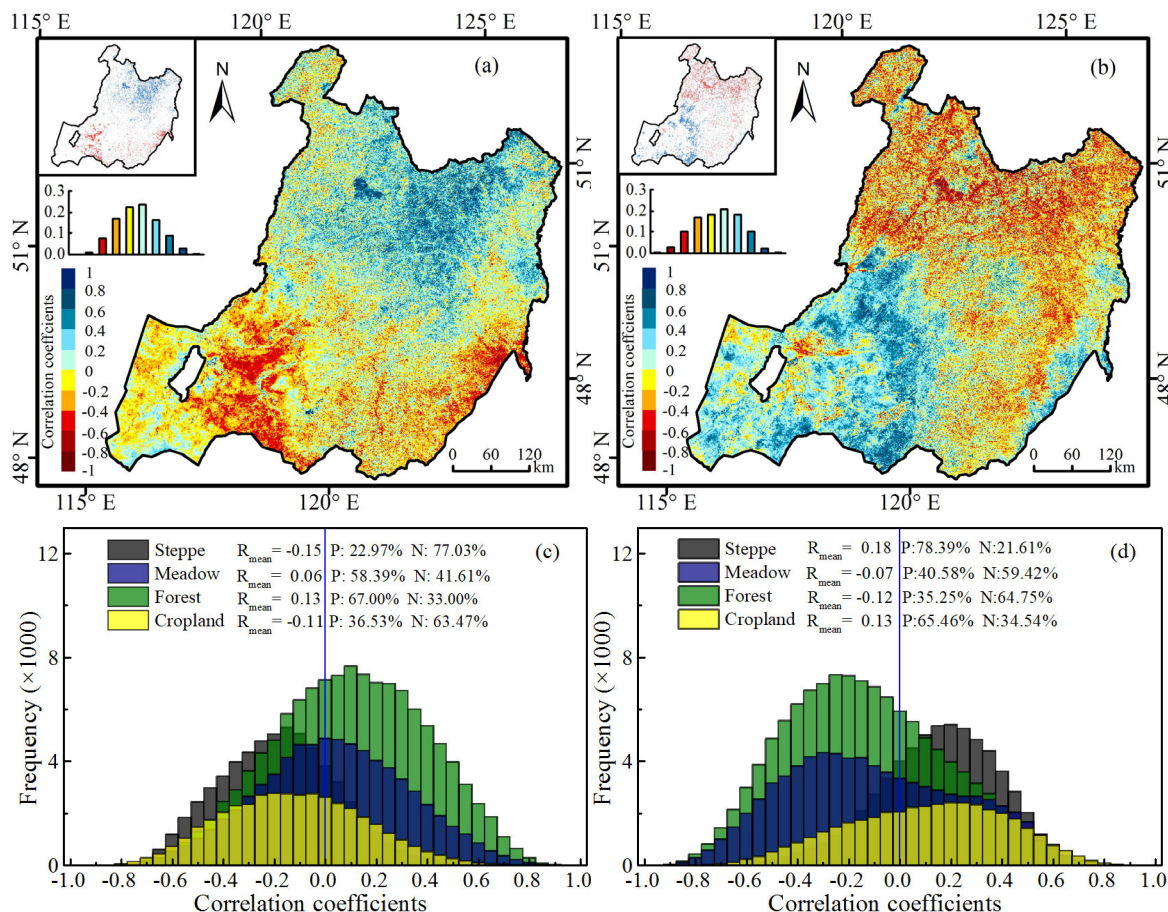


FIGURE 8. Spatial pattern of the correlation coefficients of the EOS to summer NDVI (a), and peak of growing season (POS) (b), (The red (negative) and blue (positive) pixels in the top-left (upper) inset indicate significance at $p < 0.05$; the top left inset (lower) shows the percentage of each interval that is indicated on the map legend). The frequency distribution of the correlation coefficients between the EOS and summer average NDVI (c) and POS (d) for different vegetation types, (P and N represent the positive and negative correlations, respectively).

dependent on the smoothing method rather than the identification method, and found an obvious distinction between the Tibetan Plateau EOS trends based on the cubic spline and HANTS functions. Liu and Zhan [51] also found that the DL function was better than the SG filter for describing the overall trend of the SOS. However, our results showed that the interannual variations of the EOS using various filter were in good agreement with each other for all biomes (Fig. 4), indicating that the use of different smoothing methods had little impact on the EOS trend in NIM. The inconsistency in the results of the different studies may be attributed to the differences in the methodology of phenology extraction [19], land surface conditions [28], and data resolution [52], [53].

B. SPATIAL DIFFERENCES AND TEMPORAL TRENDS

Our results showed that the EOS ranged between days 240 and 300 (Fig. 3e), which was in agreement with previous studies that found the EOS mainly occurred in late-August to mid-October in the Mongolian Plateau [16] and temperate China [19], including NIM. Despite there being no clear patterns along the latitudinal or longitudinal gradients,

the EOS of NIM displayed a spatial heterogeneity among the different vegetation types, with the forest EOS always being later than in steppe and meadow regions. This discrepancy may be attributed to plant functional types [54]. For example, the forest vegetation was more cold-resistant than the grassland as the temperature fell in autumn, therefore, leaf senescence occurred later in forest than in steppe and meadow areas [15].

In addition, this study identified a slight but non-significant advancing trend in the EOS of NIM during the past 17 years (Fig. 4). The absence of an EOS tendency was mainly due to the offsetting effect caused by spatial variations [28], [35]. Our study observed that the forest EOS was delayed with a rate of $0.14 \text{ d}\cdot\text{a}^{-1}$. The delaying trend was consistent with previous results reported in forests in the eastern United States and semi-arid mountains of China, but its magnitude was different between arid and humid areas [56]–[58]. In contrast, the EOS of steppe displayed an advanced trend at a rate of $0.33 \text{ d}\cdot\text{a}^{-1}$, and the meadow EOS had a slightly earlier trend ($0.02 \text{ d}\cdot\text{a}^{-1}$). This advancing trend of grassland was consistent with previous studies. For example, Bao *et al.* [16]

investigated the EOS of the Mongolian Plateau over a long observation period and found an earlier trend in grassland areas. Liu *et al.* [19] studied the variation of the EOS from 1982–2011 in temperate China and observed an advancing trend ($0.02 \pm 0.01 \text{ d}\cdot\text{a}^{-1}$) in grassland areas of Inner Mongolia. However, a delaying trend of the EOS was reported in some other studies. Gong *et al.* [59] found that the EOS over the entire Inner Mongolia grassland during 2002–2014 was delayed at a rate of $0.51 \text{ d}\cdot\text{a}^{-1}$. Yang *et al.* [60] found that the EOS of temperate grassland in China was delayed by $0.08 \text{ d}\cdot\text{a}^{-1}$ during 1982–2010. The different rates of change and diverse EOS trends in grassland might be due to the different types of grassland, target periods, data resolution, and extraction methods.

C. RESPONSES OF THE EOS TO POTENTIAL DRIVING FACTORS

Previous studies have reported differential warming in recent decades in terms of T_{\min} and T_{\max} , which had asymmetric effects on the land surface phenology [2], [15], [30]. However, we found an equal effect of T_{\min} and T_{\max} on the EOS for steppe and meadow areas, with an increase in both T_{\min} and T_{\max} delaying the EOS (Fig. 6). These positive correlations may be partly due to the fact that a higher T_{\min} could eliminate the risk of frost damage in autumn and slow the degradation of chlorophyll in plants [32]. An increase in T_{\max} could enhance vegetation photosynthesis with the decline in temperature in autumn and postpone the EOS date [28], [61]. Although T_{\min} is considered to be strongly related to the frequency of chilling damage in the boreal ecosystem [62], [63], our study identified a negative correlation between T_{\min} and the EOS of the forest and cropland biomes (Fig. 6). An increased nighttime temperature would strengthen leaf respiration, consume large amounts of leaf carbohydrates, and then accelerate the development of autumn leaf coloration [30], [64]. This mechanism could partly explain the negative impact of T_{\min} on the EOS. It should be noted that the cropland EOS was negatively correlated with T_{\max} , which was mainly ascribed to the fact that a higher T_{\max} may lead to decreasing the water content in the soil and restraining the vegetation growth in the irrigated agricultural area [65]. Significantly, there were great uncertainties in the relationship between the cropland EOS and climate factors due to this particular region being extraordinarily vulnerable to human management, such as changes in crop variety, irrigation, and fertilizers [66]. In most boreal and wet temperate regions, the vegetation growth was more sensitive to the photoperiod due to the seasonal temperature varying strongly [67]. Our results showed that the SSD had a positive effect on EOS for all biomes (Fig. 6). This was mainly because a longer SSD would stimulate the photosynthesis capacity of plants and thereby slow the speed of vegetation degradation [35], [68]. Additionally, we found that the EOS was negatively correlated with both RHU and precipitation for all biomes. This phenomenon may be explained by the fact that increasing precipitation was associated with lower radiation [15], and

a higher RHU could result in a higher risk of freezing injury with the drop in autumn temperature in colder areas, subsequently promoting leaf senescence in autumn [60], [69].

Plants of each life-cycle rely heavily on their previous growth stage [37], [70]. For the steppe, we found that summer vegetation growth had a negative effect on the EOS (Fig. 8c), which was in accordance with the previous study in the alpine vegetation of the Tibetan Plateau [35]. This may be caused by the vigorous vegetation growth in summer being accompanied by the over consumption of soil water, thus, resulting in an earlier EOS for water-limited ecosystem [71]. The steppe vegetation grew fastest in June and needed more water at this time [72], and therefore the EOS of steppe was most strongly related to the NDVI in June (Fig. S6b). Interestingly, the forest EOS was positively correlated with the NDVI in months prior to the EOS and most strongly related to September NDVI (Fig. S6d). This suggests that vegetation growth in all periods prior to leaf senescence would delay the EOS, especially in the autumn. Compared with herbaceous plants, woody plants with developed roots are habituated to uptake deeper soil water [20], resulting in less dependence on land surface water variability. Additionally, woody plants are likely to be more drought resistant than herbaceous plants due to their ability to store water [20]. Additionally, strong pre-season vegetation activity indicates an improvement in carbon sequestration [13]. As a result, vegetation growth in the preceding stage would slow the rate of leaf senescence and postpone the forest EOS. Furthermore, with the decline in autumn temperature, the stronger photosynthetic capacity of vegetation would have a heat preservation function, keeping the land surface temperature relatively stable in autumn [73]. This phenomenon could explain the strongest impact of NDVI on the forest EOS being strongest in September. Cong *et al.* [28] demonstrated that plants with a shorter growing season have lower plasticity in regulating the length of growing season and have a more conservative strategy. Thus, an earlier or later peak season activity is accompanied by advanced or delayed degradation of vegetation with a shorter length of growing season [74]. These results may help to explain the positive correlation between the POS and EOS in steppe and cropland areas (Fig. 8d). Nevertheless, there were negative effects of the POS on forest and meadow EOS, which could be attributed to several factors. First, the forest and meadow plants with a longer growing season had a higher plasticity in adjusting their life-cycle stage and were more sensitive to pre-season climate factors [75]. Furthermore, the earlier POS enabled the vegetation to assimilate more carbon [76] and accelerated vegetation photosynthesis in autumn [12].

V. CONCLUSION

The reliable detection and attribution of variations in the EOS are the prerequisites for simulating ecosystem carbon cycle processes under climate change. This study provided an important comparative analysis of the effect of four smoothing methods on the extraction of the EOS for different plant

functional types. Overall, there was a fairly good agreement among the EOS dates obtained with the four smoothing methods in terms of their representation of spatial patterns and interannual variations. Furthermore, we found advancing trends of EOS in the grassland and cropland regions, and an extensive delayed trend in the forest region during the period of 2001–2017. Our study also revealed that T_{\min} , T_{\max} , and SSD exerted positive effects on the EOS trends across the NIM, while an increase in RHU and precipitation would lead to an earlier EOS. We further investigated the relationship between EOS and both vegetation growth in the period before the EOS and POS, and found a heterogeneous spatial pattern. Summer vegetation growth generally advanced the steppe EOS, while delayed the EOS of meadow and forest regions. In addition, an earlier POS would advance the EOS of steppe, but the relationship was the opposite in meadow and forest areas. These observations indicated that climate factors and the preceding growth stage of vegetation jointly determined the variation of EOS in the NIM. Future studies are needed to investigate the potential interactions between the environmental controlling factors and to develop a full understanding of the mechanisms influencing the autumn phenology.

REFERENCES

- [1] A. D. Richardson, D. Y. Hollinger, D. B. Dail, J. T. Lee, J. W. Munger, and J. O'Keefe, "Influence of spring phenology on seasonal and annual carbon balance in two contrasting new england forests," *Tree Physiol.*, vol. 29, no. 3, pp. 321–331, Jan. 2009, doi: [10.1093/treephys/tpn040](https://doi.org/10.1093/treephys/tpn040).
- [2] S. Piao, J. Tan, A. Chen, Y. H. Fu, P. Ciais, Q. Liu, I. A. Janssens, S. Vicca, Z. Zeng, S.-J. Jeong, Y. Li, R. B. Myneni, S. Peng, M. Shen, and J. Peñuelas, "Leaf onset in the northern hemisphere triggered by daytime temperature," *Nature Commun.*, vol. 6, no. 1, p. 1, Nov. 2015, doi: [10.1038/ncomms7911](https://doi.org/10.1038/ncomms7911).
- [3] S.-J. Jeong, C.-H. Ho, and J.-H. Jeong, "Increase in vegetation greenness and decrease in springtime warming over East Asia: Vegetation weaken regional warming," *Geophys. Res. Lett.*, vol. 36, no. 2, pp. 1–5, Jan. 2009, doi: [10.1029/2008GL036583](https://doi.org/10.1029/2008GL036583).
- [4] R. John, J. Chen, Y. Kim, Z.-T. Ou-yang, J. Xiao, H. Park, C. Shao, Y. Zhang, A. Amarjargal, O. Batkshig, and J. Qi, "Differentiating anthropogenic modification and precipitation-driven change on vegetation productivity on the mongolian plateau," *Landscape Ecol.*, vol. 31, no. 3, pp. 547–566, Mar. 2016, doi: [10.1007/s10980-015-0261-x](https://doi.org/10.1007/s10980-015-0261-x).
- [5] Q. Du, H. Liu, Y. Li, L. Xu, and S. Diloksumpun, "The effect of phenology on the carbon exchange process in grassland and maize cropland ecosystems across a semiarid area of China," *Sci. Total Environ.*, vol. 695, Dec. 2019, Art. no. 133868, doi: [10.1016/j.scitotenv.2019.133868](https://doi.org/10.1016/j.scitotenv.2019.133868).
- [6] R. B. Myneni, C. D. Keeling, C. J. Tucker, G. Asrar, and R. R. Nemani, "Increased plant growth in the northern high latitudes from 1981 to 1991," *Nature*, vol. 386, no. 6626, pp. 698–702, Apr. 1997, doi: [10.1038/386698a0](https://doi.org/10.1038/386698a0).
- [7] J. T. Morissette, A. D. Richardson, A. K. Knapp, J. I. Fisher, E. A. Graham, J. Abatzoglou, B. E. Wilson, D. D. Breshears, G. M. Henebry, J. M. Hanes, and L. Liang, "Tracking the rhythm of the seasons in the face of global change: Phenological research in the 21st century," *Frontiers Ecol. Environ.*, vol. 7, no. 5, pp. 253–260, Jun. 2009, doi: [10.1890/070217](https://doi.org/10.1890/070217).
- [8] C. J. Tucker, D. A. Slayback, J. E. Pinzon, S. O. Los, R. B. Myneni, and M. G. Taylor, "Higher northern latitude normalized difference vegetation index and growing season trends from 1982 to 1999," *Int. J. Biometeorol.*, vol. 45, no. 4, pp. 184–190, Nov. 2001, doi: [10.1007/s00484-001-0109-8](https://doi.org/10.1007/s00484-001-0109-8).
- [9] A. Gonsamo, J. M. Chen, D. T. Price, W. A. Kurz, and C. Wu, "Land surface phenology from optical satellite measurement and CO₂ eddy covariance technique: Land surface phenology index," *J. Geophys. Res., Biogeosci.*, vol. 117, no. G3, pp. 1–18, Sep. 2012, doi: [10.1029/2012JG002070](https://doi.org/10.1029/2012JG002070).
- [10] S. Piao, Q. Liu, A. Chen, I. A. Janssens, Y. Fu, J. Dai, L. Liu, X. Lian, M. Shen, and X. Zhu, "Plant phenology and global climate change: Current progresses and challenges," *Global Change Biol.*, vol. 25, no. 6, pp. 1922–1940, Jun. 2019, doi: [10.1111/gcb.14619](https://doi.org/10.1111/gcb.14619).
- [11] A. Menzel et al., "European phenological response to climate change matches the warming pattern," *Global Change Biol.*, vol. 12, no. 10, pp. 1969–1976, Oct. 2006, doi: [10.1111/j.1365-2486.2006.01193.x](https://doi.org/10.1111/j.1365-2486.2006.01193.x).
- [12] C. Xu, H. Liu, A. P. Williams, Y. Yin, and X. Wu, "Trends toward an earlier peak of the growing season in northern hemisphere mid-latitudes," *Global Change Biol.*, vol. 22, no. 8, pp. 2852–2860, Aug. 2016, doi: [10.1111/gcb.13224](https://doi.org/10.1111/gcb.13224).
- [13] J. Tao, J. Dong, Y. Zhang, X. Yu, G. Zhang, N. Cong, J. Zhu, and X. Zhang, "Elevation-dependent effects of growing season length on carbon sequestration in xizang plateau grassland," *Ecolog. Indicators*, vol. 110, Mar. 2020, Art. no. 105880, doi: [10.1016/j.ecolind.2019.105880](https://doi.org/10.1016/j.ecolind.2019.105880).
- [14] S. Piao, P. Ciais, P. Friedlingstein, P. Peylin, M. Reichstein, S. Luysaert, H. Margolis, J. Fang, A. Barr, A. Chen, A. Grelle, D. Y. Hollinger, T. Laurila, A. Lindroth, A. D. Richardson, and T. Vesala, "Net carbon dioxide losses of northern ecosystems in response to autumn warming," *Nature*, vol. 451, no. 7174, pp. 49–52, Jan. 2008, doi: [10.1038/nature06444](https://doi.org/10.1038/nature06444).
- [15] C. Wu, X. Wang, H. Wang, P. Ciais, J. Peñuelas, R. B. Myneni, A. R. Desai, C. M. Gough, A. Gonsamo, A. T. Black, R. S. Jassal, W. Ju, W. Yuan, Y. Fu, M. Shen, S. Li, R. Liu, J. M. Chen, and Q. Ge, "Contrasting responses of autumn-leaf senescence to daytime and night-time warming," *Nature Climate Change*, vol. 8, no. 12, pp. 1092–1096, Dec. 2018, doi: [10.1038/s41558-018-0346-z](https://doi.org/10.1038/s41558-018-0346-z).
- [16] G. Bao, J. Chen, M. Chopping, Y. Bao, S. Bayarsaikhan, A. Dorjsuren, A. Tuya, B. Jirigala, and Z. Qin, "Dynamics of net primary productivity on the mongolian plateau: Joint regulations of phenology and drought," *Int. J. Appl. Earth Observ. Geoinf.*, vol. 81, pp. 85–97, Sep. 2019, doi: [10.1016/j.jag.2019.05.009](https://doi.org/10.1016/j.jag.2019.05.009).
- [17] Y. Ni, Y. Zhou, and J. Fan, "Characterizing spatiotemporal pattern of vegetation greenness breakpoints on tibetan plateau using GIMMS NDVI3g dataset," *IEEE Access*, vol. 8, pp. 56518–56527, 2020, doi: [10.1109/ACCESS.2020.2982661](https://doi.org/10.1109/ACCESS.2020.2982661).
- [18] J. Zhou, L. Jia, M. Menenti, and B. Gorte, "On the performance of remote sensing time series reconstruction methods—A spatial comparison," *Remote Sens. Environ.*, vol. 187, pp. 367–384, Dec. 2016, doi: [10.1016/j.rse.2016.10.025](https://doi.org/10.1016/j.rse.2016.10.025).
- [19] Q. Liu, Y. H. Fu, Z. Zeng, M. Huang, X. Li, and S. Piao, "Temperature, precipitation, and insolation effects on autumn vegetation phenology in temperate China," *Global Change Biol.*, vol. 22, no. 2, pp. 644–655, Feb. 2016, doi: [10.1111/gcb.13081](https://doi.org/10.1111/gcb.13081).
- [20] J. Peng, C. Wu, X. Zhang, X. Wang, and A. Gonsamo, "Satellite detection of cumulative and lagged effects of drought on autumn leaf senescence over the northern hemisphere," *Global Change Biol.*, vol. 25, no. 6, pp. 2174–2188, Jun. 2019, doi: [10.1111/gcb.14627](https://doi.org/10.1111/gcb.14627).
- [21] J. Chen, P. Jönsson, M. Tamura, Z. Gu, B. Matushita, and L. Eklundh, "A simple method for reconstructing a high-quality NDVI time-series data set based on the Savitzky–Golay filter," *Remote Sens. Environ.*, vol. 91, nos. 3–4, pp. 332–344, Jun. 2004, doi: [10.1016/j.rse.2004.03.014](https://doi.org/10.1016/j.rse.2004.03.014).
- [22] A. Moody and D. M. Johnson, "Land-surface phenologies from AVHRR using the discrete Fourier transform," *Remote Sens. Environ.*, vol. 75, no. 3, pp. 305–323, Mar. 2001, doi: [10.1016/S0034-4257\(00\)00175-9](https://doi.org/10.1016/S0034-4257(00)00175-9).
- [23] X. Zhang, M. A. Friedl, C. B. Schaaf, A. H. Strahler, J. C. Hodges, F. Gao, B. C. Reed, and A. Huete, "Monitoring vegetation phenology using MODIS," *Remote Sens. Environ.*, vol. 84, no. 3, pp. 471–475, Mar. 2003, doi: [10.1016/S0034-4257\(02\)00135-9](https://doi.org/10.1016/S0034-4257(02)00135-9).
- [24] M. A. White, K. M. de Beurs, K. Didan, D. W. Inouye, A. D. Richardson, O. P. Jensen, J. O. H. N. O'Keefe, G. Zhang, R. R. Nemani, W. J. van Leeuwen, and J. F. Brown, "Intercomparison, interpretation, and assessment of spring phenology in North America estimated from remote sensing for 1982–2006," *Global Change Biol.*, vol. 15, no. 10, pp. 2335–2359, Oct. 2009, doi: [10.1111/j.1365-2486.2009.01910.x](https://doi.org/10.1111/j.1365-2486.2009.01910.x).
- [25] N. Cong, S. Piao, A. Chen, X. Wang, X. Lin, S. Chen, S. Han, G. Zhou, and X. Zhang, "Spring vegetation green-up date in China inferred from SPOT NDVI data: A multiple model analysis," *Agric. Forest Meteorol.*, vol. 165, pp. 104–113, Nov. 2012, doi: [10.1016/j.agrformet.2012.06.009](https://doi.org/10.1016/j.agrformet.2012.06.009).
- [26] P. M. Atkinson, C. Jeganathan, J. Dash, and C. Atzberger, "Inter-comparison of four models for smoothing satellite sensor time-series data to estimate vegetation phenology," *Remote Sens. Environ.*, vol. 123, pp. 400–417, Aug. 2012, doi: [10.1016/j.rse.2012.04.001](https://doi.org/10.1016/j.rse.2012.04.001).

- [27] B. Lara and M. Gandini, "Assessing the performance of smoothing functions to estimate land surface phenology on temperate grassland," *Int. J. Remote Sens.*, vol. 37, no. 8, pp. 1801–1813, Apr. 2016, doi: [10.1080/2150704X.2016.1168945](https://doi.org/10.1080/2150704X.2016.1168945).
- [28] N. Cong, M. Shen, and S. Piao, "Spatial variations in responses of vegetation autumn phenology to climate change on the Tibetan Plateau," *JPECOL*, vol. 10, no. 5, p. rtw084, Sep. 2016, doi: [10.1093/jpe/rtw084](https://doi.org/10.1093/jpe/rtw084).
- [29] *Climate Change 2013: The Physical Science Basis. Contribution of Working Group I to the Fifth Assessment Report of the Intergovernmental Panel on Climate Change*, Cambridge Univ. Press, Cambridge, U.K., 2013.
- [30] S. Peng, S. Piao, P. Ciais, R. B. Myneni, A. Chen, F. Chevallier, A. J. Dolman, I. A. Janssens, J. Peñuelas, G. Zhang, S. Vicca, S. Wan, S. Wang, and H. Zeng, "Asymmetric effects of daytime and night-time warming on northern hemisphere vegetation," *Nature*, vol. 501, no. 7465, pp. 88–92, Sep. 2013, doi: [10.1038/nature12434](https://doi.org/10.1038/nature12434).
- [31] Y. H. Chew, A. M. Wilczek, M. Williams, S. M. Welch, J. Schmitt, and K. J. Halliday, "An augmented arabidopsis phenology model reveals seasonal temperature control of flowering time," *New Phytologist*, vol. 194, no. 3, pp. 654–665, May 2012, doi: [10.1111/j.1469-8137.2012.04069.x](https://doi.org/10.1111/j.1469-8137.2012.04069.x).
- [32] Z. Yang, M. Shen, S. Jia, L. Guo, W. Yang, C. Wang, X. Chen, and J. Chen, "Asymmetric responses of the end of growing season to daily maximum and minimum temperatures on the tibetan plateau," *J. Geophys. Res., Atmos.*, vol. 122, no. 24, pp. 13,278–13,287, Dec. 2017, doi: [10.1002/2017JD027318](https://doi.org/10.1002/2017JD027318).
- [33] J. Welty, S. Stillman, X. Zeng, and J. Santanello, "Increased likelihood of appreciable afternoon rainfall over wetter or drier soils dependent upon atmospheric dynamic influence," *Geophys. Res. Lett.*, vol. 47, no. 11, Jun. 2020, Art. no. e2020GL087779, doi: [10.1029/2020GL087779](https://doi.org/10.1029/2020GL087779).
- [34] A. D. Richardson et al., "Terrestrial biosphere models need better representation of vegetation phenology: Results from the North American carbon program site synthesis," *Global Change Biol.*, vol. 18, no. 2, pp. 566–584, Feb. 2012, doi: [10.1111/j.1365-2486.2011.02562.x](https://doi.org/10.1111/j.1365-2486.2011.02562.x).
- [35] P. Li, C. Peng, M. Wang, Y. Luo, M. Li, K. Zhang, D. Zhang, and Q. Zhu, "Dynamics of vegetation autumn phenology and its response to multiple environmental factors from 1982 to 2012 on qinghai-tibetan plateau in China," *Sci. Total Environ.*, vols. 637–638, pp. 855–864, Oct. 2018, doi: [10.1016/j.scitotenv.2018.05.031](https://doi.org/10.1016/j.scitotenv.2018.05.031).
- [36] M. Yuan, L. Zhao, A. Lin, Q. Li, D. She, and S. Qu, "How do climatic and non-climatic factors contribute to the dynamics of vegetation autumn phenology in the yellow river basin, China?" *Ecolog. Indicators*, vol. 112, May 2020, Art. no. 106112, doi: [10.1016/j.ecolind.2020.106112](https://doi.org/10.1016/j.ecolind.2020.106112).
- [37] J. Zu, Y. Zhang, K. Huang, Y. Liu, N. Chen, and N. Cong, "Biological and climate factors co-regulated spatial-temporal dynamics of vegetation autumn phenology on the tibetan plateau," *Int. J. Appl. Earth Observ. Geoinf.*, vol. 69, pp. 198–205, Jul. 2018, doi: [10.1016/j.jag.2018.03.006](https://doi.org/10.1016/j.jag.2018.03.006).
- [38] A. Gonsamo, J. M. Chen, and Y. W. Ooi, "Peak season plant activity shift towards spring is reflected by increasing carbon uptake by extratropical ecosystems," *Global Change Biol.*, vol. 24, no. 5, pp. 2117–2128, May 2018, doi: [10.1111/gcb.14001](https://doi.org/10.1111/gcb.14001).
- [39] T. Park, C. Chen, M. Macias-Fauria, H. Tømmervik, S. Choi, A. Winkler, U. S. Bhatt, D. A. Walker, S. Piao, V. Brovkin, R. R. Nemani, and R. B. Myneni, "Changes in timing of seasonal peak photosynthetic activity in northern ecosystems," *Global Change Biol.*, to be published, doi: [10.1111/gcb.14638](https://doi.org/10.1111/gcb.14638).
- [40] J. Chen, R. John, C. Shao, Y. Fan, Y. Zhang, A. Amarjargal, D. G. Brown, J. Qi, J. Han, R. Laforteza, and G. Dong, "Policy shifts influence the functional changes of the CNH systems on the mongolian plateau," *Environ. Res. Lett.*, vol. 10, no. 8, Aug. 2015, Art. no. 085003, doi: [10.1088/1748-9326/10/8/085003](https://doi.org/10.1088/1748-9326/10/8/085003).
- [41] J. Chen et al., "Prospects for the sustainability of social-ecological systems (SES) on the mongolian plateau: Five critical issues," *Environ. Res. Lett.*, vol. 13, no. 12, Dec. 2018, Art. no. 123004, doi: [10.1088/1748-9326/aaf27b](https://doi.org/10.1088/1748-9326/aaf27b).
- [42] G. Q. Tabios and J. D. Salas, "A comparative analysis of techniques for spatial interpolation of precipitation," *J. Amer. Water Resour. Assoc.*, vol. 21, no. 3, pp. 365–380, Jun. 1985, doi: [10.1111/j.1752-1688.1985.tb00147.x](https://doi.org/10.1111/j.1752-1688.1985.tb00147.x).
- [43] R. John, J. Chen, N. Lu, and B. Wilske, "Land cover/land use change in semi-arid inner mongolia: 1992–2004," *Environ. Res. Lett.*, vol. 4, no. 4, Oct. 2009, Art. no. 045010, doi: [10.1088/1748-9326/4/4/045010](https://doi.org/10.1088/1748-9326/4/4/045010).
- [44] J. Gu, X. Li, C. Huang, and G. S. Okin, "A simplified data assimilation method for reconstructing time-series MODIS NDVI data," *Adv. Space Res.*, vol. 44, no. 4, pp. 501–509, Aug. 2009, doi: [10.1016/j.asr.2009.05.009](https://doi.org/10.1016/j.asr.2009.05.009).
- [45] X. Hou, S. Gao, Z. Niu, and Z. Xu, "Extracting grassland vegetation phenology in north China based on cumulative spot-vegetation NDVI data," *Int. J. Remote Sens.*, vol. 35, no. 9, pp. 3316–3330, May 2014, doi: [10.1080/01431161.2014.903437](https://doi.org/10.1080/01431161.2014.903437).
- [46] S. Piao, A. Mohammad, J. Fang, Q. Cai, and J. Feng, "NDVI-based increase in growth of temperate grasslands and its responses to climate changes in China," *Global Environ. Change*, vol. 16, no. 4, pp. 340–348, Oct. 2006, doi: [10.1016/j.gloenvcha.2006.02.002](https://doi.org/10.1016/j.gloenvcha.2006.02.002).
- [47] P. K. Sen, "Estimates of the regression coefficient based on Kendall's tau," *J. Amer. Stat. Assoc.*, vol. 63, no. 324, pp. 1379–1389, Dec. 1968, doi: [10.1080/01621459.1968.10480934](https://doi.org/10.1080/01621459.1968.10480934).
- [48] X. Wang and C. Wu, "Estimating the peak of growing season (POS) of China's terrestrial ecosystems," *Agricult. Forest Meteorol.*, vol. 278, Nov. 2019, Art. no. 107639, doi: [10.1016/j.agrformet.2019.107639](https://doi.org/10.1016/j.agrformet.2019.107639).
- [49] R. Liu, R. Shang, Y. Liu, and X. Lu, "Global evaluation of gap-filling approaches for seasonal NDVI with considering vegetation growth trajectory, protection of key point, noise resistance and curve stability," *Remote Sens. Environ.*, vol. 189, pp. 164–179, Feb. 2017, doi: [10.1016/j.rse.2016.11.023](https://doi.org/10.1016/j.rse.2016.11.023).
- [50] S. Kandasamy and R. Fernandes, "An approach for evaluating the impact of gaps and measurement errors on satellite land surface phenology algorithms: Application to 20year NOAA AVHRR data over canada," *Remote Sens. Environ.*, vol. 164, pp. 114–129, Jul. 2015, doi: [10.1016/j.rse.2015.04.014](https://doi.org/10.1016/j.rse.2015.04.014).
- [51] J. Liu and P. Zhan, "The impacts of smoothing methods for time-series remote sensing data on crop phenology extraction," in *Proc. IEEE Int. Geosci. Remote Sens. Symp. (IGARSS)*, Jul. 2016, pp. 2296–2299, doi: [10.1109/IGARSS.2016.7729593](https://doi.org/10.1109/IGARSS.2016.7729593).
- [52] X. Wang, J. Xiao, X. Li, G. Cheng, M. Ma, T. Che, L. Dai, S. Wang, and J. Wu, "No consistent evidence for advancing or delaying trends in spring phenology on the tibetan plateau," *J. Geophys. Res., Biogeosci.*, vol. 122, no. 12, pp. 3288–3305, Dec. 2017, doi: [10.1002/2017JG003949](https://doi.org/10.1002/2017JG003949).
- [53] Y. Zhu, Y. Zhang, J. Zu, Z. Wang, K. Huang, N. Cong, and Z. Tang, "Effects of data temporal resolution on phenology extractions from the alpine grasslands of the tibetan plateau," *Ecolog. Indicators*, vol. 104, pp. 365–377, Sep. 2019, doi: [10.1016/j.ecolind.2019.05.004](https://doi.org/10.1016/j.ecolind.2019.05.004).
- [54] C. Wu, D. Peng, K. Soudani, L. Siebicke, C. M. Gough, M. A. Arain, G. Bohrer, P. M. Lafleur, M. Peichl, A. Gonsamo, S. Xu, B. Fang, and Q. Ge, "Land surface phenology derived from normalized difference vegetation index (NDVI) at global FLUXNET sites," *Agricult. Forest Meteorol.*, vol. 233, pp. 171–182, Feb. 2017, doi: [10.1016/j.agrformet.2016.11.193](https://doi.org/10.1016/j.agrformet.2016.11.193).
- [55] G. Bao, Y. Bao, A. Sanjjava, Z. Qin, Y. Zhou, and G. Xu, "NDVI-indicated long-term vegetation dynamics in mongolia and their response to climate change at biome scale: Vegetation dynamics in mongolia and their response to climate change," *Int. J. Climatol.*, vol. 35, no. 14, pp. 4293–4306, Nov. 2015, doi: [10.1002/joc.4286](https://doi.org/10.1002/joc.4286).
- [56] T. F. Keenan, J. Gray, M. A. Friedl, M. Toomey, G. Bohrer, D. Y. Hollinger, J. W. Munger, J. O'Keefe, H. P. Schmid, I. S. Wing, B. Yang, and A. D. Richardson, "Net carbon uptake has increased through warming-induced changes in temperate forest phenology," *Nature Climate Change*, vol. 4, no. 7, pp. 598–604, Jul. 2014, doi: [10.1038/nclimate2253](https://doi.org/10.1038/nclimate2253).
- [57] J. Du, Z. He, J. Yang, L. Chen, and X. Zhu, "Detecting the effects of climate change on canopy phenology in coniferous forests in semi-arid mountain regions of China," *Int. J. Remote Sens.*, vol. 35, no. 17, pp. 6490–6507, Sep. 2014, doi: [10.1080/01431161.2014.955146](https://doi.org/10.1080/01431161.2014.955146).
- [58] Z. He, J. Du, W. Zhao, J. Yang, L. Chen, X. Zhu, X. Chang, and H. Liu, "Assessing temperature sensitivity of subalpine shrub phenology in semi-arid mountain regions of China," *Agricult. Forest Meteorol.*, vol. 213, pp. 42–52, Nov. 2015, doi: [10.1016/j.agrformet.2015.06.013](https://doi.org/10.1016/j.agrformet.2015.06.013).
- [59] Z. Gong, K. Kawamura, N. Ishikawa, M. Goto, T. Wulan, D. Alateng, T. Yin, and Y. Ito, "MODIS normalized difference vegetation index (NDVI) and vegetation phenology dynamics in the inner mongolia grassland," *Solid Earth*, vol. 6, no. 4, pp. 1185–1194, Nov. 2015, doi: [10.5194/se-6-1185-2015](https://doi.org/10.5194/se-6-1185-2015).
- [60] Y. Yang, H. Guan, M. Shen, W. Liang, and L. Jiang, "Changes in autumn vegetation dormancy onset date and the climate controls across temperate ecosystems in China from 1982 to 2010," *Global Change Biol.*, vol. 21, no. 2, pp. 652–665, Feb. 2015, doi: [10.1111/gcb.12778](https://doi.org/10.1111/gcb.12778).

- [61] C. Shi, G. Sun, H. Zhang, B. Xiao, B. Ze, N. Zhang, and N. Wu, "Effects of warming on chlorophyll degradation and carbohydrate accumulation of alpine herbaceous species during plant senescence on the tibetan plateau," *PLoS ONE*, vol. 9, no. 9, Sep. 2014, Art. no. e107874, doi: [10.1371/journal.pone.0107874](https://doi.org/10.1371/journal.pone.0107874).
- [62] O. Langvall and G. Örlander, "Effects of pine shelterwoods on microclimate and frost damage to norway spruce seedlings," *Can. J. Forest Res.*, vol. 31, no. 1, pp. 155–164, Jan. 2001, doi: [10.1139/x00-149](https://doi.org/10.1139/x00-149).
- [63] M. Shen, S. Piao, X. Chen, S. An, Y. H. Fu, S. Wang, N. Cong, and I. A. Janssens, "Strong impacts of daily minimum temperature on the green-up date and summer greenness of the tibetan plateau," *Global Change Biol.*, vol. 22, no. 9, pp. 3057–3066, Sep. 2016, doi: [10.1111/gcb.13301](https://doi.org/10.1111/gcb.13301).
- [64] K. L. Griffin, M. Turnbull, R. Murthy, G. Lin, J. Adams, B. Farnsworth, T. Mahato, G. Bazin, M. Potasnak, and J. A. Berry, "Leaf respiration is differentially affected by leaf vs. Stand-level night-time warming," *Global Change Biol.*, vol. 8, no. 5, pp. 479–485, May 2002, doi: [10.1046/j.1365-2486.2002.00487.x](https://doi.org/10.1046/j.1365-2486.2002.00487.x).
- [65] Y. Feng and X. Zhao, "Daily temperature trend and sensitivity to grassland and cropland in eastern China during the past 32 years: Temperature variability and its sensitivity to grassland and cropland," *Int. J. Climatol.*, vol. 35, no. 7, pp. 1510–1518, Jun. 2015, doi: [10.1002/joc.4072](https://doi.org/10.1002/joc.4072).
- [66] W. Wu, R. Shibusaki, P. Yang, Q. Zhou, and H. Tang, "Characterizing spatial patterns of phenology in China's cropland based on remotely sensed data," in *Proc. Int. Workshop Earth Observ. Remote Sens. Appl.*, Jun. 2008, pp. 1–6.
- [67] X. Shen, B. Liu, G. Li, Z. Wu, Y. Jin, P. Yu, and D. Zhou, "Spatiotemporal change of diurnal temperature range and its relationship with sunshine duration and precipitation in China," *J. Geophys. Res., Atmos.*, vol. 119, no. 23, pp. 13163–13179, Dec. 2014, doi: [10.1002/2014JD022326](https://doi.org/10.1002/2014JD022326).
- [68] Y. Fracheboud, V. Luquez, L. Björkén, A. Sjödin, H. Tuominen, and S. Jansson, "The control of autumn senescence in European aspen," *Plant Physiol.*, vol. 149, no. 4, p. 4, Apr. 2009, doi: [10.1104/pp.108.133249](https://doi.org/10.1104/pp.108.133249).
- [69] M. Yuan, L. Wang, A. Lin, Z. Liu, and S. Qu, "Variations in land surface phenology and their response to climate change in yangtze river basin during 1982–2015," *Theor. Appl. Climatol.*, vol. 137, nos. 3–4, pp. 1659–1674, Aug. 2019, doi: [10.1007/s00704-018-2699-7](https://doi.org/10.1007/s00704-018-2699-7).
- [70] L. L. Jiang et al., "Relatively stable response of fruiting stage to warming and cooling relative to other phenological events," *Ecology*, vol. 97, no. 8, pp. 1961–1969, Aug. 2016, doi: [10.1002/ecy.1450](https://doi.org/10.1002/ecy.1450).
- [71] K. Zhang, J. S. Kimball, R. R. Nemani, S. W. Running, Y. Hong, J. J. Gourley, and Z. Yu, "Vegetation greening and climate change promote multidecadal rises of global land evapotranspiration," *Sci. Rep.*, vol. 5, no. 1, Dec. 2015, Art. no. 15956, doi: [10.1038/srep15956](https://doi.org/10.1038/srep15956).
- [72] H. Wang, H. Liu, G. Cao, Z. Ma, Y. Li, F. Zhang, X. Zhao, X. Zhao, L. Jiang, N. J. Sanders, A. T. Classen, and J. He, "Alpine grassland plants grow earlier and faster but biomass remains unchanged over 35 years of climate change," *Ecol. Lett.*, vol. 23, no. 4, pp. 701–710, Apr. 2020, doi: [10.1111/ele.13474](https://doi.org/10.1111/ele.13474).
- [73] Q. Pang, L. Zhao, Y. Ding, and S. Li, "Analysis about the influence on the thermal regime in permafrost regions with different underlying surfaces," *Sci. Cold Arid Regions*, vol. 2, no. 3, pp. 0203–0211, Feb. 2010.
- [74] Y. S. H. Fu, M. Campioli, Y. Vitasse, H. J. De Boeck, J. Van den Berge, H. AbdElgawad, H. Asard, S. Piao, G. Deckmyn, and I. A. Janssens, "Variation in leaf flushing date influences autumnal senescence and next year's flushing date in two temperate tree species," *Proc. Nat. Acad. Sci. USA*, vol. 111, no. 20, pp. 7355–7360, May 2014, doi: [10.1073/pnas.1321727111](https://doi.org/10.1073/pnas.1321727111).
- [75] Z. Shi, Y. Liu, and F. Wang, "Ecosystem respiration under different mycorrhizal strategy dominated forest and their response to temperature and precipitation," *Environ. Pollut. Public Health*, pp. 703–706, May 2012.
- [76] M. J. Duveneck and J. R. Thompson, "Climate change imposes phenological trade-offs on forest net primary productivity: Phenological trade-offs on forests," *J. Geophys. Res., Biogeosci.*, vol. 122, no. 9, pp. 2298–2313, Sep. 2017, doi: [10.1002/2017JG004025](https://doi.org/10.1002/2017JG004025).



WENDU RINA received the M.S. degree in cartography and geography information system from the College of Geographical Science, Inner Mongolia Normal University, Hohhot, China, in 2017. She is currently pursuing the Ph.D. degree with Inner Mongolia Normal University. Her research interests include vegetation dynamic monitoring and ecosystem response to climate change.



GANG BAO received the Ph.D. degree in remote sensing of resources and environment from the International Institute for Earth System Science, Nanjing University, Nanjing, in 2016. He is currently an Associate Professor with the College of Geographical Science, Inner Mongolia Normal University, Hohhot. His research interests include vegetation dynamic monitoring and remote sensing applications.



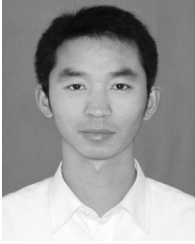
SIQIN TONG received the Ph.D. degree in cartography and geography information system from the School of Environment, Northeast Normal University, Changchun, in 2019. She is currently an Associate Professor with the College of Geographical Science, Inner Mongolia Normal University, Hohhot. Her research interests include climate change monitoring and terrestrial ecosystems productivity simulation.



YUHAI BAO received the Ph.D. degree in cartography and geography information system from the Institute of Remote Sensing Applications, Chinese Academy of Sciences, Beijing, in 1999. He is currently the Dean and a Professor with the College of Geographical Science, Inner Mongolia Normal University, Hohhot. His research interest includes 3S (GPS, GIS, and RS) integration and applications.



YIN SHAN received the Ph.D. degree in soil and water conservation and desertification combating from the College of Ecological Environment, Inner Mongolia Agricultural University, Hohhot, in 2010. He is currently a Professor with the College of Geographical Science, Inner Mongolia Normal University, Hohhot. His research interest includes desertification monitoring and assessment.



XIAOJUN HUANG received the Ph.D. degree in cartography and geography information system from the College of Earth and Environmental Sciences, Lanzhou University, Lanzhou, in 2019. He is currently a Professor with the College of Geographical Science, Inner Mongolia Normal University, Hohhot. His research interests include remote sensing monitoring of natural disasters and ecological environment.



LINGTONG DU received the Ph.D. degree in remote sensing of resources and environment from the International Institute for Earth System Science, Nanjing University, Nanjing, in 2013. He is currently a Professor with the Breeding Base for State Key Laboratory of Land Degradation and Ecological Restoration in Northwest China, Ningxia University, Yinchuan. His research interest includes remote sensing of environmental and spatial analysis.

...



HONG YING received the M.S. degree in cartography and geography information system from the School of Geographical Sciences, Northeast Normal University, Changchun, China, in 2016. She is currently pursuing the Ph.D. degree with Northeast Normal University. Her research interests include climate change and vegetation remote sensing.



Lagged feedback of peak season photosynthetic activities on local surface temperature in Inner Mongolia, China

Wendu Rina^{a,b}, Yuhai Bao^{a,b,*}, Enliang Guo^{a,c}, Siqin Tong^{a,b}, Xiaojun Huang^{a,b}, Shan Yin^{a,b}

^a College of Geographical Science, Inner Mongolia Normal University, Hohhot, 010022, China

^b Inner Mongolia Key Laboratory of Remote Sensing and Geographic Information Systems, Inner Mongolia Normal University, Hohhot, 010022, China

^c Inner Mongolia Key Laboratory of Disaster and Ecological Security on the Mongolian Plateau, Inner Mongolia Normal University, Hohhot, 010022, China

ARTICLE INFO

Handling Editor: Aijie Wang

Keywords:

Peak season photosynthetic activities
Land surface temperature
Cooling effect
Warming effect
Evapotranspiration
Structural equation model

ABSTRACT

Increased vegetation peak growth and phenological shifts toward spring have been observed in response to climate warming in the temperate regions. Such changes have the potential to modify warming by perturbing land–atmosphere energy exchanges; however, the signs and magnitudes of biophysical feedback on surface temperature in different biomes are largely unknown. Here, we synthesized information from vegetation growth proxies, land surface temperature (LST), and surface energy balance factors (surface evapotranspiration (ET), albedo, and broadband emissivity (BBE)) to investigate the variations in timing (PPT) and productivity (PP_{max}) of seasonal peak photosynthesis and their time-lagged biophysical feedbacks to the post-season LST in Inner Mongolia (IM) during 2001–2020. We found that increased PP_{max}, rather than advanced PPT, exhibited a significant impact on LST, with divergent signs and magnitudes across diurnal periods and among different biomes. In the grassland biome, increased PP_{max} cooled both LST during daytime (LST_{day}) and nighttime (LST_{night}) throughout the post-season period, with a more pronounced response during daytime and diminishing gradually from July to September. This cooling effect on LST was primarily attributed to enhanced ET, as evidenced by the greater effect of ET cooling than that of albedo warming and BBE cooling based on a structural equation model (SEM). In the forest biome, increased PP_{max} led to a symmetrical warming effect on LST_{day} and LST_{night}, and none of the surface energy balance factors were identified as significant intermediate explanatory factors for the observed warming effect. Moreover, the responses of average LST (LST_{mean}) and diurnal temperature range of LST (LST_{TR}) to variations in PP_{max} were consistent with those of LST_{day} at two biomes. The observations above elucidate the divergent feedback mechanisms of vegetation peak growth on LST among different biomes and diurnal cycles, which could facilitate the improvement of the realistic parameterization of surface processes in global climate models.

1. Introduction

Vegetation plays a fundamental role in hydrothermal cycles, acting as a link between the hydrosphere and atmosphere (Bonan et al., 1992; Piao et al., 2019). In the context of global warming, extensive vegetation greening has been observed unequivocally across the globe over the past three decades (Forzieri et al., 2017; Zhu et al., 2016). Such greening can either amplify or dampen the dominant warming signal by modifying the seasonal cycles of biochemical and biophysical processes that affect the partitioning of net radiation into latent and sensible heat fluxes at the land–atmosphere interface (Lee et al., 2011; Lian et al., 2022; Peng et al., 2014). Moreover, the associated phenological shifts exert a

regulatory effect on these feedbacks (Richardson et al., 2013), primarily because of their observed sensitivity to climate change and variability (Jeong et al., 2011a; Vitasse et al., 2018). However, previous studies have focused primarily on the overall growth status of the entire growing season and the two phenological events that determine its length (i.e., the start (SOS) and end (EOS) of the growing season) (Shen et al., 2022; Xu et al., 2020), thereby overlooking the separate feedback of peak season photosynthetic activities to climate. Peak season photosynthetic activities serve as an indicator not only of the capacity of terrestrial ecosystem productivity (Gonsamo et al., 2018; Xu et al., 2016), but also of the timing and magnitude of resource availability (Buermann et al., 2013; Huang et al., 2018). Shifts in these activities

* Corresponding author. College of Geographical Science, Inner Mongolia Normal University, Hohhot, 010022, China.

E-mail address: baoyuhai@imnu.edu.cn (Y. Bao).

<https://doi.org/10.1016/j.envres.2023.116643>

Received 22 May 2023; Received in revised form 7 July 2023; Accepted 10 July 2023

Available online 12 July 2023

0013-9351/© 2023 Elsevier Inc. All rights reserved.

represent key transition points in the surface energy budget and can have significant implications for ecosystem processes and feedbacks (Park et al., 2019; Piao et al., 2019). Consequently, there is a compelling need to assess the lagged feedback of peak season photosynthetic activity on surface temperature.

The net vegetation effect on surface temperature differs across the Northern Hemisphere (Li et al., 2015; Peng et al., 2014), owing to the involvement of multiple biophysical processes linked to vegetation modification, such as surface evapotranspiration (ET), albedo, short-wave transmissivity, and longwave air emissivity, contributing to the complexity of vegetation-climate feedbacks (Forzieri et al., 2017; Huang et al., 2022; Lian et al., 2022). In colder climates of boreal regions, greening exerts a warming effect on local temperatures through reduced albedo, which increases the amount of absorbed incoming shortwave radiation at the surface (Li et al., 2016). However, such warming effects disappear and switch to strong cooling effects in tropical lands, as a result of ET-induced cooling effect outweighing the albedo-induced warming effect (Feldman et al., 2023; Li et al., 2015). An increase in the strength of plant-mediated ET can enhance turbulent energy dissipation and cause net surface cooling (Peng et al., 2014). For temperate regions, the net effect of vegetation change on surface temperature remains controversial, because of the competing effects of albedo and ET on climate (Jeong et al., 2011b; Lee et al., 2011). Furthermore, opposing signals in different seasons may be partly responsible for conflicting conclusions regarding the feedback of annual vegetation growth (Li et al., 2016; Shen et al., 2022). For instance, Lian et al. (2022) demonstrated that the biophysical feedback effects of vegetation shift from warming-dominated in colder seasons to cooling-dominated in warmer seasons, highlighting the variability of vegetation feedbacks with intra-seasonal temperature conditions (Xue et al., 2021). However, the evaporative cooling effect in warmer seasons (such as summer) may also be constrained by soil moisture availability, as higher transpiration rates require adequate water supply (Pitman et al., 2011; Swann et al., 2012). The advanced onset of spring green-up leads to the premature depletion of summer soil moisture, especially in water-limited regions (Buermann et al., 2013), which could cause a substantial decline in latent cooling and subsequent warming of the surface temperature in summer (Peñuelas and Filella, 2009). Therefore, there is large uncertainty over the feedback mechanisms of vegetation activities during the peak season, along with the mediation of the phenological shifts. Additionally, surface broadband emissivity (BBE), as an important component characterizing the biogeophysical processes, also plays a key role in the temperature feedback of vegetation dynamics (Kuo et al., 2018; Zhou et al., 2008). Greening induced increase in BBE would enhance the outgoing longwave radiation and reduce the sensible heat flux, which further cool the surface temperature (Liu et al., 2020; Zhou et al., 2003). However, such cooling effect of BBE was more pronounced in the arid and semi-arid regions with sparse vegetation cover (Cheng and Liang, 2013; Ogawa and Schmutge, 2004), suggesting a potential discrepancy in the explanatory ability of BBE on vegetation feedback to surface temperature across different biomes. The commonly studied biophysical processes (i.e., ET and albedo) induced by vegetation greening primarily occur during daytime, thereby affecting daytime temperature more than nighttime temperature (Peng et al., 2014; Shen et al., 2015). In contrast, variations in BBE have a more substantial impact on surface temperature during nighttime compared with during daytime (Zhou et al., 2007, 2008). Therefore, it is essential to comprehensively consider these surface energy balance factors to achieve a more precise understanding of the vegetation feedback to climate.

Until recently, studies quantifying the biophysical temperature effects of vegetation change could be categorized into two types: land use/land cover change, (e.g., afforestation/deforestation) (Li et al., 2015; Peng et al., 2014), and climate change-induced greening (i.e., change in vegetation intensity) (Li et al., 2023; Shen et al., 2015, 2022). Studies based on afforestation areas typically assume the complete replacement of short vegetation (croplands and marginal lands) with forest to amplify

the signal of complete land-use transitions (Rigden and Li, 2017). However, such an empirical approach might be unable to adequately comprehend the temporal changes in vegetation biophysical effects due to the space-for-time assumption (Peng et al., 2014; Wang et al., 2018), which overlooks temporal fluctuations in vegetation growth. The persistent greening phenomenon is prevalent globally, and its temperature feedback is more constructive for global warming signals and extends beyond the cases of vegetation-type replacement that occupy only a relatively small fraction of global land. Despite systematic quantification of the feedback of widespread greening across different latitudinal zones (Forzieri et al., 2017; Jeong et al., 2011b; Lian et al., 2022), researchers often overlook the heterogeneity among different biomes. Such an approach would obscure or confound the specific biophysical feedback information of different biomes on climate even within the same latitudinal zones, owing to their distinct fundamental characteristics. Plant functional type modulates the impact of vegetation on surface energy partitioning (Zheng et al., 2019; Forzieri et al., 2020). For instance, in contrast to grasslands with shallow soil moisture, forests exhibit a lower sensitivity of energy terms to greening due to a more conservative and even utilization of water resources facilitated by a deeper rooting system (Forzieri et al., 2020). Plant functional types also directly lead to differences in albedo change trends (Yan et al., 2021). Forests, in comparison to shorter vegetation types, display intricate vertical and horizontal structures characterized by distinct canopy spectral features (Hadi Pfeifer et al., 2017). Consequently, the differential radiation transmission and absorption in the forest canopy (Richardson et al., 2013; Zhu et al., 2022) have the potential to result in divergent feedback mechanisms when compared to grasslands. Therefore, there is substantial degree of ambiguity regarding the signs and magnitudes of the temperature feedback of different biome.

To address the above issues, Inner Mongolia (IM) in northern China, a temperate region characterized by profound vegetation changes (Bao et al., 2019), was selected as an ideal region to investigate the temperature feedbacks of variations in peak season photosynthetic activities in different biomes. This study aimed to answer the following questions: (1) How have the timing (PPT) and productivity (PP_{max}) of seasonal peak photosynthesis changed in IM over the last two decades? (2) Are there variations in the signs and magnitude of the feedback of peak season photosynthetic activities on land surface temperature (LST) across the diurnal period and among different biomes? (3) Which surface energy balance factors (ET, albedo, or BBE) serve as primary, intermediate explanatory indicators in the negative/positive feedbacks of peak season photosynthetic activities? The findings of present study could enhance our understanding of the mechanisms of land surface biophysical processes and facilitate projection of the effects of future climate change.

2. Materials and methods

2.1. Study area and biome classification

Inner Mongolia (IM) Autonomous Region is located in the northern border area of China, is bordered by Mongolia to the north, spanning $97^{\circ}12' - 126^{\circ}04' E$ and $37^{\circ}24' - 53^{\circ}23' N$, and covering a total area of approximately 118.3 km^2 (Fig. 1a). The elevation of IM shows a downward sloping trend from south to north and from west to east, with majority ranging between 1000 and 1500 m (Fig. 1a). The study area spans several climate zones, transitioning from arid and semi-arid in the northwest inland region to humid and semi-humid in the southeast coastal region, with an average annual temperature of $1-15^{\circ}C$ and an average annual precipitation of 50–500 mm. The vegetation type of IM follows an evident geotropic pattern, which was controlled by the geographical location and climatic conditions, ranging from the eastern forested zone to the central grassland zone and then to the western desert zone (Li et al., 2018) (Fig. 1b). The vegetation type data used in our study were obtained from digitized results Suld et al. (2015) based

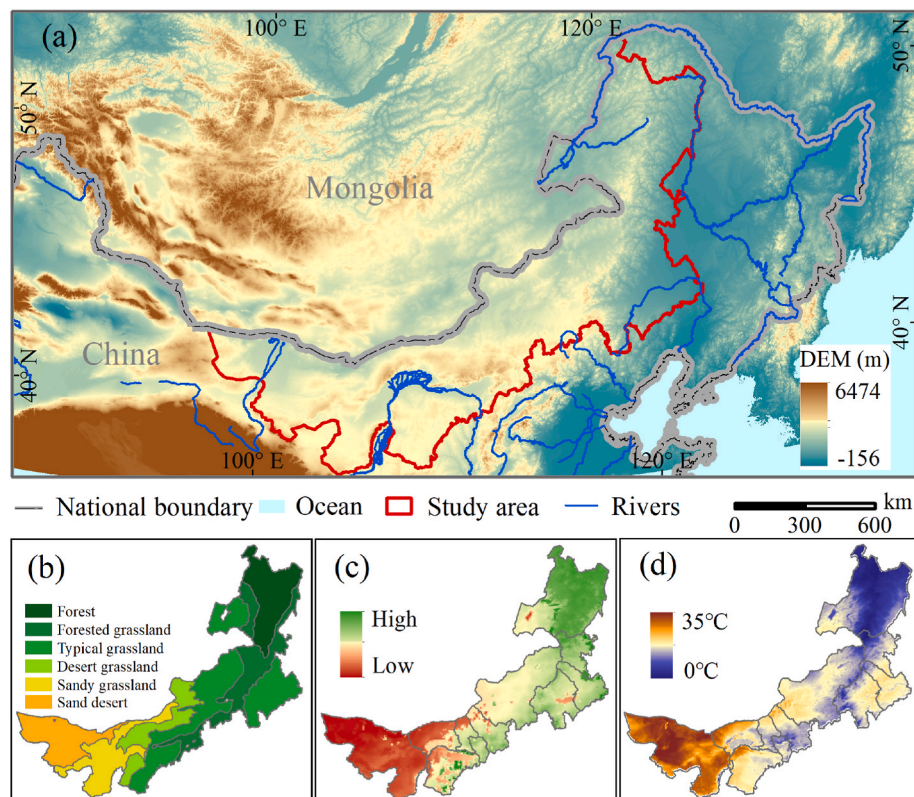


Fig. 1. Geographic location of study area (a), the distribution of vegetation types (b), summer soil moisture (c), and summer land surface temperature (LST) of daily mean (d).

on field research (Li, 1962, 1990). The undulating topography and diverse vegetation types have resulted in an extremely fragile environment that is particularly sensitive to climate change (Guo et al., 2020). To thoroughly analyze feedback across different biomes, the study area was divided geographically into two main biomes: grasslands and forests. The grassland biome included forested grassland, typical grassland, desert grassland, and sandy grassland. There was a noticeable difference in soil moisture and mean LST between the forest and grassland biomes, with higher soil moisture and lower mean LST in the forest biomes, and lower soil moisture and higher mean LST in the grassland biomes (Fig. 1b–d).

2.2. Datasets and pre-processing

2.2.1. Proxies of vegetation growth

We evaluated vegetation peak season photosynthetic activities (PPT and PP_{max}) using three different satellite-based datasets (gross primary production (GPP), normalized difference vegetation index (NDVI), and near-infrared reflectance of vegetation (NIR_v)) from 2001 to 2020. The datasets were utilized as follows:

The GPP for the period 2001–2020 was obtained from the GOSIF-GPP dataset, which utilizes a biome-specific linear relationship between flux tower-based GPP and a global sun-induced chlorophyll fluorescence (SIF) data set from the Orbiting Carbon Observatory-2 (OCO-2) (referred to as GOSIF) (<http://globalecology.unh.edu/>) (Li and Xiao, 2019). The GOSIF-GPP dataset, with a temporal resolution of 8-day and a spatial resolution of 0.05° , was estimated using a machine learning model that incorporates various variables representing vegetation conditions, meteorological conditions, and land cover information as input. The dataset exhibits reasonable seasonal and spatial patterns and high correlated with GPP data from FLUXNET (Li and Xiao, 2019).

The NDVI for the period 2001–2020 was obtained from the MOD13C1 version 6 dataset, with a temporal resolution of 16-days and a

spatial resolution of 0.05° . The dataset was pre-processed for radiation calibration, cloud detection, and atmospheric correction to remove the noise caused by sensors and other factors. In addition, a Moderate-Resolution Imaging Spectroradiometer (MODIS) specific synthesis method that adopted product quality assurance was also applied to generate 16-day composite NDVI data free of low-quality observations for phenology extraction. To focus on regions with vegetation and seasonality, the pixels with mean NDVI values < 0.1 and annual maximum NDVI failing to occur within the June–August were discarded from the analysis (Jeong et al., 2011a).

The NIR_v (Badgley et al., 2017) was calculated by NDVI and near infrared (NIR) from the MOD13C1 dataset. The NIR_v , as a direct index of photons intercepted by chlorophyll, can differentiate between the confounding effects of background brightness, leaf area and distribution of photosynthetic capacity with depth in canopies. It exhibits a higher correlation with observed GPP than with NDVI. The NIR_v were calculated as follows:

$$NIR_v = (NDVI - C) \times NIR \quad (1)$$

where the parameter C was set to 0.08 according to (Badgley et al., 2017), NIR (841–876 nm).

2.2.2. LST dataset

LST data for the period 2001–2020 were obtained from Terra/MODIS in monthly composite form and a spatial resolution of 0.05° (MOD11C3), which were downloaded from the NASA website (<http://www.nasa.gov/>). The LST data included daytime (local solar time $\sim 10:30$) and nighttime (local solar time $\sim 22:30$) temperature observations. In the present study, we aimed to investigate the impacts of peak season plant activities on post-season LST variations. Therefore, the post-season was defined as the period from July to September considering that the multiyear mean PPT of the study area primarily occurred in late June to mid-July. We first extracted the 8-day composite

of the average LST_{day} and LST_{night} bands of post season from the remote sensing products. Subsequently, the monthly mean LST_{day} and LST_{night} values were computed by aggregating the mean values of three or four images corresponding to each month. Finally, the average LST (LST_{mean}) and the diurnal temperature range of LST (LST_{DTR}) were constructed from LST_{day} and LST_{night}.

2.2.3. Surface energy balance factors

Surface ET, albedo, and BBE are the three major surface energy balance factors that determine the positive/negative feedback of vegetation activity in climate systems (Peng et al., 2014; Shen et al., 2015; Zhou et al., 2008). In the present study, ET, albedo, and BBE were employed as the intermediate explanatory factors in the relationships between LST and PPT and PP_{max} to investigate the feedback mechanisms of the variations in peak season photosynthetic activities on LST.

The monthly ET utilized in this study was obtained from the Global Land Data Assimilation System (GLDAS) version 2.1 datasets, which provided by the Goddard Earth Sciences Data and Information Services Center (https://disc.gsfc.nasa.gov/datasets/GLDAS_NOAH025_M_2.1/). The GLDAS datasets ingest satellite- and ground-based observational data products and use advanced land surface modeling data assimilation techniques to provide optimal fields of land surface states and fluxes. In the present study, the GLDAS-ET dataset spanning the period 2001–2020, with a spatial resolution of 0.25°, was resampled to 0.05° using the nearest neighbor method to match the spatial resolution of the vegetation growth proxies and LST data.

Shortwave white-sky albedo and longwave (window: 8–13.5 μm) BBE datasets for the period 2001–2020 were obtained from the Global Land Surface Satellite (GLASS) product (<http://glass-product.bnu.edu.cn/index.html>), generated by the Advanced Very High-Resolution Radiometer (AVHRR) at a temporal resolution of 8-days and a spatial resolution of 0.05°. The GLASS albedo product was validated using FLUXNET observation data and showed high quality and accuracy compared to the MODIS instrument Bidirectional Reflectance Distribution Function (BRDF)/albedo product. The dataset provides black-sky and white-sky albedo, and the white-sky data can more closely reflect the condition of the surface land cover and is more stable for long-term global environmental change observation (Liang et al., 2013). The GLASS BBE was derived by utilizing transfer models that incorporate both AVHRR visible and near-infrared reflectance and MODIS short-wave albedos. In this study, monthly white-sky albedo and BBE were generated by aggregating the mean values of three or four images corresponding to each month.

2.3. Methods

2.3.1. Phenological metrics retrieval

A sixth-degree polynomial function (Piao et al., 2006) was first used to construct daily vegetation proxies (GPP, NDVI, and NIR_v) for each pixel using Eq. (2). Subsequently, the maximum value of sixth-degree polynomial function fitted curves was defined as PP_{max}, and its corresponding date was then defined as PPT for each vegetation proxy.

$$VI_t = a_0 + a_1t + a_2t^2 + a_3t^3 + \dots + a_6t^6 \tag{2}$$

where, VI_t is the sixth-degree polynomial function fitted vegetation proxy for Julian date *t*; a₀, ..., a_n are the fitted coefficients derived from least-squares regression.

2.3.2. Theil–Sen slope estimation and Mann–Kendall significance test

The Theil–Sen slope estimator is a median-based non-parametric trend test estimator, which has no strict requirement of the time series to meet the assumptions of serial autocorrelation and normal distribution, and can effectively deal with small outliers and missing value noise (Akritas et al., 1995). In this study, the trends of PP_{max} and PPT in the

time series were calculated using the Theil–Sen slope estimator. The calculation method is as follows:

$$\beta = \text{Median}\left(\frac{X_j - X_i}{j - i}\right), \forall j > i \tag{3}$$

where, β is the median value of the slope of all data. If β > 0, the vegetation change shows an upward trend, and if β < 0, the vegetation change shows a downward trend. X_i and X_j are the variables value at a time *i* and *j*, respectively, and Median represents the median value.

The Mann–Kendall (M–K) significance test is a non-parametric test method, which supplements Theil–Sen slope statistics, and is used to test the significance of the time series trend. The calculation method is as follows:

$$Z = \begin{cases} \frac{S - 1}{\sqrt{\text{var}(S)}}, S > 0 \\ 0, S = 0 \\ \frac{S + 1}{\sqrt{\text{var}(S)}}, S < 0 \end{cases} \tag{4}$$

$$S = \sum_{i=1}^{n-1} \sum_{j=i+1}^n \text{sign}(VI_{S_j} - VI_{S_i}) \tag{5}$$

$$\text{var}(S) = \frac{n(n-1)(2n+5)}{18} \tag{6}$$

$$\text{sign}(X_j - X_i) = \begin{cases} 1, X_j - X_i > 0 \\ 0, X_j - X_i = 0 \\ -1, X_j - X_i < 0 \end{cases} \tag{7}$$

where, X_i and X_j are the variable values at times *i* and *j*, respectively, *n* is the length of the time series, sign is the sign function, and Z value of less than 0 indicates a downward trend; while a value of greater than 0 indicates an upward trend. When the absolute value of Z is > 1.65, 1.96, and 2.58, it means that the trend has passed the significance test with reliabilities of 90%, 95%, and 99%, respectively. At 95% reliability test was used in the present study.

2.3.3. Pearson correlation analysis

To investigate the relationship between PPT and PP_{max} and their impacts on LST variations, Pearson’s correlation analysis was used to examine the correlation between vegetation peak season photosynthetic activities (PPT and PP_{max}) and LST (LST_{day}, LST_{night}, LST_{mean}, and LST_{DTR}) of each month of the post-season for the entire study area. All variables were linearly detrended before the Pearson’s correlation analysis. This approach allowed us to disentangle the unidirectional PPT/PP_{max}-LST effect from the simultaneously changing climate and vegetation dynamic signal. The formula of Pearson’s correlation method is as follows:

$$r_{xy} = \frac{\sum_{i=1}^n (x_i - \bar{x})(y_i - \bar{y})}{\sqrt{\sum_{i=1}^n (x_i - \bar{x})^2 (y_i - \bar{y})^2}} \tag{8}$$

where, x_i and y_i were the values of the *i* year, \bar{x} and \bar{y} are the average values of all years, *n* is the length of the time series. When *r* > 0, the two variables are positively correlated, and when *r* < 0, the two variables are negatively correlated.

2.3.4. Structural equation model

Structural equation modeling (SEM), as a confirmatory factor analysis, can partition the direct and indirect causal relationships of a complex natural system, and has been widely applied in ecological research (Xie et al., 2021; Yu and Leng, 2022). The SEM not only

identifies the influence degree (standardized path coefficient) for each influence path, but also estimates the goodness-of-fit of the whole model to determine whether to modify the possible conceptual model (Yu and Leng, 2022). In this study, we utilized SEM to explore the regulating roles of surface ET and albedo in PP_{max} feedbacks on LST (Fig. 2). The SEM model is defined as follows:

$$y = By + \Gamma x + \zeta \quad (9)$$

where, y and x indicate the column vectors of the exogenous and endogenous variables, respectively; B , Γ , and ζ are the relationships between the endogenous variables, influence of exogenous variables on endogenous variables, and residual term of the structural equation, respectively. Note that all the input parameters of the model were linearly detrended.

3. Results

3.1. Spatiotemporal patterns of peak season photosynthetic activities

All three indices (GPP, NDVI, and NIR_v) were found to have similar spatial heterogeneity gradients (Fig. S1) and interannual variation (Fig. 3a–c, and 3e–g) in peak season photosynthetic activities (PP_{max} and PPT) of the IM during the period 2001–2020. However, the PPT inferred from the GPP generally occurred earlier than that inferred from VI-based estimates (NDVI and NIR_v) (Figs. S1e–g). On average, the forest ecosystem in the northeastern part of the study area had a higher PP_{max} and attained a PPT earlier than the grassland ecosystem (Figs. S1d and h). Specifically, the multi-year averaged PPT of the forest and grassland biomes occurred on the 200th and 219th days of the year (DOY), respectively. Furthermore, the multi-year averaged PP_{max} of the forest biome (0.66) was nearly twice as high as that of the grassland biome (0.29).

Temporally, the different data-averaged PP_{max} experienced a widespread increasing trend, occupying 93.24% of the entire region, and the pixels with a significant increasing trend (41.96%) were distributed in the southwestern and eastern areas of IM, such as the Mu Us Sandy Land, Hetao irrigation areas, and Horqin Sandy Land (Fig. 3d). Regionally, PP_{max} increased significantly in both grassland ($0.29 \times 10^{-2} \text{ year}^{-1}$, $P < 0.01$) and forest ($0.30 \times 10^{-2} \text{ year}^{-1}$, $P < 0.01$) biomes (Fig. 4a).

Regarding PPT variations, the different data-averaged PPT exhibited a complex spatial pattern, with mixed advanced (59.21%) and delayed (40.79%) signals (Fig. 3h), evidenced by a non-significant change trend ($0.01 \text{ days year}^{-1}$, $P > 0.05$) in the regional mean PPT (Fig. 4b). Advanced PPT pixels were spread over most areas of IM, and areas with significant advancement (14.09%, $P < 0.05$) were mainly in the north-eastern forest ecosystems of the interest region (Fig. 3h). Therefore, the regional mean PPT of the forest biome showed a significant advancing trend ($0.32 \text{ days year}^{-1}$, $P < 0.01$; Fig. 4b). In contrast, the pixels of the delayed PPT were primarily concentrated in grassland ecosystems, such as the Xilingole Grasslands in the central part and Hulunbuir Grasslands in the northern part of the study area (Fig. 3h), resulting in a delayed but insignificant trend at the regional mean scale of the grassland biome ($0.05 \text{ days year}^{-1}$, $P > 0.05$; Fig. 4b).

Furthermore, we found a close relationship between the interannual variations in PP_{max} and PPT, with high spatial heterogeneity across the study region (Fig. S2). Increased PP_{max} was accompanied by advanced PPT in more than a half of IM (62.31%), which mainly occurred in the Mu Us Sandy Land in southwestern part of IM and most of northeastern part of IM, where the forest ecosystem was dominant. The remaining areas (37.69%) experienced a delayed PPT (Fig. 3h) and had an increased PP_{max} accompanying the delayed PPT (positive correlation coefficients), which were found mostly in the Hetao irrigation areas in western IM, the Xilingole Grasslands in central IM, and the Hulunbuir Grasslands in northern IM.

3.2. Cooling/warming effects of peak season photosynthetic activities on local LST

We hypothesize that increased PP_{max} and delayed/advanced PPT will turbulently affect the surface energy balance, and exert a sizable time-lagged influence on the post-season (July–September) LST. To test this hypothesis, we initially examined the correlation between inter-annual fluctuations of LST and PP_{max} and PPT. The analysis revealed that PP_{max} had an extensive negative spatial correlation with LST_{day} in grasslands over all months of the post-season, occupying 98.68% (July), 98.25% (August), and 91.37% (September) of the grasslands in IM (Fig. 5a–c), and implying a cooling effect of enhanced peak season photosynthetic production on LST during the daytime in grassland

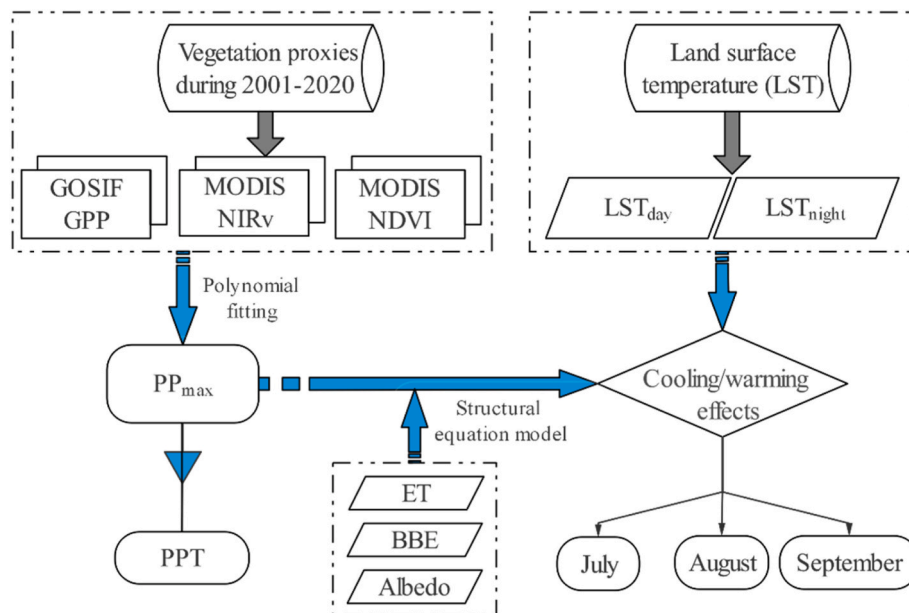


Fig. 2. Flowchart of steps in the methodology (GPP: Gross Primary Production; NIR_v : Near-infrared Reflectance of Vegetation; NDVI: Normalized Difference Vegetation Index; PPT: Timing of seasonal peak photosynthesis; PP_{max} : Productivity of seasonal peak photosynthesis; ET: Evapotranspiration; BBE: Broad-band Emissivity).

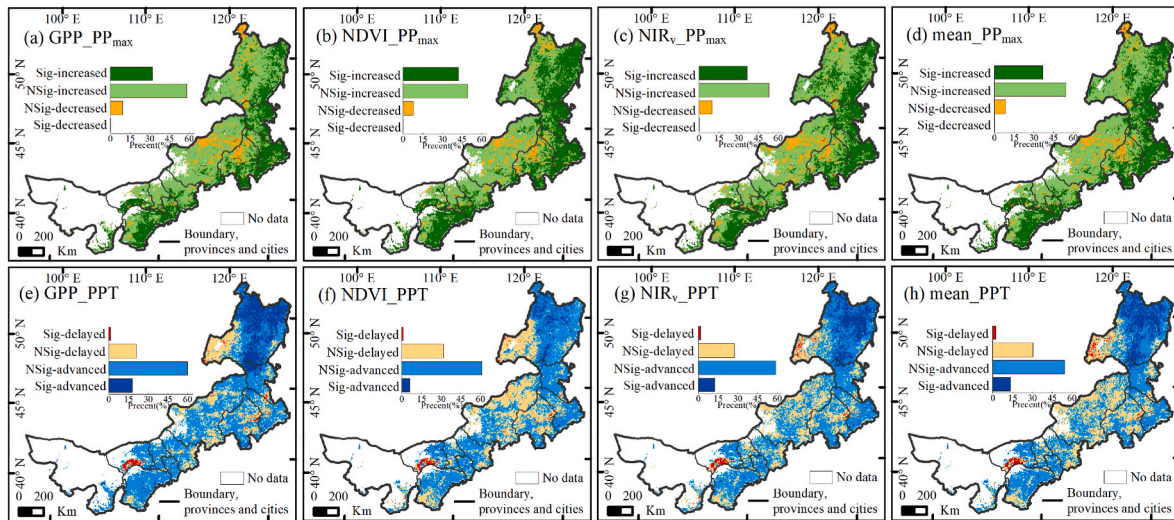


Fig. 3. Spatial distributions of linear trends of PP_{max} and PPT over Inner Mongolia (IM) during 2001–2020 based on GPP (a and e), NDVI (b and f), NIR_v (c and g), and different data averages (d and h), respectively. (Sig, significantly changed; NSig, changed but not significantly; significant at $P < 0.05$).

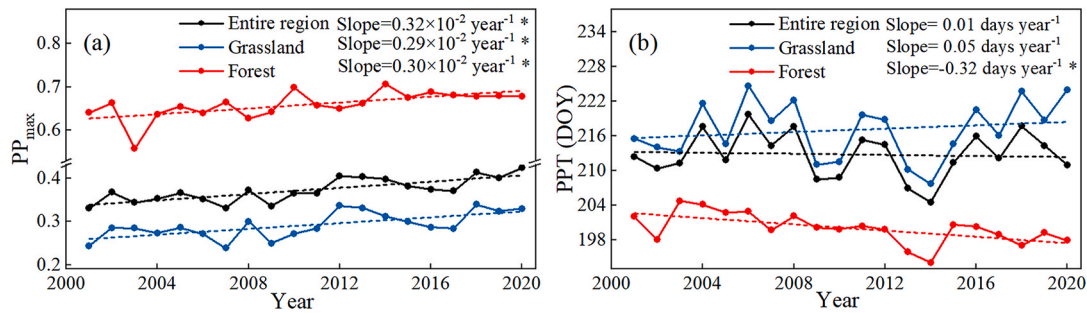


Fig. 4. Interannual variations of PP_{max} (a) and PPT (b) from 2001 to 2020 averaged for three data for the entire study area and two vegetation types (*represent significant trends at $P < 0.05$).

biomes. Interestingly, the magnitude of the cooling effect reduced gradually from July to September, as evidenced by the decreased area proportion (Fig. 5a–c) and the magnitude of the negative correlation coefficients (Fig. 6a). In contrast to grasslands, the PP_{max} of forested regions were positively correlated with LST_{day} throughout the post-season (Fig. 6c), with positive correlation coefficients of 57.37% (July), 80.57% (August), and 87.05% (September) (Fig. 5a–c). This phenomenon implies that enhanced PP_{max} had a warming effect on the post-season LST_{day} of the forest ecosystem, and such effects are more pronounced in the later months of the post-season. Similar to LST_{day} , PP_{max} had an opposite effect on the post-season LST_{night} of the grassland and forest biomes, despite having different degrees of effect compared to LST_{day} (Fig. 5d–f and Fig. 6b, d). Specifically, LST_{night} exhibited a non-significant negative correlation ($P > 0.05$) with the PP_{max} of grassland ecosystem across all months of the post-season (Fig. 6b), indicating that the impact of PP_{max} on LST_{night} was weaker than that on LST_{day} . Regarding the forest biome, LST_{night} had a significant negative correlation ($P < 0.05$) with PP_{max} in the majority months of the post-season, being comparable to LST_{day} in terms of magnitude and signals of correlation coefficients, indicating a symmetrical influence of PP_{max} on the daytime and nighttime LST in the forest biome. Furthermore, the relationships between PP_{max} and LST_{mean} and LST_{DTR} exhibited features similar to those with LST_{day} at both the pixel-scale and biome-scale across all months (Figs. S3–4), that is, increased PP_{max} cooled the LST_{mean} and LST_{DTR} of the grassland ecosystem, while it warmed the LST_{mean} and LST_{DTR} of the forest ecosystem.

Contrary to PP_{max} , the feedbacks of PPT variations on LST_{day} and LST_{night} were neither significant across the post-season, nor dependent

on the different biomes (Figs. 7–8). However, the relationship between the PPT and LST (daytime and nighttime) demonstrated a clear discrepancy among the different months over the entire study area. In July, the PPT was positively correlated with both LST_{day} and LST_{night} in the majority of pixels (more than a half of the total pixels), although this was not significant (Fig. 7a, d), indicating that advanced PPT had a cooling effect on both LST_{day} and LST_{night} over the regions of interest to some extent. However, in August and September, PPT had opposite effects on LST_{day} and LST_{night} over the IM, that is, advancing PPT cooled LST_{day} , while warming LST_{night} (Fig. 7b and c, e, f). Similar to the relationships observed between PP_{max} and LST indices, the relationships between PPT with LST_{mean} and LST_{DTR} exhibited comparable characteristics to those of LST_{day} in terms of spatial patterns and regional scale throughout all months (Figs. S5–6). Typically, the feedback of PP_{max} interannual fluctuations on LST was relatively significant compared with PPT, with considerable diurnal and between biome diversity. As a result, we exclusively used PP_{max} in the subsequent analyses to reveal differences in land surface feedback mechanisms across different biomes and diurnal LST. In addition, the mechanisms of land surface feedback of PP_{max} to LST_{mean} and LST_{DTR} were not considered further because their responses to peak season photosynthetic activities were consistent with LST_{day} .

3.3. Explanatory roles of surface energy balance factors in the cooling/warming effect of PP_{max} on LST

SEM was used to elucidate the indirect effects of increased PP_{max} on LST by regulating ET, albedo, and BBE. There were three main pathways

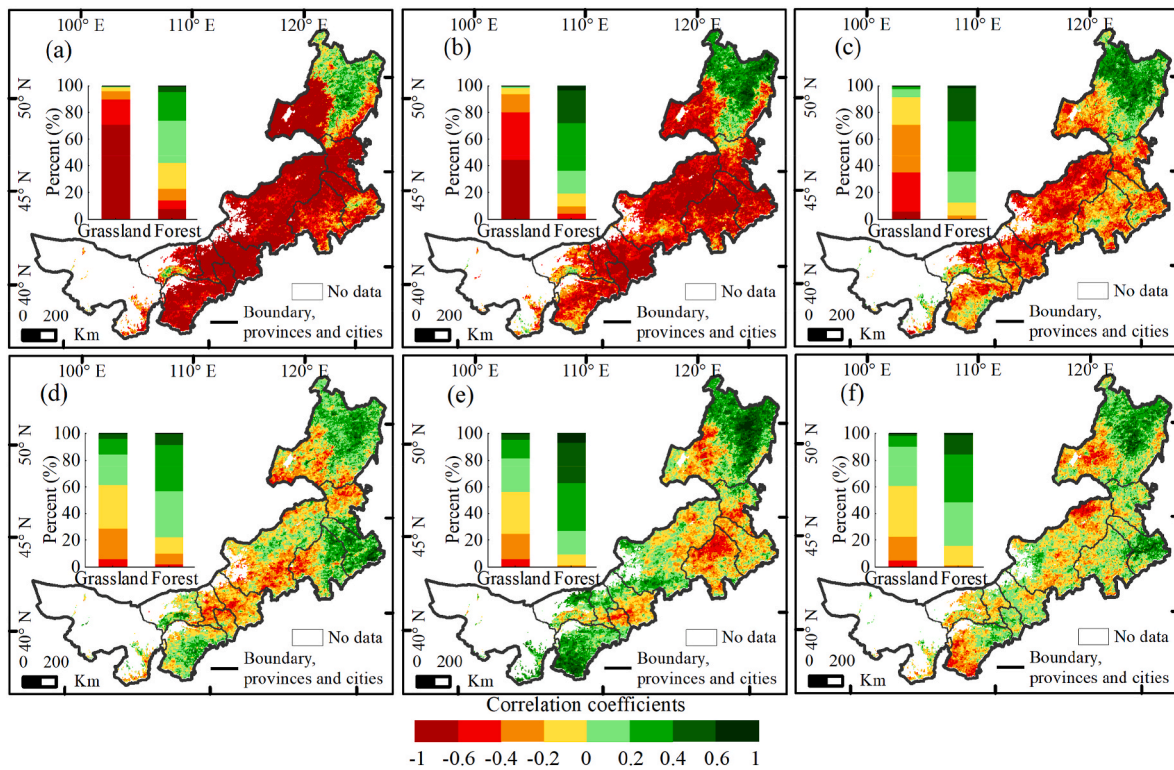


Fig. 5. Spatial distributions of the correlation coefficients between PP_{max} and LST_{day} (a–c) and LST_{night} (d–f) of July (a, d), August (b, e), and September (c, f) over the study areas from 2001 to 2020.

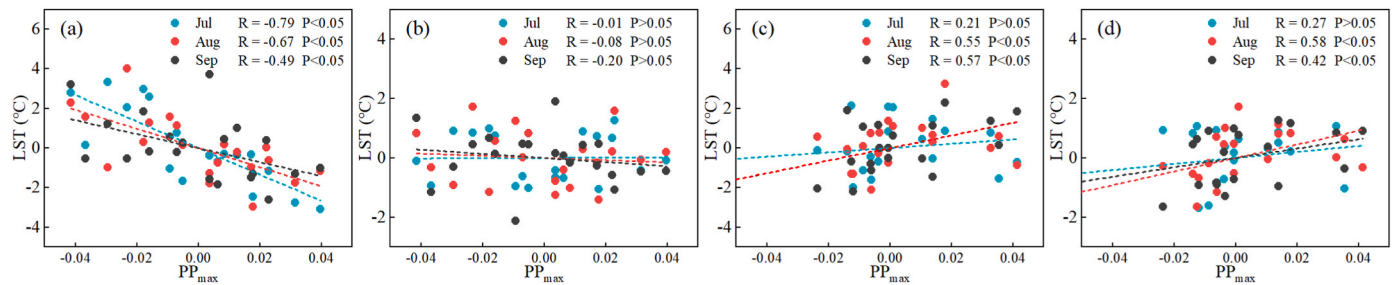


Fig. 6. Correlations between PP_{max} and LST_{day} (a, c) and LST_{night} (b, d) for different biomes: grassland (a, b) and forest (b, d). (Jul: July, Aug: August, Sep: September).

by which PP_{max} affected LST indirectly: the “ET effect” (“ PP_{max} - ET - LST”), “albedo effect” (“ PP_{max} - albedo - LST”), and “BBE effect” (“ PP_{max} - BBE - LST”). In the grassland biome, the SEM results showed that PP_{max} enhancement significantly increased both ET ($P < 0.001$) and BBE ($P < 0.001$), and decreased albedo ($P < 0.001$) in all months of the post-season (Fig. 9a–c). However, only the “ET effect” was a primary pathway responsible for the variation in LST_{day} based on its significant pathway coefficient ($P < 0.05$), suggesting that enhanced peak photosynthetic production cooled the LST_{day} through increasing ET during the late growing season. Interestingly, such a cooling effect of PP_{max} on LST_{day} was weakened progressively from July (standardized indirect effect (SIE) = -0.94) to September (SIE = -0.54) (Fig. 9a–c). With regard to LST_{night} , variations in ET, albedo, and BBE induced by increased PP_{max} were not the intermediate explanatory factors in the correlation between LST_{night} and PP_{max} , primarily due to non-significant pathway coefficients (ET/albedo/BBE \rightarrow LST_{night} : $P > 0.05$; Fig. 9a–c), as well as very low SIE values for all months (Fig. 10).

In the forest biome, although PP_{max} affected some surface energy balance factors (such as albedo in all months and BBE in September) significantly, variations in PP_{max} had a limited effect on both LST_{day} and

LST_{night} over all months of the post-season via the “ET effect,” “albedo effect,” and “BBE effect,” as observed by inapparent pathway coefficients ($P > 0.05$; Fig. 9d–f) and negligible SIE values (almost all < 0.3 ; Fig. 10). The phenomenon suggests that the warming effects of increased peak photosynthetic production on LST variations during the daytime and nighttime were independent of variations in ET, albedo, and BBE in the forest ecosystem. In addition, we observed similar patterns for each biome and month when employing the ridge regression model (Tables S2–3), to further verify the robustness of the SEM results. In other words, variations in LST_{day} in the grassland biome were more sensitive (as reflected by the regression coefficient being significant at a level of 0.05) to ET than to albedo and BBE during all months (Table S2). However, there was no significant regression coefficients between LST and the three surface energy balance factors in grassland LST_{night} or forest LST_{day}/LST_{night} in most months (Tables S2–3).

4. Discussion

Peak season photosynthetic activities (PP_{max} and PPT) derived from SIF GPP, NDVI, and NIR_v had similar spatial heterogeneity gradients

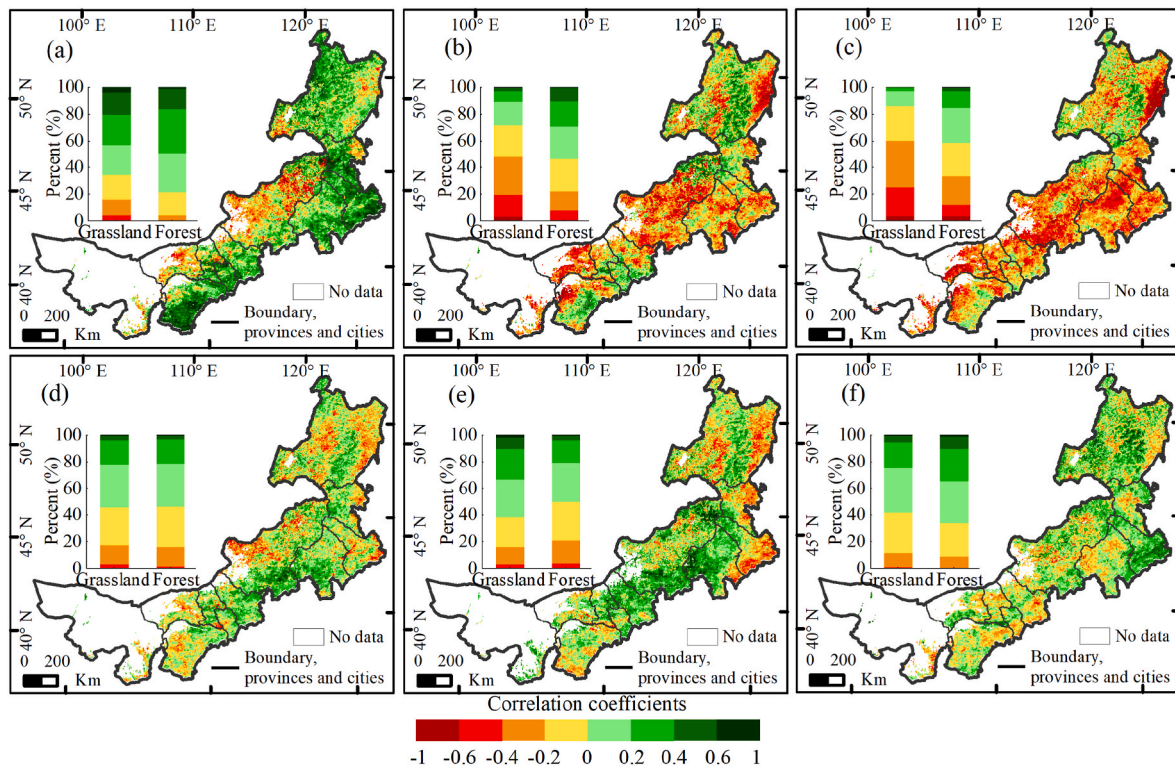


Fig. 7. Spatial distributions of the correlation coefficients between PPT and LST_{day} (a–c) and LST_{night} (d–f) of July (a, d), August (b, e), and September (c, f) over the study area from 2001 to 2020.

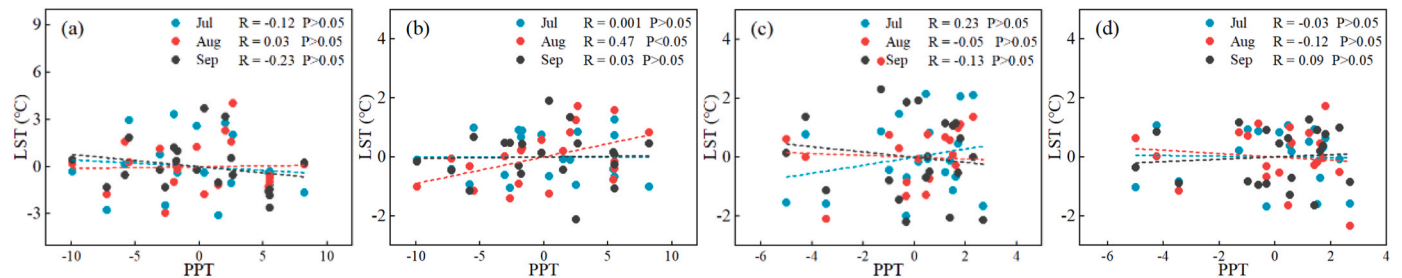


Fig. 8. Correlations between PPT and LST_{day} (a, c) and LST_{night} (b, d) for different biomes: grassland (a, b) and forest (b, d). (Jul: July, Aug: August, Sep: September).

across the IM (Fig. S1). On average, the forest biome in northeastern IM had a higher PP_{max} and attained an earlier PPT than the grassland biome. However, it is noteworthy that PPT inferred from the SIF GPP generally occurred earlier than the other VI-based estimates (NDVI and NIR_v) (Fig. S1). This finding is consistent with the global scale work of Wang et al. (2020), who investigated the patterns of peak growing season based on optical, microwave, and fluorescence satellite data, and found that SIF-PPT occurred earlier than NDVI-PPT and Vegetation optical depth (VOD)-PPT for temperate grasslands. SIF is an optical signal directly emitted by plants during the light-based reactions of photosynthesis, whereas NDVI and NIR_v are greenness indices based on canopy reflectance of vegetation seasonality (Badgley et al., 2017; Tucker et al., 2001). Photosynthesis begins to translate prior to changes in leaf coloration in response to biophysical constraints such as shorter day length, cooler temperatures, and/or progressive water constraints (Buermann et al., 2018; Estiarte and Peñuelas, 2015), while canopy chlorophyll content appears to persist for a significant amount of time following the downregulation of photosynthesis (Zhang et al., 2019). This probably explains why the SIF GPP-based PPT occurred relatively early compared with the PPT derived from the vegetation greenness indices. Nevertheless, the discrepancy among the different datasets did

not affect the interannual variations in either PP_{max} or PPT. Overall, we found enhanced PP_{max} and advanced PPT across the study region during 2001–2020 (4), which is consistent with previous findings of increased net carbon uptake and a shift toward an earlier peak growing season owing to climate warming (Gonsamo et al., 2018; Park et al., 2019). Our findings further confirmed those of many other studies showing that, in terms of temporal trends, the SIF and vegetation greenness indices were highly consistent in temperate grasslands (Wang et al., 2020).

It is widely acknowledged that phenological events, such as SOS and EOS, play crucial roles in regulation of vegetation feedbacks to climate via the exertion of a paramount influence on the intra-seasonal variation in surface biophysical properties (Shen et al., 2022; Xu et al., 2020). However, we found a weak impact of PPT on post-season (July to September) LST over the last two decades (Figs. 7–8). This discrepancy in the roles of different seasonal phenological events may be attributed to differences in the magnitudes of changes in vegetation growth before and after these events. Rapid changes in plant growth status accompanying spring onset and autumn dormancy can induce radiative (related to surface albedo changes) and non-radiative (related to changes in ET) biophysical changes, resulting in abrupt shifts in surface water fluxes and energy partitioning between sensible and latent heat (Moore et al.,

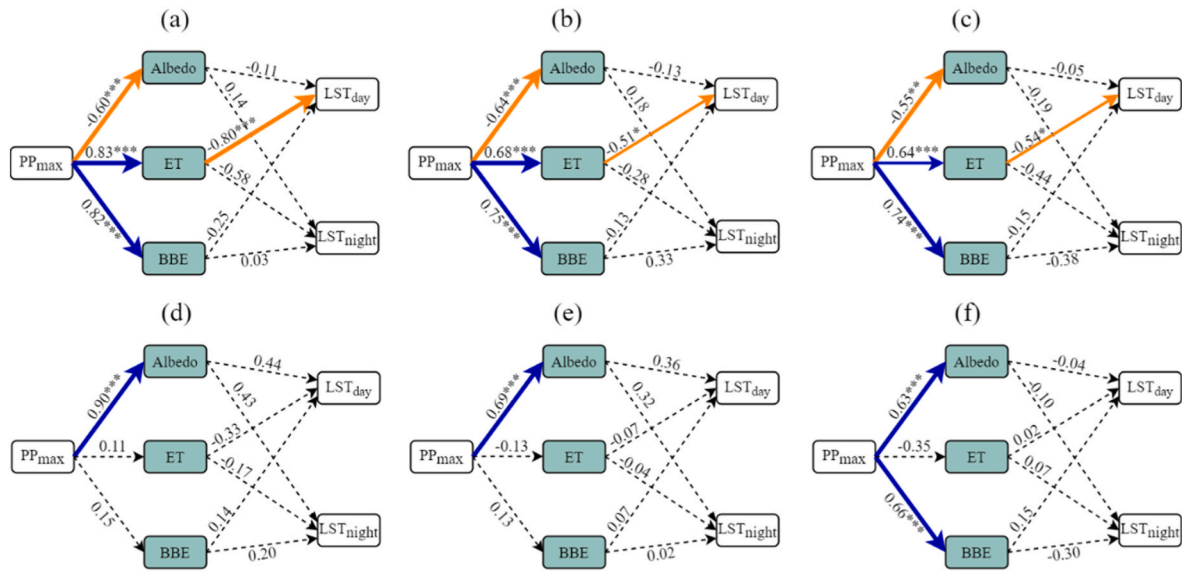


Fig. 9. Structural equation modeling (SEM) results of the relationships between PP_{max} and ET, BBE and albedo attributes of LST in grassland (a, July; b, August; c, September) and forest (d, July; e, August; f, September) biomes. Blue arrows indicate significant positive relationships while red arrows indicate significant negative relationships. Black dashed arrows indicate insignificant relationships. Numbers adjacent to arrows are pathway coefficients and are indicative of the effect size of the relationship. (*, **, and *** represent significance levels at $P < 0.05$, $P < 0.01$, and $P < 0.001$, respectively). Goodness-of-fit statistics for SEM are shown in Table S1.

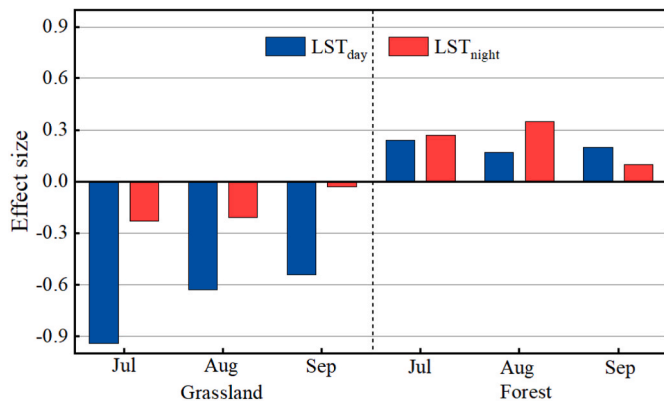


Fig. 10. Standardized indirect effect (SIE) of PP_{max} on the variation in LST_{day} and LST_{night} for grassland and forest biomes in each month. Positive and negative values indicate warming and cooling effects of PP_{max} on LST, respectively. (Jul: July, Aug: August, Sep: September).

1996; Piao et al., 2019; Richardson et al., 2013). However, owing to the persistent nature of the maturity stage (Gonsamo et al., 2018), the occurrence of the PPT rarely results in significant changes in surface biophysical processes (Li et al., 2015). Compared with PPT, PP_{max} exhibited a significant time-lagged effect on LST for the post-season period, with considerable differences between diurnal periods (daytime and nighttime) and among different biomes (grassland and forest) (Figs. 5–6). Additionally, our analysis revealed that the relationship between PP_{max} and LST_{mean} and LST_{DTR} exhibited similar patterns to the relationships observed between PP_{max} and LST_{day} (Figs. S3-4). This finding implies a major determinant of the change trend of LST_{day} for the variations of LST_{mean} and LST_{DTR} , and underscores the importance of understanding the feedback mechanisms of PP_{max} on LST_{day} .

In the grassland biome, PP_{max} was negatively correlated with LST_{day} during the post-season period (Fig. 5a–c), indicating that enhanced PP_{max} had a cooling effect on LST_{day} during the late growing season in the grassland ecosystem. Additionally, the SEM result displayed that this negative legacy feedback of PP_{max} on LST_{day} in grasslands was primarily caused by increase in ET, rather than a decrease in albedo or an increase

in BBE. This result is consistent with previous research on Tibetan alpine grasslands reported by Shen et al. (2015), who revealed that enhanced vegetation activity during the growing season may mitigate daytime warming by enhancing ET, a cooling process, based on coupling regional weather research and forecasting mesoscale model simulations. An increase in ET induced by greening was paralleled by a proportional decrease in sensible heat, and less available surface energy dissipated as latent heat favors evaporative cooling of the surface (Lian et al., 2022; Xu et al., 2020). Nevertheless, some studies have demonstrated that the greening-induced warming effect of lower albedo would offset the cooling effect of higher ET on temperature during the growing season, owing to the greater absorption of incoming shortwave radiation over the temperate grasslands of China (Shen et al., 2022). In the present study, although the surface albedo decreased with an increase in PP_{max} , albedo variations had no decisive effect on post-season LST_{day} variations in the grassland biome. Such uncertainties are predominantly a result of the season-dependent balance between the ET-induced cooling effect and albedo-induced warming effect; that is, the strength of evaporative cooling dwindles gradually toward colder and drier seasons, while the strength of albedo warming increases (Li et al., 2015; Lian et al., 2022). Consequently, the warming effect of vegetation greening throughout the growing season can be attributed to the masking effect of warming induced by decreased albedo during spring and autumn on the cooling effect of increased ET during summer (Shen et al., 2022). This phenomenon may also be the reason that the cooling effect of PP_{max} on LST_{day} weakened progressively from July to September (Fig. 6a). Furthermore, the cooling effect resulting from enhanced PP_{max} persists at nighttime, albeit at a significantly lower magnitude compared with the daytime (Fig. 5d-f), which is consistent with previous studies that demonstrated a stronger interplay between vegetation greening and surface temperature during the daytime than nighttime in arid regions (Forzieri et al., 2017). During the daytime, vegetation can dissipate sensible heat more efficiently through turbulent diffusion and cools down faster than at nighttime under stably stratified conditions (Rigden and Li, 2017). Such a diurnal difference may also be partially attributed to the intensity of ET. Generally, ET is a major contributor to daytime cooling owing to higher transpiration rates during the daytime, while its contribution is relatively low during the nighttime (Wang et al., 2014). In addition, it is worth mentioning that, despite the lack of statistical significance ($P > 0.05$) in the pathway coefficients (BBE →

LST_{day}/LST_{night}), an increase in BBE may have a complementary role in the cooling effect of PP_{max} on LST, which varies within a diurnal cycle (Fig. 9a–c). An increase in PP_{max} enhances BBE, resulting in greater transmission of longwave energy from land surface to atmosphere. This amplifies atmospheric thermal forcing and cools the land surface, especially at night (Liu et al., 2020).

For the forest biome, we found a symmetrical warming effect of PP_{max} on LST_{day} and LST_{night} throughout the post-season, as evidenced by similar signs and magnitudes (Fig. 6c and d). In contrast to the grassland biome, SEM analysis showed that the direct effects of ET, albedo, and BBE on LST in the forest biome were relatively negligible (Fig. 9d–f). Despite the cooling effect of ET being amplified under humid conditions (Li et al., 2015), it is restricted to the high-latitude northern boreal and Arctic regions with colder temperatures and lower solar radiation (Forzieri et al., 2017; Zeng et al., 2017), implying a weaker explanatory power of ET for LST in colder regions (Peng et al., 2014). This partially explains why ET cooling had a limited influence on LST over the forest biome in our study, which was mainly distributed in higher latitudes between 48 and 54° N, as well as higher altitudes in the Greater Khingan Mountains. Notably, in addition to affecting how the land surface dissipates absorbed energy, ET affects how much energy the surface absorbs indirectly through water vapor and clouds (Ramstein et al., 1998). For instance, Xu et al. (2020) found that ET-induced greening enhanced the water vapor release from the surface to the upper layers of the atmosphere in the northern temperate and boreal regions without water stress. Consequently, the additional boundary-layer water vapor increases the frequency of cumulus clouds, which absorb surface long-wave radiation and emit part of it back to the surface as downward longwave radiation, ultimately warming the LST (Xu et al., 2020). In terms of albedo, our study observed an increased albedo in the forest biome instead of the expected decrease associated with greening, and the variation in albedo exerted a greater impact on LST than did either ET or BBE, despite the non-significance of these variables (Fig. 9d–f). There exists a critical threshold at approximately 50% canopy cover where a turning point in albedo change trends occurs with greening (Lukeš et al., 2014). Below the threshold, albedo decreases as vegetation coverage increases, while above the threshold, albedo increases with an increase in vegetation coverage (Lukeš et al., 2014). The observed increase in albedo as forest greening can presumably be explained by the fact that increasing forest coverage is accompanied by more bright canopies and less dark gaps, leading to an increasing albedo in summer (Abera et al., 2019; Yan et al., 2021). Therefore, findings from grassland or afforested areas cannot simply be transferred to a forest biome with lower interannual variance (Fig. S7). In addition, unlike grassland biome, the greening of forest biome has a minor impact on the BEE at forest biome (Fig. 9), which can be attributed to the fact that the BBE remains relatively constant over dense vegetation (Ogawa and Schmugge, 2004). Furthermore, the symmetrical feedback of PP_{max} to LST during the daytime and nighttime in the forest biome can be attributed to its larger heat capacity compared to the grassland biome (Richardson et al., 2013), which leads to slower heat loss and warm canopies at night (Houspanossian et al., 2013).

In summary, our study examined the signs, magnitude, and underlying mechanism of feedback of peak season photosynthetic activities to LST within grassland and forest biomes. The result revealed divergent impacts of interannual variations in peak season photosynthetic productivity on LST across different biomes, highlighting the different feedbacks between widespread greening and cases of vegetation-type replacement (i.e., afforestation). However, it is worth mentioning that the widespread greening observed in the grassland biome may include the relative contributions of ecological engineering efforts (Tong et al., 2018), as reforestation and afforestation programmes have been actively implemented since the 1980s (Chen et al., 2019). Consequently, it is necessary to conduct a comprehensive examination into vegetation type alterations and elucidate the temperature feedback mechanisms associated with different conversion types in future research. Furthermore,

the dominant evaporative cooling effect identified in our study demonstrates a diminishing or potentially reversing trend with increasing surface moisture content (Fig. 11), exactly as the observed shifts from substantial cooling effects in grassland areas to non-significant effect in forested regions. Nevertheless, it should be noted that while it is widely acknowledged that the greening-induced ET affects the dissipation of surface energy, it also has an impact on the absorption of surface energy through water vapor and clouds (Ramstein et al., 1998). Therefore, the effect of cloud cover also needs to be considered in further attribution analysis to accurately quantify another facet of the ET effect induced by greening. Moreover, there are uncertainties regarding the robustness of satellite-derived LST in accurately capturing the local thermal conditions, despite previous studies advocating that LST can better reflect the pure climate impact from land surface greening (Li et al., 2023). Future studies need to integrate adequate observations and credible climate model estimates of thermal conditions. Additionally, considering that phenological events exhibit interannual variations typically on the scale of a few days, the use of monthly mean LST in our study may result in the underestimation of the phenological effects on LST. Therefore, subsequent studies require more detailed LST data, such as daily-scale observations, to quantify the feedback of phenological changes on LST.

5. Conclusions

In this study, we utilized a SEM to investigate the feedback of peak season photosynthetic activities (PP_{max} and PPT) on local surface temperature, mediated by key surface energy balance factors (ET, albedo, and BBE) over IM during the period 2001–2020. Our analysis presents robust and conclusive evidence of the time-lagged influence of increased PP_{max} , rather than advanced PPT, on LST during the post-season period (July to September), with divergent signs and magnitudes across diurnal periods and among different biomes. Specifically, increased PP_{max} cooled the LST_{day}/LST_{night} in the grassland biome, with a stronger response observed on LST_{day} than in the LST_{night} . However, increased PP_{max} resulted in a symmetrical warming effect on LST_{day}/LST_{night} in the forest biome. Our pathway analysis further revealed that the “ET effect”, which outweighs the “albedo effect” and “BBE effect”, was the primary intermediate explanatory factor for the cooling effect of greening on the LST in the grassland biome, particularly during the daytime, with its influence gradually diminishing as the season progressed. However, none of these effects had a direct impact on the correlation between PP_{max} and LST during either the daytime or the nighttime in the forest biome. The findings underscore the divergent feedback mechanisms of peak season photosynthetic productivity on LST across different biomes, which are influenced by background climatic conditions and extent of greening. The results of the present study provide valuable insights that facilitate the comprehension of greening-induced biophysical feedbacks in an ecosystem sense.

CRedit authorship contribution statement

Wendu Rina: Conceptualization, Data curation, Formal analysis, Writing – original draft. **Yuhai Bao:** Writing – review & editing, Project administration, Supervision. **Enliang Guo:** Methodology, Software, Investigation. **Siqin Tong:** Data curation, Software. **Xiaojun Huang:** Visualization, Funding acquisition. **Shan Yin:** Supervision, Investigation.

Declaration of competing interest

The authors declare that they have no known competing financial interests or personal relationships that could have appeared to influence the work reported in this paper.

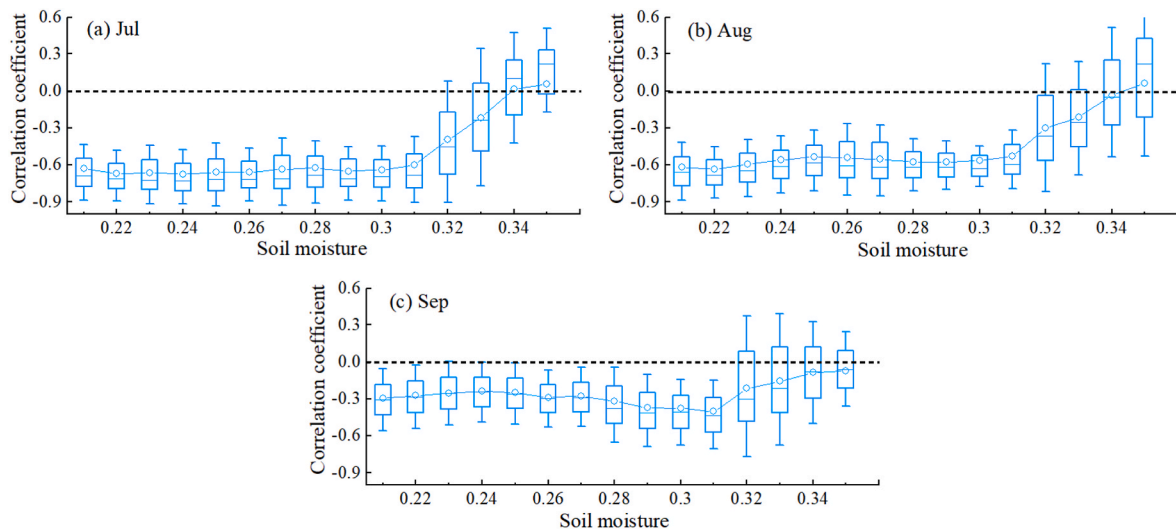


Fig. 11. Correlation coefficients between ET and LST_{day} during the period 2001–2020 along soil moisture gradient across IM. Error bars show standard deviation of pixels in each soil moisture bin.(Jul: July, Aug: August, Sep: September)

Data availability

No data was used for the research described in the article.

Acknowledgments

This work was financially supported by the INTERNATIONAL COOPERATION and Exchange Programs under Grant 41961144019, and the National Natural Science Foundation of China under Grant 41861056. We thankfully acknowledge MODIS, GLASS, GLDAS, and SIF-GPP datasets Science team members for their data making available. We also like to thank anonymous referees and subject editor for the helpful comments.

Appendix A. Supplementary data

Supplementary data to this article can be found online at <https://doi.org/10.1016/j.envres.2023.116643>.

References

- Abera, T.A., Heiskanen, J., Pellikka, P., Rautiainen, M., Maeda, E.E., 2019. Clarifying the role of radiative mechanisms in the spatio-temporal changes of land surface temperature across the Horn of Africa. *Remote Sens. Environ.* 221, 210–224.
- Akritas, M.G., Murphy, S.A., Lavalley, M.P., 1995. The Theil-Sen estimator with doubly censored data and applications to astronomy. *J. Am. Stat. Assoc.* 90, 170–177.
- Badgley, G., Field, C.B., Berry, J.A., 2017. Canopy near-infrared reflectance and terrestrial photosynthesis. *Sci. Adv.* 3, e1602244.
- Bao, G., Chen, J., Chopping, M., Bao, Y., Bayarsaikhan, S., Dorjsuren, A., Tuya, A., Jirigala, B., Qin, Z., 2019. Dynamics of net primary productivity on the Mongolian Plateau: joint regulations of phenology and drought. *Int. J. Appl. Earth Obs. Geoinf.* 81, 85–97.
- Bonan, G.B., Pollard, D., Thompson, S.L., 1992. Effects of boreal forest vegetation on global climate. *Nature* 359.
- Buermann, W., Bikash, P.R., Jung, M., Burn, D.H., Reichstein, M., 2013. Earlier springs decrease peak summer productivity in North American boreal forests. *Environ. Res. Lett.* 8.
- Buermann, W., Forkel, M., O'sullivan, M., Sitch, S., Friedlingstein, P., Haverd, V., Jain, A. K., Kato, E., Kautz, M., Lienert, S., 2018. Widespread seasonal compensation effects of spring warming on northern plant productivity. *Nature* 562, 110–114.
- Chen, C., Park, T., Wang, X., Piao, S., Xu, B., Chaturvedi, R.K., Fuchs, R., Brovkin, V., Ciais, P., Fensholt, R., Tommervik, H., Bala, G., Zhu, Z., Nemani, R.R., Myneni, R.B., 2019. China and India lead in greening of the world through land-use management. *Nat. Sustain.* 2, 122–129.
- Cheng, J., Liang, S., 2013. Effects of thermal-infrared emissivity directionality on surface broadband emissivity and longwave net radiation estimation. *Geosci. Rem. Sens. Lett. IEEE* 11 (2), 499–503.
- Estiarte, M., Peñuelas, J., 2015. Alteration of the phenology of leaf senescence and fall in winter deciduous species by climate change: effects on nutrient proficiency. *Global Change Biol.* 21, 1005–1017.
- Feldman, A.F., Short Gianotti, D.J., Dong, J., Trigo, I.F., Salvucci, G.D., Entekhabi, D., 2023. Tropical surface temperature response to vegetation cover changes and the role of drylands. *Global Change Biol.* 29, 110–125.
- Forzieri, G., Alkama, R., Miralles, D.G., Cescatti, A., 2017. Satellites reveal contrasting responses of regional climate to the widespread greening of Earth. *Science* 356, 1180–1184.
- Forzieri, G., Miralles, D.G., Ciais, P., Alkama, R., Ryu, Y., Duveiller, G., Zhang, K., Robertson, E., Kautz, M., Martens, B., 2020. Increased control of vegetation on global terrestrial energy fluxes. *Nat. Clim. Change* 10, 356–362.
- Gonsamo, A., Chen, J.M., Ooi, Y.W., 2018. Peak season plant activity shift towards spring is reflected by increasing carbon uptake by extratropical ecosystems. *Global Change Biol.* 24, 2117–2128.
- Guo, E., Wang, Y., Jirigala, B., Jin, E., 2020. Spatiotemporal variations of precipitation concentration and their potential links to drought in mainland China. *J. Clean. Prod.* 267.
- Hadi Pfeifer, M., Korhonen, L., Wheeler, C., Rautiainen, M., 2017. Forest canopy structure and reflectance in humid tropical Borneo: a physically-based interpretation using spectral invariants. *Remote Sens. Environ.* 201, 314–330.
- Houspanossian, J., Noretto, M., Jobbagy, E.G., 2013. Radiation budget changes with dry forest clearing in temperate Argentina. *Global Change Biol.* 19, 1211–1222.
- Huang, K., Xia, J., Wang, Y., Ahlstrom, A., Chen, J., Cook, R.B., Cui, E., Fang, Y., Fisher, J.B., Huntzinger, D.N., Li, Z., Michalak, A.M., Qiao, Y., Schaefer, K., Schwalm, C., Wang, J., Wei, Y., Xu, X., Yan, L., Bian, C., Luo, Y., 2018. Enhanced peak growth of global vegetation and its key mechanisms. *Nature Ecology & Evolution* 2, 1897–1905.
- Huang, A., Xu, X., Jia, G., Shen, R., 2022. Asymmetrical cooling effects of Amazonian protected areas across spatiotemporal scales. *Environ. Res. Lett.* 17.
- Jeong, S.-J., Ho, C.-H., Gim, H.-J., Brown, M.E., 2011a. Phenology shifts at start vs. end of growing season in temperate vegetation over the Northern Hemisphere for the period 1982–2008. *Global Change Biol.* 17, 2385–2399.
- Jeong, S.-J., Ho, C.-H., Park, T.-W., Kim, J., Levis, S., 2011b. Impact of vegetation feedback on the temperature and its diurnal range over the Northern Hemisphere during summer in a 2× CO₂ climate. *Clim. Dynam.* 37, 821–833.
- Kuo, C., Feldman, D.R., Huang, X., Flanner, M., Yang, P., Chen, X., 2018. Retracted: time-dependent cryospheric longwave surface emissivity feedback in the community earth system model. *J. Geophys. Res. Atmos.* 123, 789–813.
- Lee, X., Goulden, M.L., Hollinger, D.Y., Barr, A., Black, T.A., Bohrer, G., Bracho, R., Drake, B., Goldstein, A., Gu, L., Katul, G., Kolb, T., Law, B.E., Margolis, H., Meyers, T., Monson, R., Munger, W., Oren, R., Paw, U.K., Richardson, A.D., Schmid, H.P., Staebler, R., Wofsy, S., Zhao, L., 2011. Observed increase in local cooling effect of deforestation at higher latitudes. *Nature* 479, 384–387.
- Li, B., 1962. The basic types of the zonal vegetation on Inner Mongolia and its ecological geographic rule. *Journal of Inner Mongolia University (Natural Sciences Edition)* 4, 41–71.
- Li, B., 1990. The principle, method, and application of ecological regionalization—explanation of the ecological regionalization map of the Inner Mongolia Autonomous Region. *Chinese Journal of Plant Ecology* 14, 55.
- Li, X., Xiao, J., 2019. A global, 0.05-degree product of solar-induced chlorophyll fluorescence derived from OCO-2, MODIS, and reanalysis data. *Rem. Sens.* 11, 517.
- Li, Y., Zhao, M., Motesharrei, S., Mu, Q., Kalnay, E., Li, S., 2015. Local cooling and warming effects of forests based on satellite observations. *Nat. Commun.* 6, 1–8.
- Li, Y., Zhao, M., Mildrexler, D.J., Motesharrei, S., Mu, Q., Kalnay, E., Zhao, F., Li, S., Wang, K., 2016. Potential and actual impacts of deforestation and afforestation on land surface temperature. *J. Geophys. Res. Atmos.* 121 (14), 314–386, 372.

- Li, C., Wang, J., Hu, R., Yin, S., Bao, Y., Ayal, D.Y., 2018. Relationship between vegetation change and extreme climate indices on the Inner Mongolia Plateau, China, from 1982 to 2013. *Ecol. Indic.* 89, 101–109.
- Li, Y., Li, Z.L., Wu, H., Zhou, C., Liu, X., Leng, P., Yang, P., Wu, W., Tang, R., Shang, G.F., Ma, L., 2023. Biophysical impacts of earth greening can substantially mitigate regional land surface temperature warming. *Nat. Commun.* 14, 121.
- Lian, X., Jeong, S., Park, C.E., Xu, H., Li, L.Z.X., Wang, T., Gentine, P., Penuelas, J., Piao, S., 2022. Biophysical impacts of northern vegetation changes on seasonal warming patterns. *Nat. Commun.* 13, 3925.
- Liang, S., Zhao, X., Liu, S., Yuan, W., Cheng, X., Xiao, Z., Zhang, X., Liu, Q., Cheng, J., Tang, H., 2013. A long-term Global Land Surface Satellite (GLASS) data-set for environmental studies. *International Journal of Digital Earth* 6, 5–33.
- Liu, Y., Zhang, Y., Huang, K., Zu, J., Chen, N., Cong, N., 2020. Increased surface broadband emissivity driven by denser vegetation on the Tibetan plateau grassland area. *Journal of the Indian Society of Remote Sensing* 48, 1845–1859.
- Lukes, P., Rautiainen, M., Manninen, T., Stenberg, P., Möttönen, M., 2014. Geographical gradients in boreal forest albedo and structure in Finland. *Remote Sens. Environ.* 152, 526–535.
- Moore, K.E., Fitzjarrald, D.R., Sakai, R.K., Goulden, M.L., Munger, J.W., Wofsy, S.C., 1996. Seasonal variation in radiative and turbulent exchange at a deciduous forest in central Massachusetts. *J. Appl. Meteorol. Climatol.* 35, 122–134.
- Ogawa, K., Schmugge, T., 2004. Mapping surface broadband emissivity of the Sahara Desert using ASTER and MODIS data. *Earth Interact.* 8, 1–14.
- Park, T., Chen, C., Macias-Fauria, M., Tommervik, H., Choi, S., Winkler, A., Bhatt, U.S., Walker, D.A., Piao, S., Brovkin, V., Nemani, R.R., Myneni, R.B., 2019. Changes in timing of seasonal peak photosynthetic activity in northern ecosystems. *Global Change Biol.* 25, 2382–2395.
- Peng, S.S., Piao, S., Zeng, Z., Ciais, P., Zhou, L., Li, L.Z., Myneni, R.B., Yin, Y., Zeng, H., 2014. Afforestation in China cools local land surface temperature. *Proc. Natl. Acad. Sci. U.S.A.* 111, 2915–2919.
- Peñuelas, J., Filella, I., 2009. Phenology feedbacks on climate change. *Science* 324, 887–888.
- Piao, S., Fang, J., Zhou, L., Ciais, P., Zhu, B., 2006. Variations in satellite-derived phenology in China's temperate vegetation. *Global Change Biol.* 12, 672–685.
- Piao, S., Wang, X., Park, T., Chen, C., Lian, X., He, Y., Bjerke, J.W., Chen, A., Ciais, P., Tommervik, H., Nemani, R.R., Myneni, R.B., 2019. Characteristics, drivers and feedbacks of global greening. *Nat. Rev. Earth Environ.* 1, 14–27.
- Pitman, A.J., Avila, F.B., Abramowitz, G., Wang, Y.P., Phipps, S.J., de Noblet-Ducoudré, N., 2011. Importance of background climate in determining impact of land-cover change on regional climate. *Nat. Clim. Change* 1, 472–475.
- Ramstein, G., Treut, S.L., Treut, H.L., Forichon, M., Joussaume, S., 1998. Cloud processes associated with past and future climate changes. *Clim. Dynam.* 14, 233–247.
- Richardson, A.D., Keenan, T.F., Migliavacca, M., Ryu, Y., Sonnentag, O., Toomey, M., 2013. Climate change, phenology, and phenological control of vegetation feedbacks to the climate system. *Agric. For. Meteorol.* 169, 156–173.
- Rigden, A.J., Li, D., 2017. Attribution of surface temperature anomalies induced by land use and land cover changes. *Geophys. Res. Lett.* 44, 6814–6822.
- Shen, M., Piao, S., Jeong, S.J., Zhou, L., Zeng, Z., Ciais, P., Chen, D., Huang, M., Jin, C.S., Li, L.Z., Li, Y., Myneni, R.B., Yang, K., Zhang, G., Zhang, Y., Yao, T., 2015. Evaporative cooling over the Tibetan Plateau induced by vegetation growth. *Proc. Natl. Acad. Sci. U.S.A.* 112, 9299–9304.
- Shen, X., Liu, B., Henderson, M., Wang, L., Jiang, M., Lu, X., 2022. Vegetation greening, extended growing seasons, and temperature feedbacks in warming temperate grasslands of China. *J. Clim.* 35, 5103–5117.
- Suld, B., Jie, Y., Zhiqiang, W., Rui, G., Yulong, Y., Qingzhu, G., 2015. Climate change and its impacts on distribution pattern of grassland types in inner Mongolia. *Chin. J. Agrometeorol.* 36 (2), 139.
- Swann, A.L., Fung, I.Y., Chiang, J.C., 2012. Mid-latitude afforestation shifts general circulation and tropical precipitation. *Proc. Natl. Acad. Sci. U.S.A.* 109, 712–716.
- Tong, X., Brandt, M., Yue, Y., Horion, S., Wang, K., Keersmaecker, W.D., Tian, F., Schurgers, G., Xiao, X., Luo, Y., Chen, C., Myneni, R., Shi, Z., Chen, H., Fensholt, R., 2018. Increased vegetation growth and carbon stock in China karst via ecological engineering. *Nat. Sustain.* 1, 44–50.
- Tucker, C.J., Slayback, D.A., Pinzon, J.E., Los, S.O., Myneni, R.B., Taylor, M.G., 2001. Higher northern latitude normalized difference vegetation index and growing season trends from 1982 to 1999. *Int. J. Biometeorol.* 45, 184–190.
- Vitasse, Y., Signarbieux, C., Fu, Y.H., 2018. Global warming leads to more uniform spring phenology across elevations. *Proc. Natl. Acad. Sci. U.S.A.* 115, 1004–1008.
- Wang, L., Good, S.P., Caylor, K.K., 2014. Global synthesis of vegetation control on evapotranspiration partitioning. *Geophys. Res. Lett.* 41, 6753–6757.
- Wang, L., Lee, X., Schultz, N., Chen, S., Wei, Z., Fu, C., Gao, Y., Yang, Y., Lin, G., 2018. Response of surface temperature to afforestation in the Kubuqi desert, inner Mongolia. *J. Geophys. Res. Atmos.* 123, 948–964.
- Wang, X., Dannenberg, M.P., Yan, D., Jones, M.O., Kimball, J.S., Moore, D.J.P., Leeuwen, W.J.D., Didan, K., Smith, W.K., 2020. Globally consistent patterns of asynchrony in vegetation phenology derived from optical, microwave, and fluorescence satellite data. *J. Geophys. Res.: Biogeosciences* 125.
- Xie, Z., Zhu, W., Qiao, K., Li, P., Liu, H., 2021. Joint influence mechanism of phenology and climate on the dynamics of gross primary productivity: insights from temperate deciduous broadleaf forests in North America. *J. Geophys. Res.: Biogeosciences* 126, e2020JG006049.
- Xu, C., Liu, H., Williams, A.P., Yin, Y., Wu, X., 2016. Trends toward an earlier peak of the growing season in Northern Hemisphere mid-latitudes. *Global Change Biol.* 22, 2852–2860.
- Xu, X., Riley, W.J., Koven, C.D., Jia, G., Zhang, X., 2020. Earlier leaf-out warms air in the north. *Nat. Clim. Change* 10, 370–375.
- Xue, Y., Lu, H., Guan, Y., Tian, P., Yao, T., 2021. Impact of thermal condition on vegetation feedback under greening trend of China. *Sci. Total Environ.* 785, 147380.
- Yan, H., Wang, S., Dai, J., Wang, J., Chen, J., Shugart, H.H., 2021. Forest greening increases land surface albedo during the main growing period between 2002 and 2019 in China. *J. Geophys. Res. Atmos.* 126 (6), e2020JD033582.
- Yu, L., Leng, G., 2022. Identifying the paths and contributions of climate impacts on the variation in land surface albedo over the Arctic. *Agric. For. Meteorol.* 313, 108772.
- Zeng, Z., Piao, S., Li, L.Z.X., Zhou, L., Ciais, P., Wang, T., Li, Y., Lian, X., Wood, E.F., Friedlingstein, P., Mao, J., Estes, L.D., Myneni, Ranga B., Peng, S., Shi, X., Seneviratne, S.I., Wang, Y., 2017. Climate mitigation from vegetation biophysical feedbacks during the past three decades. *Nat. Clim. Change* 7, 432–436.
- Zhang, Z., Chen, J.M., Guanter, L., He, L., Zhang, Y., 2019. From canopy-leaving to total canopy far-red fluorescence emission for remote sensing of photosynthesis: first results from TROPOMI. *Geophys. Res. Lett.* 46, 12030–12040.
- Zheng, L., Zhao, G., Dong, J., Ge, Q., Tao, J., Zhang, X., Qi, Y., Doughty, R.B., Xiao, X., 2019. Spatial, temporal, and spectral variations in albedo due to vegetation changes in China's grasslands. *ISPRS J. Photogrammetry Remote Sens.* 152, 1–12.
- Zhou, L., Dickinson, R.E., Tian, Y., Jin, M., Ogawa, K., Yu, H., Schmugge, T., 2003. A sensitivity study of climate and energy balance simulations with use of satellite-derived emissivity data over Northern Africa and the Arabian Peninsula. *J. Geophys. Res. Atmos.* 108 (D24).
- Zhou, L., Dickinson, R.E., Tian, Y., Vose, R.S., Dai, Y., 2007. Impact of vegetation removal and soil aridation on diurnal temperature range in a semiarid region: application to the Sahel. *Proc. Natl. Acad. Sci. USA* 104, 17937–17942.
- Zhou, L., Dickinson, R., Dirmeyer, P., Chen, H., Dai, Y., Tian, Y., 2008. Asymmetric response of maximum and minimum temperatures to soil emissivity change over the Northern African Sahel in a GCM. *Geophys. Res. Lett.* 35 (5).
- Zhu, Z., Piao, S., Myneni, R.B., Huang, M., Zeng, Z., Canadell, J.G., Ciais, P., Sitch, S., Friedlingstein, P., Arneeth, A., Cao, C., Cheng, L., Kato, E., Koven, C., Li, Y., Lian, X., Liu, Y., Liu, R., Mao, J., Pan, Y., Peng, S., Peñuelas, J., Poulter, B., Pugh, T.A.M., Stocker, B.D., Viovy, N., Wang, X., Wang, Y., Xiao, Z., Yang, H., Zaehle, S., Zeng, N., 2016. Greening of the earth and its drivers. *Nat. Clim. Change* 6, 791–795.
- Zhu, Y., Zhang, Y., Zheng, Z., Liu, Y., Wang, Z., Cong, N., Zu, J., Tang, Z., Zhao, G., Gao, J., Sun, Y., 2022. Converted vegetation type regulates the vegetation greening effects on land surface albedo in arid regions of China. *Agric. For. Meteorol.* 324.



Parallel acceleration of vegetation growth rate and senescence rate across the Northern Hemisphere from 1982 to 2015

Wendu Rina^{a,b}, Gang Bao^{a,b,*}, Quansheng Hai^{c,d}, Jiquan Chen^e, Enliang Guo^a, Fei Li^f, Yuhai Bao^{a,b}, Lijuan Miao^g, Xiaojun Huang^{a,b}

^a College of Geographical Science, Inner Mongolia Normal University, Hohhot 010022, China

^b Inner Mongolia Key Laboratory of Remote Sensing and Geographic Information Systems, Inner Mongolia Normal University, Hohhot 010022, China

^c Department of Geography, School of Arts and Sciences, National University of Mongolia, Ulaanbaatar 14200, Mongolia

^d Baotou Normal College, Baotou 014030, China

^e Department of Geography, Environment, and Spatial Sciences, Michigan State University, East Lansing, MI 48823, USA

^f Grassland Research Institute, Chinese Academy of Agricultural Sciences, Hohhot 010010, China

^g School of Geographical Sciences, Nanjing University of Information Science & Technology, Nanjing 210044, China

ARTICLE INFO

Keywords:

Vegetation growth and senescence rates
Peak growth
Phenology
Northern Hemisphere
Climate-phenology-canopy development linkages

ABSTRACT

Growth and senescence rates are critical ecological indicators of seasonality shifts of vegetation, with both sensitive to climate change. Here we investigated daily mean vegetation growth and senescence rates, and the major climate forcing across the Northern Hemisphere ($>30^{\circ}\text{N}$) using satellite-derived normalized difference vegetation index (NDVI) and flux-based gross primary productivity (GPP) from 1982 through 2015. Both growth and senescence rates are higher at high latitudes than those at low latitudes, with spatially-averaged values increased by 1.0×10^{-4} and 0.7×10^{-4} NDVI-units-day⁻¹ per degree latitude. These increases were greater in Eurasia than in North America. A parallel acceleration of growth (0.8×10^{-4} NDVI-units-day⁻¹.decade⁻¹) and senescence (0.6×10^{-4} NDVI-units-day⁻¹.decade⁻¹) rates was found for the 34-year study period. The warming-induced increases in vegetation peak growth (peak NDVI) contributed strongly to this parallel acceleration, while unequal advances or delays of three key phenological indicators (the start (SOS), peak (POS), and end (EOS) of the growing season) exerted influential effects on the rates. However, no single climatic factor during any period appeared responsible for the variations in growth and senescence rates. In areas with growth and senescence rates that are determined by peak growth, temperature and precipitation during the growth period accelerated both rates through elevating peak growth. On the other hand, in areas with growth rate determined by SOS, rising temperature before SOS decelerated the growth rate by advancing SOS. In areas with senescence rate determined by EOS, both temperature and radiation during the senescence period contributed to changes in senescence rate by influencing EOS. In sum, a central focus should be placed on the linkages among climate, phenology, and growth and senescence rates for quantifying vegetation seasonality and associated ecosystem function under the changing climate.

* Corresponding author at: College of Geographical Science, Inner Mongolia Normal University, Hohhot 010022, China.
E-mail address: baogang@imnu.edu.cn (G. Bao).

<https://doi.org/10.1016/j.gecco.2023.e02622>

Received 6 April 2023; Received in revised form 30 July 2023; Accepted 4 September 2023

Available online 6 September 2023

2351-9894/© 2023 The Authors. Published by Elsevier B.V. This is an open access article under the CC BY-NC-ND license (<http://creativecommons.org/licenses/by-nc-nd/4.0/>).

1. Introduction

Seasonality shifts in vegetation are one of the most sensitive biological indicators of climate change (Menzel and Fabian, 1999; Park et al., 2015; Richardson et al., 2013). A small change in climate can be directly reflected by shifts in vegetation seasonality, such as the timings of green-up, peak growth, and dormancy (Gonsamo et al., 2015; Liu et al., 2016; Piao et al., 2015). This seasonal variation is a fundamental determinant of many ecosystem processes and functions in earth-atmosphere systems (Peng et al., 2014; Chen et al., 2018; Ma et al., 2022; Shen et al., 2022). In the mid to high latitudes of the Northern Hemisphere (generally North of 30°, NH), vegetation turns green at the start of the growing season (SOS) in spring, reaches its peak growth in summer, and fades at the end of the growing season (EOS) in autumn, with seasonal climate fluctuations (Jeong et al., 2011; Richardson et al., 2009). In recent years, several studies have been conducted on the vegetation growth rate during SOS and the peak of the growing season (POS), showing that the growth rate in the NH has been significantly accelerated due to the rising temperature (Park et al., 2020; Wang et al., 2020). For example, Park et al. (2020) showed that the vegetation green-up rate across the high latitudes (>60°N) of the NH has accelerated by 1.8% month⁻¹.decade⁻¹ in North America and of 1.0% month⁻¹.decade⁻¹ in Eurasia from 1982 to 2016 due to increases in temperature before SOS and atmospheric CO₂ concentration. Wang et al. (2020) reported an accelerated growth rate of alpine grasslands in the Tibetan plateau during 1980–2014. However, these studies focused mostly on the maximum growth rate of vegetation, which corresponds only to the instantaneous growth rate on the date when the vegetation achieves maximum growth during SOS and POS. In contrast, daily mean vegetation growth rate during SOS and POS might be a more important indicator of how climate fine-tunes vegetation growth rate during the entire growth period rather than only at one instantaneous timeframe (Wang et al., 2018). In addition, both SOS and POS tend to advance over the past three decades in most mid- to high-latitudes of the NH (Gonsamo et al., 2015; Jeong et al., 2011). Yet whether these advances have (un)equal responses to climate change and how they influence daily growth rate remain unknown. Here we hypothesize that POS is more responsive to the warming trend and has advanced more than SOS. Consequently, the daily mean growth rate may accelerate due to the shortened growth period, and vice versa. These premises would become more complex if peak growth of vegetation, which was reported to enhance globally (Huang et al., 2018), is considered in the estimates of daily growth rate. Unfortunately, the role of peak growth in vegetation growth rate cannot be well investigated by considering only changes during the growth period, such as from the maximum growth rate.

The vegetation senescence rate from POS in summer to EOS in autumn is another key indicator of canopy development, which reflects the seasonality of vegetation through regulating ecosystem functioning and climate feedback (Piao et al., 2022). However, it is unclear whether the daily mean senescence rate in the NH has accelerated synchronously with the growth rate, as suggested previously (Hong et al., 2022; Wang et al., 2018) due to the normal distribution of vegetation growth cycles (Huete et al., 2002), or has decelerated due to the alleviation of temperature constraints caused by rising temperatures in autumn (Wu et al., 2018). Similar to our hypothesis on the growth rate, (un)equal advances (delays) of the POS and EOS, as well as the enhancement of peak growth (Huang et al., 2018) may have strong influences on variations in daily senescence rate.

Although temperature has been recognized as the primary driver of intra- and inter-annual variations in plant growth in temperate and boreal regions of the NH (Menzel et al., 2006; Jeong et al., 2011), the extent of its influence on plant growth depends largely on the sequence of developmental stages (Seyednasrollah et al., 2018), introducing significant ambiguity regarding vegetation growth and senescence rates. For instance, temperature increase has a strong positive impact on the growth rate during the early growth period, but as spring progresses into summer and the canopy gradually closes, this positive causal relationship diminishes generally, or can be even attenuated by negative impacts (Hong et al., 2022; Piao et al., 2022). In addition, the observed acceleration in growth rate during the early growth period and the deceleration in senescence rate during the early senescence period appeared to attribute earlier SOS and later EOS induced by rising temperatures (Jeong et al., 2011; Liu et al., 2016; Piao et al., 2022), implying the important role of the responses of phenological metrics to temperature in canopy development. Undoubtedly, accurate characterization of the responses of canopy development rate to temperature change requires understanding the linkages among temperature, phenology, and canopy development. Moreover, it is essential to consider the interactive effects from other climatic factors (e.g., precipitation, radiation) on phenological metrics and peak growth of vegetation, because these factors also contribute to vegetation growth (Huang et al., 2018; Liu et al., 2016; Flynn and Wolkovich, 2018). Wu et al. (2021b) revealed that higher radiation advances EOS due to photooxidative stress and/or sink limitation, thereby counteracting the warming-induced delay in EOS. Precipitation not only determines water availability, but is also related to freeze damage during the progression of vegetation growth, but also defining variations in growth and senescence rates through interaction with temperature (Fu et al., 2014; Shen et al., 2014). Clearly, it is necessary to fully consider multiple inter-seasonal climatic factors, from before SOS to arrival of EOS, to comprehensively quantify variations of growth and senescence rates.

In the present study, we used four algorithms to estimate vegetation growth and senescence rates for the NH from 1982 to 2015, using satellite-based normalized difference vegetation index (NDVI) and flux-based gross primary production (GPP) data. The study aimed to answer the following questions: (a) Did growth and senescence rates accelerate synchronously across the NH? (b) How did the phenologies (SOS, POS, and EOS) and summer peak growth (peak NDVI) of vegetation determine variations in growth and senescence rates? (c) How did climate factors affect vegetation growth and senescence rates by altering phenologies and summer peak growth? Answering these questions is of particular importance for a deep understanding of vegetation seasonality during the entire growing period and its responses to climate change at fine temporal scales.

2. Data and methods

2.1. Study area

The study area includes the north of 30°N, where vegetation has clear seasonal variations such as apparent growth and senescence processes (Xu et al., 2016). The climate in the study area broadly includes (B) arid, (C) temperate, (D) continental, and (E) polar and alpine climates, with twenty-four climate subtypes and apparent latitudinal gradients from temperate and arid climates in the low latitudes to continental climates in the middle latitudes and then to polar and alpine climates in the high latitudes and at high altitudes (Fig. 1a). Vegetation in the area encompasses grasslands and croplands at low latitudes, forests at middle latitude, and shrublands and savannas at high latitudes (Fig. 1b). The geographical distributions of climates and vegetation types can be clearly identified in the Köppen-Geiger climate classification map (Fig. 1a) and the MODIS land-cover product (MCD12C1; Fig. 1b), respectively.

2.2. Data

2.2.1. Meteorological data

The meteorological data used in this study include monthly air temperature, precipitation and radiation data of the land component of the fifth generation of the European ReAnalysis (ERA5-Land) dataset with a spatial resolution of 0.1° during 1982–2015. The ERA5-Land dataset was produced by replaying the land component of the European Centre for Medium-Range Weather Forecasts (ECMWF) ERA5 climate reanalysis by incorporating model data together with abundant observations across the globe (<https://cds.climate.copernicus.eu/cdsapp>) (Wu et al., 2022). These data provided continuous global land variables over several decades at an enhanced resolution compared to the previous version, ERA5, and have been successfully used to study ecosystem responses to climate change (Wu et al., 2021a).

2.2.2. NDVI data

The third-generation Global Inventory Modelling and Mapping Studies (GIMMS) NDVI dataset, with a spatial resolution of 0.0833° and a temporal resolution of 15-day for 1982–2015 (Pinzon and Tucker, 2014), was used to determine daily growth rate and senescence rate. The GIMMS NDVI is the most widely used NDVI dataset in vegetation dynamics studies at large spatial and long temporal scales due to its (1) longest temporal coverage (1982–2015) at global scale and (2) corrections to the various deleterious effects of satellite drift and volcanic aerosols. In this study, pixels with the NDVI values of < 0.1 during the winter months (December to March) were regarded as snow-influenced pixels and replaced by the mean value of snow-free pixels for the winter months (Zhang et al., 2007). To further eliminate the impacts of non-vegetated areas (e.g., barren and saline-alkali land, or other areas with very low vegetation coverage), pixels with annual mean NDVI value of < 0.1 and maximum NDVI not occurring within June–August were removed from the analysis (Shen et al., 2020). To match the spatial resolution of the meteorological data, the GIMMS NDVI data were spatially aggregated at 0.1° using nearest-neighbor interpolation before the following analysis.

2.2.3. Flux data

GPP data estimated at the flux measurement sites were used to analyze variations in vegetation growth and senescence rates at landscape scale. The 45 flux sites of 554 site-years from the global FLUXNET2015 dataset (<http://fluxnet.fluxdata.org/>) across the NH

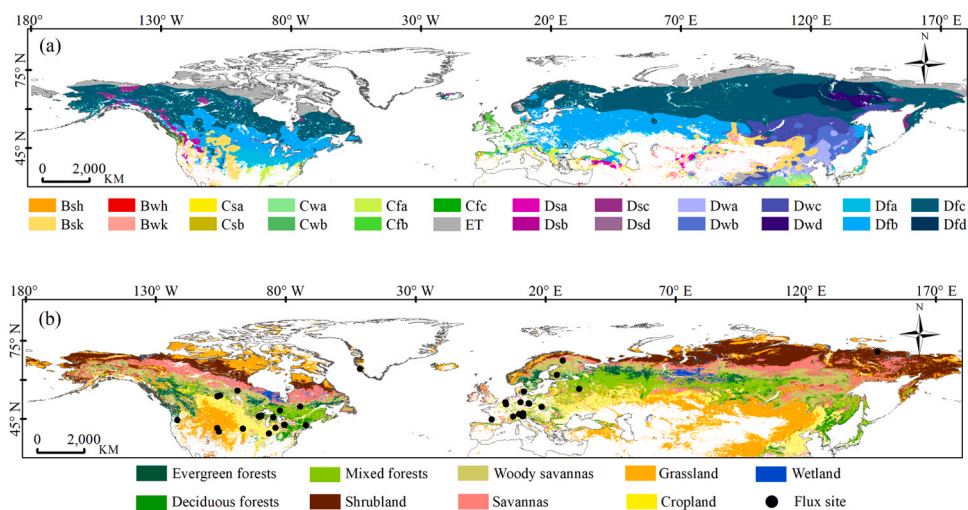


Fig. 1. Spatial distribution of (a) climates and (b) vegetation types of the NH, with flux measurement sites used to estimate GPP-based vegetation growth and senescence rates. Detailed information of the subtypes of climate and MCD12C1 are shown in Table S1.

were selected based on the following criteria: (1) no missing values of daily GPP observations, (2) located within the set of effective remote-sensing pixels on land north of > 30° N, and (3) with at least daily GPP observations for five consecutive years between 1982 and 2015 (Wu et al., 2017). Monthly temperature, precipitation, and radiation data from the corresponding sites were also used to quantify how climatic variables affect variations in vegetation growth and senescence rates by altering the phenology and peak growth of vegetation at flux sites. Detailed information of the sites can be found in Table S2.

2.3. Methods

2.3.1. Estimates of vegetation growth and senescence rates

The vegetation growth rate is the daily mean greening rate of vegetation from SOS to POS; it thereby represents the daily growth speed from initial appearance of leaves to peak growth (Wang et al., 2018). The vegetation senescence rate is the mean yellowing rate of vegetation from POS to EOS, representing the daily speed of senescence from peak growth to dormancy. In this study, the growth rate was estimated by dividing the NDVI difference between SOS and POS (NDVI_{POS} – NDVI_{SOS}) by the time interval between SOS and POS (POS – SOS, green-up period), and the senescence rate was estimated by dividing the NDVI difference between POS and EOS (NDVI_{POS} – NDVI_{EOS}) by the time interval between POS and EOS (EOS – POS, green-down period). Accurate estimates of the three phenological metrics (SOS, POS, and EOS) and their corresponding NDVI values (NDVI_{SOS}, NDVI_{POS}, and NDVI_{EOS}) are a prerequisite for determining vegetation growth and senescence rates. Here, four methods, referred as the Ployfit6-Maximum of change rate (Ployfit6-RC), the Savitzky-Golay filter-NDVI_{ratio} (SG-NDVI_{ratio}), the Double logistic model-First derivative (DL-β), and the Harmonic Analyses of Time-Series-30% of amplitude (HANTS-A₃₀), were used to determine the three key phenological metrics and their corresponding NDVI values basing on the corresponding filtering function and threshold criterion (Table 1). Once the phenological metrics and NDVI are estimated by each method, daily mean vegetation growth and senescence rates were first calculated for each method, and then mean values were calculated by the four methods to represent final growth and senescence rates. These methods were also used for vegetation growth and senescence rates at flux sites. Detailed information of the methods is shown in Text S2 and Fig. S1.

2.3.2. Data analysis

Temporal changes of growth and senescence rates were determined by the Theil-Sen slope estimator and the Mann-Kendall test (Akritas et al., 1995; Hamed, 2008). This estimator is a stable non-parametric median-based slope estimator that is insensitive to outliers. To explore the mechanisms causing the daily vegetation growth (senescence) rates variations, the relationship between growth (senescence) rates and two phenological metrics (SOS and POS for growth rate, POS and EOS for senescence rate) and the corresponding NDVI values (NDVI_{SOS} and NDVI_{POS} for growth rate, NDVI_{POS} and NDVI_{EOS} for senescence rate) that were used to estimate the growth (senescence) rates was calculated, and the maximum correlation coefficient between each phenological metric and NDVI and vegetation growth (senescence) rates was then chosen as the major determinant of vegetation growth (senescence) rates. Once the significant determinant (P < 0.05) is identified, the correlations between each major determinant and pre-season climatic variables (i.e., temperature, precipitation, and radiation) were calculated to investigate how climate factors affected vegetation growth (senescence) rates by altering phenology and peak growth of vegetation. Taking vegetation growth rate as an example, if SOS was a major determinant of growth rate, various correlation coefficients between the climate variables (e.g., temperature, precipitation, and radiation) and SOS in the area where the growth rate was determined by SOS were first estimated by changing the numbers of months by one-month steps from May to January. The time window where the temperature (precipitation or radiation) was best correlated with SOS was defined as the pre-season; the corresponding correlation coefficients between SOS and temperature (precipitation or radiation) during the pre-season represent the impacts of the climate factor that influences vegetation growth rate by altering SOS. Similar estimates were made for POS, peak NDVI and EOS, with the months of climate variables used to calculate the correlation coefficients being selected as August-April for POS and peak NDVI and October-June for EOS. All performances were calculated at pixel level to characterize the spatial patterns of the linkages among climate, phenology, and vegetation growth (senescence) rates, as well as at each flux site.

Table 1
Algorithms of the four methods for extracting key phenological metrics and corresponding NDVI values.

Methods	Data filter function	Threshold criterion
Ployfit6-RC	$NDVI_t = a_0 + a_1t + a_2t^2 + a_3t^3 + \dots + a_6t^6$	Maximum increase and decrease in fitted NDVI curve
SG-NDVI _{ratio}	$NDVI_t = \frac{1}{n} \sum_{i=t-m}^m c_i \times NDVI_{i+t}$	NDVI _{ratio} of 20%
DL-β	$NDVI_t = \frac{1}{1 + e^{\left(\frac{a_1 - t}{a_2}\right)}} - \frac{1}{1 + e^{\left(\frac{a_3 - t}{a_4}\right)}}$	Local minima and maxima for the derivatives of fitted NDVI curve
HANTS-A ₃₀	$NDVI_t = a_0 + \sum_{i=1}^n a_i \cos(\omega_i t - \varphi_i)$	30% of NDVI amplitude

Data filter function was used to reconstruct time series of NDVI, and the threshold was adopted to determine SOS and EOS from reconstructed NDVI time series. In the data filter function, t is the Julian date, NDVI_t is the fitted NDVI value by the equation of each filter function.

3. Results

3.1. Spatiotemporal variations of vegetation growth and senescence rates

The mean vegetation growth rate (Fig. 2a) and senescence rate (Fig. 2b) during 1982–2015 showed wide spatial variability across the NH. Specifically, the growth rate varied from 0.1×10^{-2} NDVI-units-day⁻¹ at low latitudes to 0.7×10^{-2} NDVI-units-day⁻¹ at high latitudes, with an average of 0.4×10^{-2} NDVI-units-day⁻¹. The high growth rates were observed in the central part of Eurasia ($>0.8 \times 10^{-2}$ NDVI-units-day⁻¹), followed by the northeastern part of Eurasia and certain small western regions of North America (0.6×10^{-2} – 0.8×10^{-2} NDVI-units-day⁻¹). The low growth rates were mostly found at low latitudes, with an average of $< 0.3 \times 10^{-2}$ NDVI-units-day⁻¹ (Fig. 2a). The vegetation senescence rate showed lower spatial variability than the growth rate, with a range between 0.1×10^{-2} and 0.5×10^{-2} NDVI-units-day⁻¹ and the low senescence rates at low latitudes (Fig. 2b). The growth and senescence rates increased with latitude, with an increase of 1.0×10^{-4} and 0.7×10^{-4} NDVI-units-day⁻¹ per degree latitude (Fig. 2c). Continentally, both rates were greater in Eurasia than in North America (Fig. S2). Interestingly, there was a strong positive relationship between growth and senescence rates ($R = 0.9$, $P < 0.05$) (Fig. 2d), suggesting that a fast growth rate was generally accompanied by a fast senescence rate across the study area. However, the magnitude of the growth rate was greater than that of the senescence rate over 79.8% of the study region (Fig. 2e), especially at latitudes between 50°N and 74°N (Fig. 2f) in areas such as Siberia, the northern and southeastern regions of Europe, and most of northern North America (Fig. 2e). The areas having a lower growth rate than senescence rate were generally distributed in the central and southeastern parts of Eurasia and on the southern and northern edges of North America.

From 1982–2015, the growth (Fig. 3a) and senescence rates (Fig. 3b) accelerated over 60.0% and 61.5% of the study area, respectively, with 46.1% and 46.4% of the acceleration change being significant ($P < 0.05$), and with similar spatial distributions occurring in the northern and northeastern parts of Eurasia (0.4×10^{-3} NDVI-units-day⁻¹.decade⁻¹) and most of North America (0.4×10^{-3} NDVI-units-day⁻¹.decade⁻¹). In contrast, decelerations of both rates were observed in the western and southern parts of Eurasia and in the western and southeastern regions of North America. At hemispherical scale, both growth and senescence rates accelerated, with a stronger acceleration of growth rate (0.8×10^{-4} NDVI-units-day⁻¹.decade⁻¹) than that of senescence rate (0.6×10^{-4} NDVI-units-day⁻¹.decade⁻¹), especially during the period 2000–2013 (Fig. 3c). By latitude, the acceleration of growth rate was greater than that of senescence rate at 35–46°N and 64–69°N, but lower at 50–63°N (Fig. 3d). Importantly, the growth and senescence rates were positively correlated over 83.6% of the study domain (Fig. 3e), and 64.2% of these correlations were statistically significant ($P < 0.05$; Fig. 3f), suggesting a parallel acceleration of vegetation growth and senescence rates across the study area. The acceleration of both rates was also confirmed by GPP-based estimates at the flux measurement sites, where vegetation growth and senescence rates accelerated at 68.8% (31 sites) and 62.2% (28 sites) of all sites, with 45.2% (14 sites; 4.1×10^{-2} g C·m⁻².day⁻¹.decade⁻¹) and 39.3% (11 sites; 3.4×10^{-2} g C·m⁻².day⁻¹.decade⁻¹) of these accelerations being significant ($P < 0.05$). On the other hand, vegetation growth and senescence rates decelerated at 31.1% and 37.7% of all sites, with 21.4% (3 sites) and 17.6%

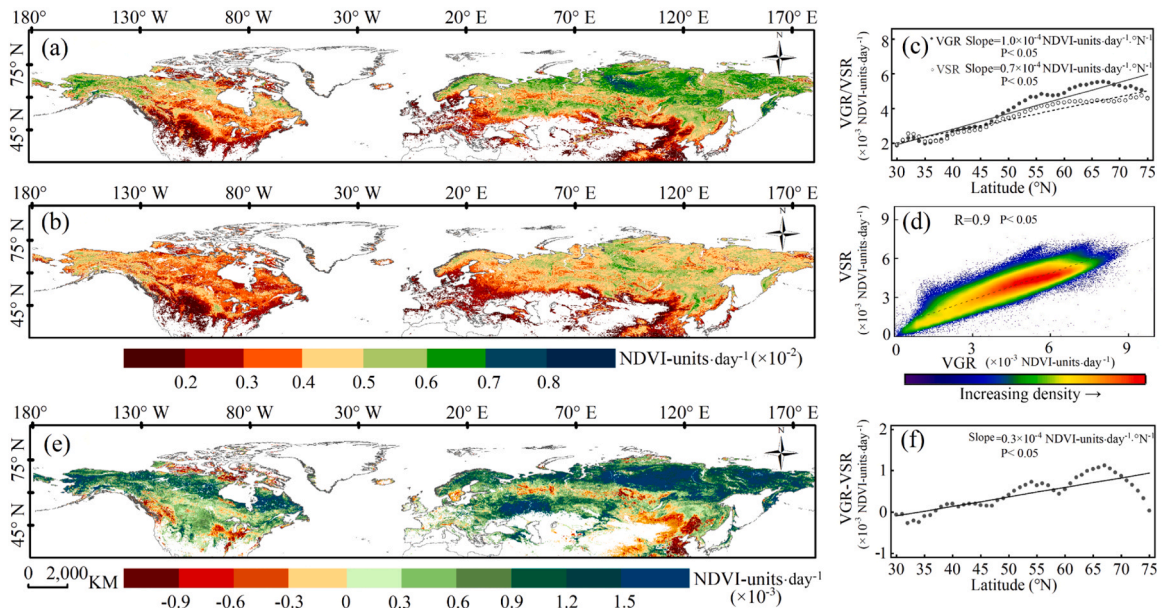


Fig. 2. Spatial changes of mean (a) growth and (b) senescence rates over the NH during 1982–2015 averaged from the four methods. (c) Variation of mean growth and senescence rates with latitude. (d) Spatial relationship between growth and senescence rates. (e) Spatial distribution of differences between growth and senescence rates (growth rate minus senescence rate) and (f) their latitudinal variations. VGR and VSR represent vegetation growth rate and senescence rate, respectively.

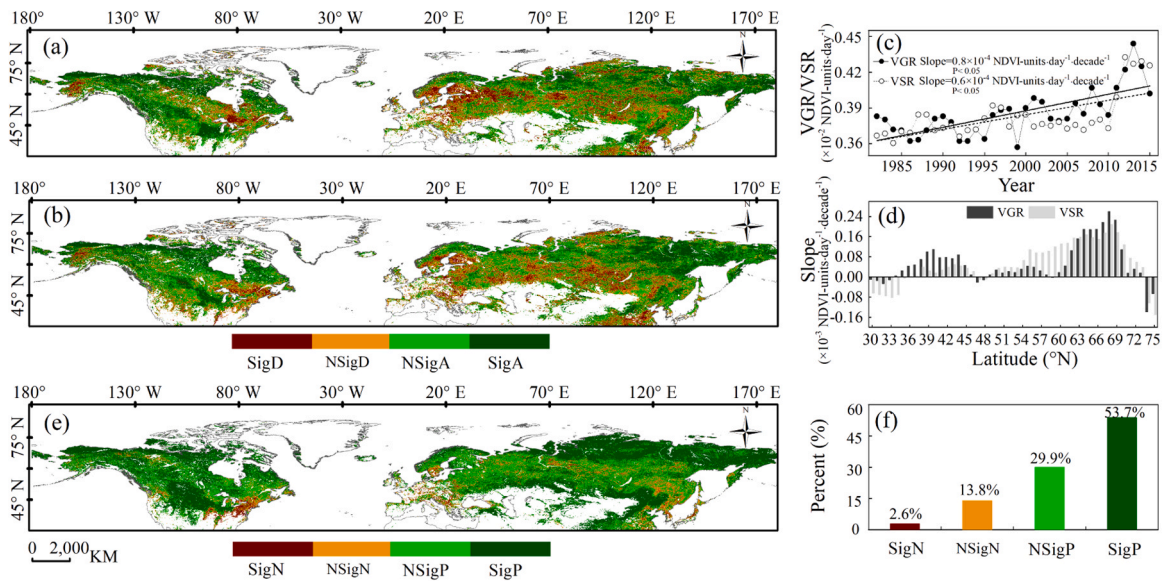


Fig. 3. Spatial changes in the trend of (a) growth rate and (b) senescence rate during 1982–2015, with (c) the trends of hemispherical averaged growth and senescence rates, and (d) the trends of the various latitudinal zones. (e) The correlations between growth and senescence rates and (f) the corresponding area percentages. SigA and SigD represent the significant ($P < 0.05$) acceleration and deceleration; NSigA and NSigD represent the corresponding in-significant trends; SigN and SigP represent significant ($P < 0.05$) negative and positive correlation; NSigN and NSigP represent the corresponding in-significant correlation; VGR and VSR represent vegetation growth rate and senescence rate, respectively.

(3 sites) of these decelerations being significant, respectively (Fig. 4).

3.2. Spatial changes in the driving variables

To identify the area distribution of the direct determinants of vegetation growth (senescence) rates, the correlation coefficients between the growth (senescence) rates and the phenological metrics, as well as the corresponding NDVIs that were used to estimate growth (senescence) rates were calculated. Growth rate was positively correlated with both SOS (Fig. S3a; 87.1%) and NDVI_{POS} (Fig. S3d; 98.6%), and negatively correlated with POS (Fig. S3c; 90.8%) over most of the study area. The senescence rate was positively correlated with both POS (Fig. S4a; 82.6%) and NDVI_{POS} (Fig. S4b; 98.6%), but negatively correlated with EOS (Fig. S4c; 77.9%). In contrast, both NDVI_{SOS} and NDVI_{EOS} were weakly correlated with growth and senescence rates (Figs. S3b and S4d).

To further identify areas where the growth (senescence) rates were affected by phenological metrics or NDVIs, spatial changes in the significant drivers on growth (senescence) rates were constructed based on the maximum correlation coefficients between growth (senescence) rates and phenological metrics and NDVIs (Fig. 5). The growth rate over 59.7% of the study area were mainly determined by NDVI_{POS} (Fig. 5b), with 99.8% of the correlations being positive and significant ($P < 0.05$) (Fig. 5a). The regions covered included Siberia, the inland portions of Asia and North America, and the northern part of North America, indicating that an increase in NDVI_{POS} led to an acceleration of growth rate in these regions (Fig. 3a). In contrast, the area proportions with growth rate determined by SOS and POS were 17.1% and 17.8%, respectively (Fig. 5a, b).

For senescence rate, NDVI_{POS} also played a significant role over 48.8% of the study area (Fig. 5c, d). However, the spatial changes were not the same as for growth rate, with strong NDVI_{POS} influence mostly occurring in the inland portions of Asia and most regions of North America on excluding the southeastern part (Fig. 5d). The regions with senescence rate determined by POS and EOS accounted for 23.0% and 25.9% of the study area, respectively, exhibiting highly pronounced latitudinal variation (Fig. 5d). Specifically, the POS-determined areas were primarily concentrated at lower latitudes, such as the temperate band south of 60°N in Eurasia and the

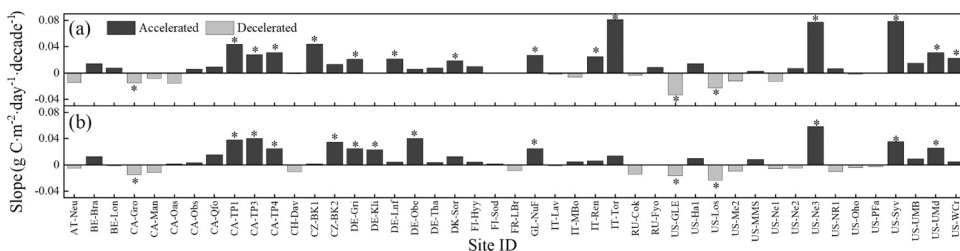


Fig. 4. Trends of (a) growth rate and (b) senescence rate estimated by daily GPP data at flux sites. * represents the significant trend at $P < 0.05$.

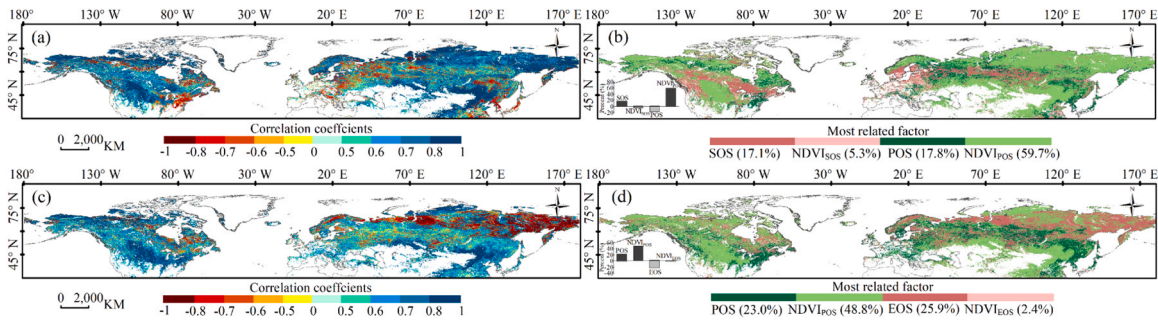


Fig. 5. Spatial changes in (a) the maximum correlation coefficient between growth rate and key phenological (SOS and POS) and productive (NDVI_{SOS} and NDVI_{POS}) metrics, and (b) the major determinant of growth rate. Spatial distributions of (c) the maximum correlation coefficient between senescence rate and key phenological (POS and EOS) and productive (NDVI_{POS} and NDVI_{EOS}) metrics, and (d) the major determinant of senescence rate. The inserted bars shown in the lower left of (b) indicate the frequency distributions of the positive and negative correlation coefficients between growth rate and key phenological and productive metrics. The inserted bars shown in the lower left of (d) indicate the frequency distributions of the positive and negative correlation coefficients between senescence rate and key phenological and productive metrics.

southeastern part of North America, whereas the EOS-determined areas were mainly distributed in higher latitudes, such as Siberia and northern North America. Interestingly, neither NDVI_{SOS} nor NDVI_{EOS} played a significant role on growth (5.3%) and senescence (2.4%) rates (Fig. 5b, d), likely due to the low vegetation productivity at the onset of spring green-up and autumn senescence. Consequently, NDVI_{SOS} and NDVI_{EOS} were neglected in the following analysis.

At flux sites, growth and senescence rates were also positively and strongly correlated with GPP_{POS} (Fig. 6b), confirming that summer peak growth is the major determinant of vegetation growth and senescence rates, although earlier SOS and EOS tended to cause slower growth rate and faster senescence rate (Fig. 6a, c).

3.3. Linkages among climate, phenology, and vegetation growth (senescence) rates

According to the spatial distribution of the major drivers on growth rate (Fig. 5b) and senescence rate (Fig. 5d), the climatic factors were further explored (Figs. 7 and 8). In areas with growth rate determined by SOS, the SOS was negatively controlled by pre-season temperature in 88.0% of its total pixels (Fig. 7a, b), indicating that high temperature led to an earlier SOS, and subsequently decelerated vegetation growth rate in these regions (Fig. 3a). Consistent with SOS, in areas with growth rate mainly determined by POS and NDVI_{POS}, these metrics were also associated with pre-season temperature in over 62.3% (Figs. 7c) and 53.3% (Fig. 7e) of their total pixels, indicating that rising temperature can accelerate growth rate by advancing POS (Fig. 7d) and increasing NDVI_{POS} (Fig. 7f). Note that pre-season precipitation also accelerated growth rate by increasing NDVI_{POS} in arid and semi-arid regions (23.6%) (Fig. 7e, f), especially in the Great Plains of central North America and in the Mongolian Plateau and Kazakh Uplands of northern Eurasia (Fig. 3a). However, pre-season precipitation can decelerate growth rate by delaying POS in arid and semi-arid regions (18.8%) (Fig. 7c). The importance of radiation on growth rate by changing SOS, POS, and NDVI_{POS} were relatively minor, and spatially spotty over the study area.

For senescence rate, in lands with senescence rate determined by POS and NDVI_{POS}, POS and NDVI_{POS} appeared controlled by pre-season temperature over 58.3% (negative correlations; Fig. 8a) and 49.4% (positive correlations; Fig. 8c) of their total pixels. This implied that warming-induced higher NDVI_{POS} (Fig. 8d) also accelerated senescence rate, whereas warming-induced earlier POS (Fig. 8b) decelerated senescence rate (Fig. 3b). In POS-influenced areas, the remaining 20.2% and 21.6% of pixels were affected by pre-season precipitation and radiation, mainly in southeastern North America, southern Europe, and southeast Asia (Fig. 8a). Notably, precipitation also accelerated senescence rate in arid and semi-arid ecosystems by increasing NDVI_{POS}, such as in the inland areas of Eurasia and North America (Fig. 8c; positive correlations in Fig. 8d). The influences of radiation on NDVI_{POS} (24.4%) appeared as

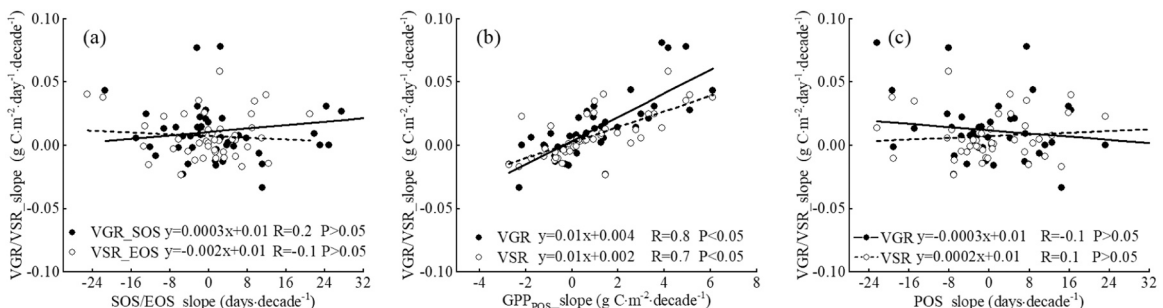


Fig. 6. Relationships of growth/senescence rate trends with (a) SOS/EOS, (b) GPP_{POS}, and (c) POS trends at flux measurement sites.

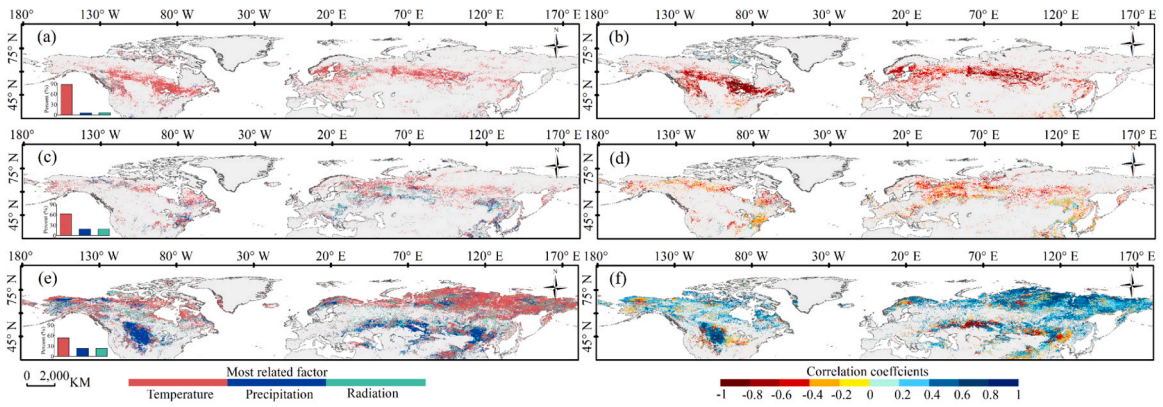


Fig. 7. Spatial changes in important climatic factor on growth rate: (a) SOS, (c) POS, and (e) NDVI_{POS}, and the correlation coefficient between the major determinant of growth rate and the dominant climatic factors: (b) SOS, (d) POS, and (f) NDVI_{POS}. The inserted bars shown in the lower left of (a, c, and d) indicate the corresponding data frequencies.

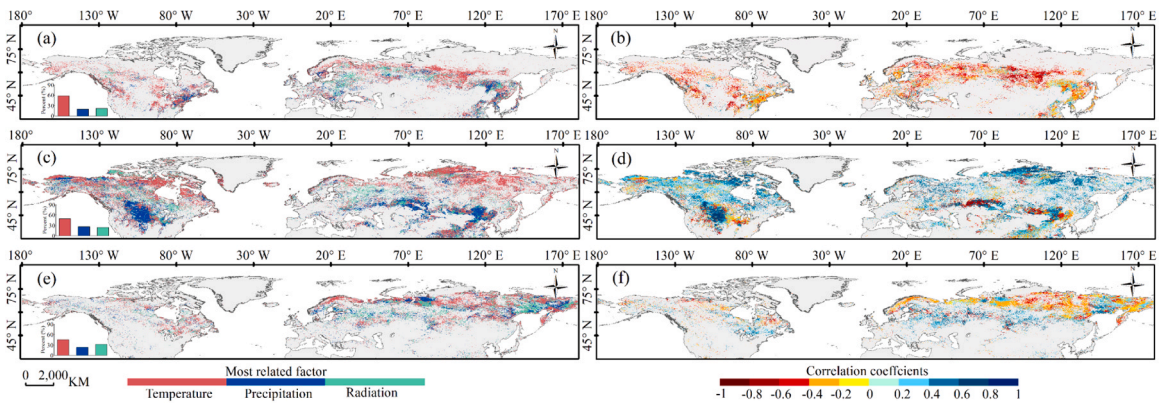


Fig. 8. Spatial changes of important climatic factor on senescence rate: (a) POS, (c) NDVI_{POS}, and (e) EOS, and the correlation coefficient between the major determinant of senescence rate and the dominant climatic factors: (b) POS, (d) NDVI_{POS}, and (f) EOS. The inserted bars shown in the lower left of (a, c, and d) indicate the corresponding data frequencies.

spatial fragments, with a tendency towards positive effects at high latitudes and negative effects in arid and semi-arid mid-latitude regions (Fig. 8c, d). The regions where senescence rate was determined by EOS were mainly distributed at high latitudes in Eurasia, with a complex spatial pattern in the impacts of climatic variables on EOS. Preseason temperature negatively regulated EOS variations over 45.7%, whereas radiation positively controlled EOS variations over 31.3% of their total pixels (Fig. 8e, f). Moreover, increasing precipitation accelerated senescence rate by advancing EOS in the remaining 23.0% of the area (Fig. 8e).

At flux site scale, the GPP_{POS}, as the major driver on growth and senescence rates (Fig. 6b), was more from preseason temperature (Fig. 9a), whereas the impacts of precipitation and radiation were not significant (Fig. 9b, c).

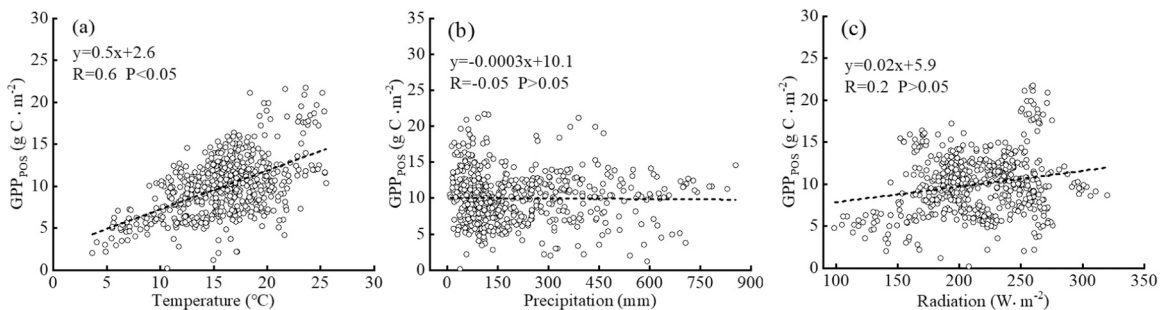


Fig. 9. Relationships of GPP_{POS} and preseason (a) temperature, (b) precipitation, and (c) radiation at the 45 flux sites.

4. Discussion

The rates of vegetation development for green-up and green-down periods are critical ecological indicators of canopy seasonality shifts in response to climate change (Richardson et al., 2010; Wang et al., 2020). Remotely-sensed 15-days NDVI and flux GPP data revealed a parallel acceleration of vegetation growth and senescence rates during 1982–2015, with a greater acceleration of the former than the latter (Fig. 3c, d). These spatiotemporal variations of growth and senescence rates were strongly related to whether the three phenological metrics (SOS, POS, and EOS) responded equally or divergently to climate warming and to how peak growth of vegetation (NDVI_{POS}) responded to climate warming. For example, a faster growth rate at high latitudes (0.7×10^{-2} NDVI-units-day⁻¹), which is in line with the maximum green-up rate by Park et al. (2020), was tightly related to later start of spring green-up at high latitude and to the associated shorter green-up period. This occurred because vegetation at high latitudes, which is acclimated to low temperature and limited photoperiod, has evolved a faster growth rate than vegetation at low latitudes to complete its annual growth sooner and make use of limited resources (Flynn and Wolkovich, 2018; Vitasse et al., 2018). This latitudinal dependence was more distinct in Eurasia than in North America (Fig. 2a). The faster senescence rate at high latitudes than at low latitudes can be directly inferred from the faster growth rate at high latitudes than at low latitudes because earlier vegetation dormancy at high latitudes resulting from limited heat and insolation availability leads to a shorter green-down period between peak growth and dormancy. This is further confirmed by the significant correlation between growth and senescence rates ($R=0.9$, $P < 0.05$; Fig. 2d). However, the magnitudes of growth and senescence rates varied with latitude, with growth rate being faster than senescence rate at latitudes north of 50° N and lower at latitudes south of 36° N (Fig. 2f). The lower growth rate than senescence rate south of 36° N could be attributed to the longer duration of the green-up period in contrast to the green-down period (Fig. S5).

Previous studies have showed that SOS and POS of vegetation have advanced over the NH (>30°N) (Gonsamo et al., 2015; Jeong et al., 2011; Xu et al., 2016) and peak growth has enhanced globally (Huang et al., 2018). However, little is known about whether SOS and POS have advanced equally, or differently, on canopy development. By exploring the direct relationships of growth rate, we found that POS advanced more rapidly than SOS from 1982 to 2015 in regions where vegetation growth accelerated (1.7 days-decade⁻¹ vs 0.1 days-decade⁻¹; Fig. 10a). The estimate of POS advance in this study is highly consistent with the results of 1.2 ± 0.6 days-decade⁻¹ during 1982–2015 (Gonsamo et al., 2015), 1.7 ± 0.3 days-decade⁻¹ during 2000–2016 in the NH (Park et al., 2019) and 1.8 days-decade⁻¹ during 1982–2015 in the continental United States (Liu et al., 2021). In contrast, the SOS advance estimated in this study during 1982–2015 is smaller than the estimates before the 1990 s (Tucker et al., 2001; Zhou et al., 2001) or 2000 s (Jeong et al., 2011; Park et al., 2018), additionally confirming the slowdown of SOS advance with an extension of the observation period (Park et al., 2018; Wang et al., 2015). This larger advance of POS than SOS confirms not only the spring-ward movement of plant growth (Piao et al., 2019; Xu et al., 2016), but also the shortened growing duration between SOS and POS by 1.5 days-decade⁻¹ (Fig. 10a) and the accelerated vegetation growth rate by 2.4×10^{-4} NDVI-units-day⁻¹·decade⁻¹. These unequal advances of two phenologies may have considerable, but different impacts on ecosystem carbon cycle processes. For example, fewer days may be available for carbon uptake due to reduced growth time, or the peak of carbon assimilation may be negatively related to the advance in POS (Gonsamo et al., 2015). Admirably, we focused on the parallel acceleration of vegetation growth and senescence rates and their underlying mechanisms, further studies with quantitative analyses are needed on the geographical distribution of the unequal responsiveness of these three phenologic metrics to climate and their consequences for ecosystem functioning.

As a result of this shortened growing duration and the concurrent increase in vegetation peak growth (0.02 NDVI-units-decade⁻¹, $P < 0.05$) caused by the larger advance of POS than SOS, the average growth rate over the study area accelerated significantly, with a rate of 0.8×10^{-4} NDVI-units-day⁻¹·decade⁻¹ (Fig. 3c), which is consistent with results from previous studies using leaf area index (LAI) data at global scale (Wang et al., 2018) and north of 60° NH (Park et al., 2020). In temperate China, Piao et al. (2022) showed a significant acceleration of vegetation growth only in April (7.75×10^{-3} NDVI-units-decade⁻¹). In parallel with vegetation growth rate, the vegetation senescence rate has also accelerated, albeit at lower magnitude of acceleration (0.6×10^{-4} NDVI-units-day⁻¹·decade⁻¹; Fig. 3c). The weaker acceleration of senescence rate compared to growth rate can be attributed to a non-significantly shortened green-down duration during POS and EOS (-0.2 days-decade⁻¹, $P > 0.05$; Fig. 10b), resulting from the simultaneous advancement of POS and EOS (0.9 days-decade⁻¹ vs 0.6 days-decade⁻¹; Fig. 10b). However, the enhancement peak growth of vegetation, which was

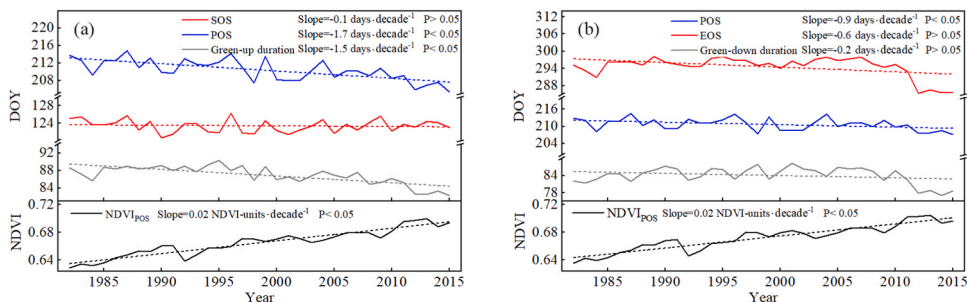


Fig. 10. (a) Trends of SOS, POS, green-up duration and NDVI_{POS} in growth rate accelerated regions. (b) Trends of POS, EOS, green-down duration and NDVI_{POS} in senescence rate accelerated regions. Green-up and green-down durations represent the time interval between SOS and POS, and between POS and EOS, respectively.

also reported globally by Huang et al. (2018), contributed largely to the senescence rate and eventually caused a parallel acceleration of growth and senescence rates. To the best of our knowledge, the accelerated vegetation senescence rate has not been investigated by hemisphere, except for temperate China where an acceleration of senescence rate occurred in October (Piao et al., 2022). Interestingly, it was found that vegetation in Eurasia and North America exhibited different mechanisms of acceleration of the senescence rate, with a strong contribution of advanced EOS in Eurasia and a strong contribution of enhanced NDVI_{POS} in North America (Fig. 5d).

There was no single climatic factor during a specific period that was responsible for variations in growth and senescence rates in different regions of the study area. In contrast to previous studies showing that the growth rate acceleration resulted from warming during the green-up period (Wang et al., 2018), we emphasize that warming prior to SOS had strong impacts on the growth rate variation in areas where growth rate was determined by SOS. In these areas, an earlier SOS in response to 1 °C warming prior to SOS indirectly led to a 0.4×10^{-2} NDVI-units-day⁻¹ deceleration of growth rate by prolonging the time interval between SOS and POS, implying the importance of the links among warming, earlier SOS, and growth rate deceleration. Another possible explanation is that the warming-induced earlier SOS may suppress vegetation growth rate by increasing soil water evaporation and imposing drought stress on vegetation growth (Buenmann et al., 2013; Xie et al., 2020; Yu et al., 2018). Importantly, warming during the green-up period had strong influences on both growth and senescence rates in regions where these rates were dependent on POS and NDVI_{POS}, especially by increasing NDVI_{POS}. However, the contribution of NDVI_{POS} to growth and senescence rates varied spatially (Fig. 5b, d), highlighting the need for future studies of plant peak growth and its key drivers for projections of vegetation development. Huang et al. (2018) attributed the enhanced peak growth of global vegetation to expanding cropland, increasing CO₂, and nitrogen deposition. However, we found that temperature during the green-up period contributed to the accelerating vegetation growth and senescence rates by enhancing NDVI_{POS} in approximately 53.3% and 49.4% of the study area (Figs. 7e and 8c). This was also confirmed at flux sites (Figs. 6b and 9a). In water-limited ecosystems, an increase in precipitation during the green-up period strongly accelerated the two rates still by increasing NDVI_{POS}, which may not have been well quantified previously (Park et al., 2015; Piao et al., 2022), if the different determinants of growth and senescence rates were not partitioned. In addition to NDVI_{POS}, advanced EOS was also responsible for the acceleration of senescence rate over a considerable area in the Eurasian continent (20.7%) (Fig. 5c, d). However, in these areas, EOS was correlated negatively and significantly with temperature during the green-down period, which is not in agreement with the assertion that higher temperatures could delay EOS (Keenan et al., 2014; Wu et al., 2018). The mechanisms of EOS changes, which can alter the senescence rate, are more complicated than for SOS changes (Wu et al., 2022; Zani et al., 2020) due to the interactive effects of multiple climate variables on EOS, such as daytime and nighttime temperature (Wu et al., 2018), winds (Wu et al., 2021a), droughts (Wu et al., 2022), photoperiod (Wu et al., 2021b), and growing-season productivity (Zani et al., 2020). Combining the significant negative correlation between EOS and temperature in our study with the results of drought effects on EOS (Wu et al., 2018, 2022), we speculated that climate warming in Eurasia during the green-down period has advanced EOS, probably by increasing drought stresses on ecosystems, further leading to an accelerated senescence rate. Radiation was another important variable decelerating vegetation senescence at high latitudes (Fig. 8e, f) by delaying EOS due to increased photoperiod and photosynthesis.

Given these linkages among climate, phenology, and canopy development in this study, it must be emphasized that growth and senescence rates are determined by multiple biological and environmental factors, and that the mechanisms linking climate-SOS-climate-POS/NDVI_{POS} to growth rate acceleration and climate-POS/NDVI_{POS}-climate-EOS to senescence rate acceleration must be properly represented for the entire vegetation growth period, instead of focusing only on warming during the green-up period or instantaneous maximum growth rate (Park et al., 2015). This is important because unequal advances in phenology metrics (i.e., SOS, POS, and EOS) caused by climate change during different time period may lead to shortened or lengthened green-up and green-down periods, which will be coupled with variations in summer peak growth to determine vegetation growth and senescence rates (Fig. 11). This assertion was also supported by GPP-based rates of vegetation growth and senescence at flux sites, with warming-induced GPP_{POS} determining the variation in growth and senescence rates and providing robust evidence of their acceleration.

Although the previous discussion has highlighted a parallel acceleration of vegetation growth and senescence rates and the importance of well representation of climate-phenology-canopy development linkages, the limitations and uncertainties in the study should further be addressed for the benefit of future efforts exploring variations in vegetation growth and senescence rates. First, accurate estimates of the three phenological metrics and of peak NDVI are a prerequisite for accurately assessing changes in vegetation growth and senescence rates. In this study, four methods with different filtering functions and thresholds were used to extract key phenological metrics and peak NDVI to minimize the uncertainties in determining phenology, as was done in previous studies (Liu et al., 2016; Shen et al., 2014). Second, NDVI only captures the spectral reflectance of leaves in the red and near-infrared bands and provides information on greenness as a surrogate for photosynthesis, rather than observing actual photosynthetic activities and growth/senescence processes, with some biases resulting from atmospheric contamination and satellite drift (Huete et al., 2002). Therefore, the unit of growth and senescence rates in the present study is only a NDVI-units instead of actual biomass growth and biomass units (i.e., g-day⁻¹). However, it is well known that remotely sensed vegetation index is a currently unique technique for studying earth surface features at large spatial and long temporal scales (Shen et al., 2021; Tucker et al., 2001; White et al., 2009), and the consistent results obtained here between NDVI-based and GPP-based vegetation growth and senescence rates have confirmed that NDVI data are a very important proxy for studying long-term vegetation growth and senescence rates. It can be speculated that the accuracy of growth and senescence rates was markedly enhanced by the use of newly developed data sets such as satellite-derived solar-induced-fluorescence (SIF), although current SIF data is too short and the spatial resolution is low (Guanter et al., 2014; Walther et al., 2016). A third concern arises from the fact that GPP-based estimates of growth and senescence rates were performed at only 45 flux sites due to limited data availability for a sufficiently long time period, as discussed earlier in the section on Data. Especially in Asia where there is only one flux site for this study. Finally, in addition to climate-phenology-canopy development linkages, vegetation growth and senescence rates are also influenced by natural and human disturbances, which calls for further

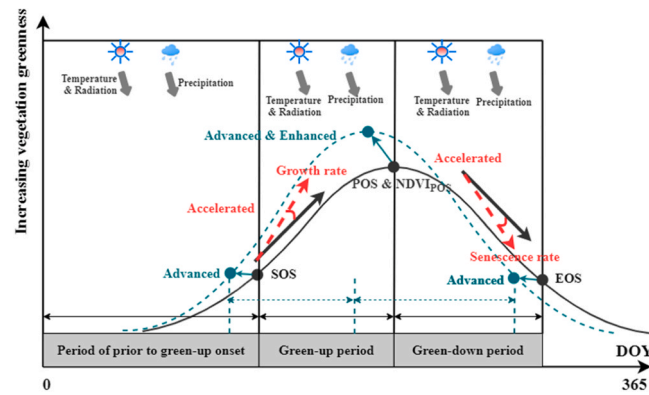


Fig. 11. Conceptual illustration of the linking mechanisms climate warming-phenology shifts to growth/senescence rate acceleration in the NH. The solid and dotted curve represent the seasonal dynamics of vegetation greenness during the prophase and post phase of study period, respectively, and the points on the curve represent the key phenological metrics. Linking paths: climate factors prior to green-up onset → SOS → growth rate, climate factors during green-up period → POS/NDVI_{POS} → growth/senescence rate, climate factors during green-down period → EOS → senescence rate.

comprehensive studies introducing the linear and nonlinear effects of multiple factors on canopy development.

5. Conclusion

Using two types of data (satellite-based NDVI and flux-based GPP data) and four methods, we explored the spatiotemporal variability of vegetation growth and senescence rates and potential drivers in the temperate and boreal regions of the NH during 1982–2015. We found a parallel acceleration of vegetation growth and senescence rates across the NH, with enhanced peak growth of vegetation in summer acting as the major driver on the parallel acceleration in most of the study area despite the existence of substantial spatial heterogeneity, which may not have been well investigated in earlier vegetation development studies. However, it is worth noting the difficulties in characterizing the variations in growth and senescence rates using a simple climate factor in a specific time period because of geographical differences in links among climate, phenology, and canopy development. Such a linkage should be explicitly considered in canopy development studies by partitioning the major determinant of growth and senescence rates and the dominant climate factors causing the changes of major determinants. Moreover, the discovery of the faster advancement of POS compared to SOS, resulting in a shortened duration between SOS and POS and an accelerated growth rate, further emphasizes the value of precise description of the unequal responsiveness of different phenology indicators (SOS, POS, and EOS) to the warming climate and should be emphasized in future vegetation seasonality. Further studies are needed with more physiological mechanisms, based either on field observations with more flux sites or on manipulative experiments for a specific species.

Declaration of Competing Interest

The authors declare that they have no known competing financial interests or personal relationships that could have appeared to influence the work reported in this paper.

Data Availability

Data will be made available on request.

Acknowledgments

This work was financially supported by the Natural Science Foundation of Inner Mongolia, China under Grant 2021MS04014, and the International Cooperation and Exchange Programme under Grant 41961144019. We would like to thank the National Aeronautics and Space Administration (NASA) GIMMS team for providing the GIMMS NDVI3g.v1 dataset, the FLUXNET community for providing FLUXNET2015 dataset, the European Centre for Medium-Range Weather Forecasts for providing the ERA5-Land dataset, and the Land Processes Distributed Active Archive Center (LPDAAC) for providing MCD12C1 land cover product.

Appendix A. Supporting information

Supplementary data associated with this article can be found in the online version at [doi:10.1016/j.gecco.2023.e02622](https://doi.org/10.1016/j.gecco.2023.e02622).

References

- Akritis, M.G., Murphy, S.A., Lavalley, M.P., 1995. The Theil-Sen estimator with doubly censored data and applications to astronomy. *J. Am. Stat. Assoc.* 90 (429), 170–177.
- Buermann, W., Bikash, P.R., Jung, M., et al., 2013. Earlier springs decrease peak summer productivity in North American boreal forests. *Environ. Res. Lett.* 8 (2), 024027.
- Chen, J., John, R., Sun, G., et al., 2018. Prospects for the sustainability of social-ecological systems (SES) on the Mongolian plateau: five critical issues. *Environ. Res. Lett.* 13 (12), 123004.
- Flynn, D.F.B., Wolkovich, E.M., 2018. Temperature and photoperiod drive spring phenology across all species in a temperate forest community. *New Phytol.* 219, 1353–1362.
- Fu, Y.H., Piao, S., Zhao, H., et al., 2014. Unexpected role of winter precipitation in determining heat requirement for spring vegetation green-up at northern middle and high latitudes. *Glob. Change Biol.* 20 (12), 3743–3755.
- Gonsamo, A., Croft, H., Chen, J.M., et al., 2015. Radiation contributed more than temperature to increased decadal autumn and annual carbon uptake of two eastern North America mature forests. *Agric. For. Meteorol.* 201, 8–16.
- Guanter, L., Zhang, Y., Jung, M., et al., 2014. Global and time-resolved monitoring of crop photosynthesis with chlorophyll fluorescence. *Proc. Natl. Acad. Sci. USA* 111 (14), E1327–E1333.
- Hamed, K.H., 2008. Trend detection in hydrologic data: the Mann–Kendall trend test under the scaling hypothesis. *J. Hydrol.* 349 (3–4), 350–363.
- Hong, S., Zhang, Y., Yao, Y., et al., 2022. Contrasting temperature effects on the velocity of early- versus late-stage vegetation green-up in the Northern Hemisphere. *Glob. Change Biol.* 28 (23), 6961–6972.
- Huang, K., Xia, J., Wang, Y., et al., 2018. Enhanced peak growth of global vegetation and its key mechanisms. *Nat. Ecol. Evol.* 2 (12), 1897–1905.
- Huete, A., Didan, K., Miura, T., et al., 2002. Overview of the radiometric and biophysical performance of the MODIS vegetation indices. *Remote Sens. Environ.* 83 (1–2), 195–213.
- Jeong, S.-J., Ho, C.-H., Gim, H.J., et al., 2011. Phenology shifts at start vs. end of growing season in temperate vegetation over the Northern Hemisphere for the period 1982–2008. *Glob. Change Biol.* 17 (7), 2385–2399.
- Keenan, T.F., Gray, J., Friedl, M.A., et al., 2014. Net carbon uptake has increased through warming-induced changes in temperate forest phenology. *Nat. Clim. Change* 4 (7), 598–604.
- Liu, Q., Fu, Y.H., Zeng, Z., et al., 2016. Temperature, precipitation, and insolation effects on autumn vegetation phenology in temperate China. *Glob. Change Biol.* 22 (2), 644–655.
- Liu, Y., Wu, C., Wang, X., et al., 2021. Impacts of global change on peak vegetation growth and its timing in terrestrial ecosystems of the continental US. *Glob. Planet. Change* 207, 103657.
- Ma, X., Zhu, X., Xie, Q., et al., 2022. Monitoring nature's calendar from space: Emerging topics in land surface phenology and associated opportunities for science applications. *Glob. Change Biol.* 28 (24), 7186–7204.
- Menzel, A., Fabian, P., 1999. Growing season extended in Europe. *Nature* 397 (6721), 659–659.
- Menzel, A., Sparks, T.H., Estrella, N., et al., 2006. European phenological response to climate change matches the warming pattern. *Glob. Change Biol.* 12 (10), 1969–1976.
- Park, H., Jeong, S.-J., Ho, C.-H., Kim, J., et al., 2015. Nonlinear response of vegetation green-up to local temperature variations in temperate and boreal forests in the Northern Hemisphere. *Remote Sens. Environ.* 165, 100–108.
- Park, H., Jeong, S.-J., Ho, C.-H., et al., 2018. Slowdown of spring green-up advancements in boreal forests. *Remote Sens. Environ.* 217, 191–202.
- Park, H., Jeong, S., Penuelas, J., 2020. Accelerated rate of vegetation green-up related to warming at northern high latitudes. *Glob. Change Biol.* 26 (11), 6190–6202.
- Park, T., Chen, C., Macias-Fauria, M., et al., 2019. Changes in timing of seasonal peak photosynthetic activity in northern ecosystems. *Glob. Change Biol.* 25 (7), 2382–2395.
- Peng, S.S., Piao, S., Zeng, Z., et al., 2014. Afforestation in China cools local land surface temperature. *Proc. Natl. Acad. Sci.* 111 (8), 2915–2919.
- Piao, S., Tan, J., Chen, A., Fu, Y.H., et al., 2015. Leaf onset in the northern hemisphere triggered by daytime temperature. *Nat. Commun.* 6 (1), 1–8.
- Piao, S., Wang, X., Park, T., et al., 2019. Characteristics, drivers and feedbacks of global greening. *Nat. Rev. Earth Environ.* 1 (1), 14–27.
- Piao, S., Wang, J., Li, X., et al., 2022. Spatio-temporal changes in the speed of canopy development and senescence in temperate China. *Glob. Change Biol.* 28 (24), 7366–7375.
- Pinzon, J.E., Tucker, C.J., 2014. A non-stationary 1981–2012 AVHRR NDVI3g time series. *Remote Sens.* 6 (8), 6929–6960.
- Richardson, A.D., Hollinger, D.Y., Dail, D.B., et al., 2009. Influence of spring phenology on seasonal and annual carbon balance in two contrasting New England forests. *Tree Physiol.* 29 (3), 321–331.
- Richardson, A.D., Black, T.A., Ciais, P., et al., 2010. Influence of spring and autumn phenological transitions on forest ecosystem productivity. *Philos. Trans. R. Soc. B: Biol. Sci.* 365 (1555), 3227–3246.
- Richardson, A.D., Keenan, T.F., Migliavacca, M., et al., 2013. Climate change, phenology, and phenological control of vegetation feedbacks to the climate system. *Agric. For. Meteorol.* 169, 156–173.
- Seyednasrollah, B., Swenson, J.J., Domec, J.-C., et al., 2018. Leaf phenology paradox: Why warming matters most where it is already warm. *Remote Sens. Environ.* 209, 446–455.
- Shen, M., Zhang, G., Cong, N., et al., 2014. Increasing altitudinal gradient of spring vegetation phenology during the last decade on the Qinghai–Tibetan Plateau. *Agric. For. Meteorol.* 189, 71–80.
- Shen, M., Jiang, N., Peng, D., et al., 2020. Can changes in autumn phenology facilitate earlier green-up date of northern vegetation? *Agric. For. Meteorol.* 291, 108077.
- Shen, X., Jiang, M., Lu, X., et al., 2021. Aboveground biomass and its spatial distribution pattern of herbaceous marsh vegetation in China. *Sci. China Earth Sci.* 64 (7), 1115–1125.
- Shen, X., Liu, B., Henderson, M., et al., 2022. Vegetation greening, extended growing seasons, and temperature feedbacks in warming temperate grasslands of China. *J. Clim.* 35 (15), 5103–5117.
- Tucker, C.J., Slayback, D.A., Pinzon, J.E., et al., 2001. Higher northern latitude normalized difference vegetation index and growing season trends from 1982 to 1999. *Int. J. Biometeorol.* 45, 184–190.
- Vitasse, Y., Signarbieux, C., Fu, Y.H., 2018. Global warming leads to more uniform spring phenology across elevations. *Proc. Natl. Acad. Sci.* 115 (5), 1004–1008.
- Walther, S., Voigt, M., Thum, T., et al., 2016. Satellite chlorophyll fluorescence measurements reveal large-scale decoupling of photosynthesis and greenness dynamics in boreal evergreen forests. *Glob. Change Biol.* 22 (9), 2979–2996.
- Wang, H., Liu, H., Cao, G., et al., 2020. Alpine grassland plants grow earlier and faster but biomass remains unchanged over 35 years of climate change. *Ecol. Lett.* 23 (4), 701–710.
- Wang, L., Tian, F., Wang, Y., et al., 2018. Acceleration of global vegetation greenup from combined effects of climate change and human land management. *Glob. Change Biol.* 24 (11), 5484–5499.
- Wang, X., Piao, S., Xu, X., et al., 2015. Has the advancing onset of spring vegetation green-up slowed down or changed abruptly over the last three decades? *Glob. Ecol. Biogeogr.* 24 (6), 621–631.
- White, M.A., de Beurs, K.M., Didan, K., et al., 2009. Intercomparison, interpretation, and assessment of spring phenology in North America estimated from remote sensing for 1982–2006. *Glob. Change Biol.* 15 (10), 2335–2359.
- Wu, C., Peng, D., Soudani, K., et al., 2017. Land surface phenology derived from normalized difference vegetation index (NDVI) at global FLUXNET sites. *Agric. For. Meteorol.* 233, 171–182.
- Wu, C., Wang, X., Wang, H., et al., 2018. Contrasting responses of autumn-leaf senescence to daytime and night-time warming. *Nat. Clim. Change* 8 (12), 1092–1096.

- Wu, C., Wang, J., Ciais, P., et al., 2021a. Widespread decline in winds delayed autumn foliar senescence over high latitudes. *Proc. Natl. Acad. Sci.* 118 (16), e2015821118.
- Wu, C., Peng, J., Ciais, P., et al., 2022. Increased drought effects on the phenology of autumn leaf senescence. *Nat. Clim. Change* 12 (10), 943–949.
- Wu, Z., Chen, S., De Boeck, H.J., et al., 2021b. Atmospheric brightening counteracts warming-induced delays in autumn phenology of temperate trees in Europe. *Glob. Ecol. Biogeogr.* 30 (12), 2477–2487.
- Xie, X., Li, A., Tan, J., et al., 2020. Uncertainty analysis of multiple global GPP datasets in characterizing the lagged effect of drought on photosynthesis. *Ecol. Indic.* 113, 106224.
- Xu, C., Liu, H., Williams, A.P., et al., 2016. Trends toward an earlier peak of the growing season in Northern Hemisphere mid-latitudes. *Glob. Change Biol.* 22 (8), 2852–2860.
- Yu, Z., Lu, C., Cao, P., et al., 2018. Earlier leaf-flushing suppressed ecosystem productivity by draining soil water in the Mongolian Plateau. *Agric. For. Meteorol.* 250, 1–8.
- Zani, D., Crowther, T.W., Mo, L., et al., 2020. Increased growing-season productivity drives earlier autumn leaf senescence in temperate trees. *Science* 370 (6520), 1066–1071.
- Zhang, X., Tarpley, D., Sullivan, J.T., 2007. Diverse responses of vegetation phenology to a warming climate. *Geophys. Res. Lett.* 34 (19), 255–268.
- Zhou, L., Tucker, C.J., Kaufmann, R.K., et al., 2001. Variations in northern vegetation activity inferred from satellite data of vegetation index during 1981 to 1999. *J. Geophys. Res.: Atmos.* 106 (D17), 20069–20083.

